AN ABSTRACT OF THE THESIS OF

Jad G. Touma for the degree of Master of Science in Chemical Engineering presented on September 19, 2018

Title: Reversible Covalent Immobilization of Desferrioxamine B (DFOB) on Aminated Polystyrene Beads for Citrate-Bound Fe(III) Chelation

Abstract approved: _____

Christine J. Kelly Kate F. Schilke

The immobilization of chelators to solid supports has recently gained renewed interest due to the increasing biomedical and environmental applications made possible by these molecules' ability to bind Fe(III) and other metal ions. The uses of immobilized chelators have expanded to include the treatment of metal overload in serum, the detection of metal ions and living bacteria, the reduction of tissue degradation and inflammation, and the separation of high-valence metal ions, among other applications.

In this work, desferrioxamine B (DFOB) was reversibly and covalently immobilized to aminated 1 μm polystyrene beads for the chelation of Fe(III)-citrate complex. This iron complex was chosen given its relevancy in blood plasma, natural waters, plants and pathogenic bacteria. After linking Pyridyldithiol-Activated DFOB to the polymeric support via cleavable disulfide bonds, citrate-bound Fe(III) prepared in HEPES at a pH of 7.4 was successfully complexed by the immobilized chelator. It was subsequently shown that the active DFOB species were mostly covalently bound to the beads and not adsorbed on the polymeric surface. Additionally, the polystyrene support was effectively regenerated via cleaving the disulfide linkage between the resulting DFOB-Fe(III) complex and the surface, followed by recoupling to fresh DFOB. This

ability to regenerate the support allows for its multiple use and can prove economically advantageous for small and large-scale operations.

The kinetics and equilibrium studies for the adsorption of citrate-bound Fe(III) on DFOB-activated beads have also been performed under a constant chelator loading on the beads. Fitting the pseudo first-order, pseudo second-order and Elovich kinetics models to the experimental data did not lead to a firm conclusion regarding the most suitable model due to the similar calculated values of the correlation coefficients R^2. Moreover, modelling the Langmuir and Freundlich adsorption isotherms yielded relatively close correlation coefficients R^2 values of 0.992 and 0.953, respectively. However, since the Langmuir physics closely matches our understanding of the iron chelation by DFOB system, we expected that the Langmuir model offers a better description of the adsorption data, with a calculated Langmuir constant K_L = 12.81 $L/mg_{Fe(III)}$ and a maximum iron coverage q_{max} = 0.206 $mg_{Fe(III)}/g_{adsorbent}$. Additionally, relating the pseudo first and pseudo second-order models via the Langmuir kinetics equation using the previously obtained K_L and q_{max} values showed a dependency of the adsorption kinetics on the initial Fe(III) concentration; with a pseudo first-order model expected to most accurately describe the adsorption kinetics for initial Fe(III) concentrations lower than 22 μM or higher than 68 μM, while a pseudo second-order model was expected to offer the best fit to the data for values approaching 35 μM. Moreover, comparing the kinetics profiles of immobilized and free DFOB, it was found that approximately 180 minutes were required to reach constant concentration values of adsorbed Fe(III) with immobilized DFOB, compared to 30 minutes with the chelator in solution. These results showed that the immobilization of DFOB significantly reduced the rate of citrate-bound Fe(III) adsorption, which can be attributed to a possible hindrance of the iron's citrate-DFOB ligand exchange mechanism. The causes of this obstruction

can be related to a reduced diffusion of dimeric iron citrate complexes to the immobilized DFOB and/or a slower mechanism of metal ion complexation by the chelator's hydroxamates groups. The effects of serum protein on the activity of immobilized DFOB were also investigated. Washing DFOB-activated beads with bovine serum albumin in phosphate-buffered saline (BSA-PBS) at its serum concentration of 40 mg/mL, and a total exposure time of 30 minutes, reduced the amount of chelated iron by more than 50% compared to washing with PBS. Additionally, Fe(III)-citrate solutions prepared in BSA (40 mg/mL) and 25% v/v equine plasma diluted with HEPES buffer had approximately 80% and 70% less iron chelation levels compared to protein-free Fe(III)-citrate, respectively. These results illustrate the negative effects of protein surface adhesion on the activity of DFOB. This can be possibly ascribed to a reduced access of Fe(III)-citrate molecules to the immobilized chelator caused by the presence of the larger surface proteins and/or their negative effects on the ability of the DFOB's hydroxamates to complex the metal ions.

Given the versatility of DFOB in chelating different metal ions, coupled with the polystyrene's suitability for mass-production and support generation, it is hoped that this study can contribute in diffusing affordable and small-scale microfluidics and biosensors technologies, suited for different biomedical and environmental applications. Provided that the required protein-repulsing surface modifications are performed, this system can potentially offer a safer chelation treatment for metal overload patients. Other immediate applications can include the simple detection of metals and bacteria in physiological and environmental fluids and the separation of high-valence metals, along other potential applications.

Reversible Covalent Immobilization of Desferrioxamine B (DFOB) on Aminated Polystyrene Beads for Citrate-Bound Fe(III) Chelation

by

Jad G. Touma

A THESIS

submitted to

Oregon State University

in partial fulfillment of
the requirements for the
degree of

Master of Science

Presented September 19, 2018
Commencement June 2019

Master of Science thesis of Jad G. Touma presented on September 19, 2018

APPROVED:

Co-major Professor, representing Chemical Engineering

Co-major Professor, representing Chemical Engineering

Head of the School of Chemical, Biological, and Environmental Engineering

Dean of the Graduate School

I understand that my thesis will become part of the permanent collection of Oregon State University libraries. My signature below authorizes release of my thesis to any reader upon request.

Jad G. Touma, Author

ACKNOWLEDGEMENTS

This thesis would not have been possible without the contribution of many amazing individuals that I met at OSU; My major advisor Dr. Christine Kelly, My co-advisor Dr. Kate Schilke, Dr. Goran Jovanovic, The CBEE faculty and staff, Curtis Lajoie, Matt Coblyn, Anita Hughes, Elisha Brackett, many graduate and undergraduate students that helped me along the way and Subway for the coffee and LBT's at 4:00 am while taking my lab break.

Thank you Dr. Christine Kelly for supporting me, guiding my work, motivating at all times and always dedicating the effort to help me do my best. Thanks for all the meetings and for giving me your much needed advices along the way, and thank you for your patience. You helped me grow, I am forever grateful to you.

To my co-advisor Dr. Kate Schilke, your love for what you do is contagious! Thank you for taking the time and effort to answer all my endless questions. Thank you for all the time you dedicated to my work, even though I always knew how busy you were. I will always miss your office (probably the best on campus!).

I am also forever indebted to Dr. Goran Jovanovic. His ideas, teachings and vision were always a source of inspiration to me. Thank you for helping me think inside and outside the box and for supporting me on all levels.

I want to thank my family, you are always, always on my mind and always in my heart; Rima Michel Chakar (7attet esmik!), Gerard (My small/big brother), Jean-Michel (Je T'aime!) and Maroun (3ammey!).

Last but definitely not least, I want to thank my one and only Vanessa. Soos and Edie, you are always in my heart.

Jad G. Touma, 09, 2018.

TABLE OF CONTENTS

Page

TABLE OF CONTENTS (Continued)

Page

TABLE OF CONTENTS (Continued)

Page

TABLE OF CONTENTS (Continued)

Page

TABLE OF CONTENTS (Continued)

LIST OF FIGURES

Figure Page

LIST OF FIGURES (Continued)

Figure Page

LIST OF FIGURES (Continued)

Figure Page

LIST OF TABLES

Table Page

1 INTRODUCTION

1.1 Desferrioxamine B (DFOB): A Brief Introduction

Desferrioxamine B (DFOB) is a bacterial hexadentate siderophore produced by the soil bacterium *Streptomyces pilosus* (Richardson, 2002). Due to its remarkable ability to strongly bind different trivalent, and to a lesser extent, divalent metal ions, DFOB has been used for various medical, environmental and industrial applications since its discovery in the late 1950's (Kiss et al., 1998; Hernlem et al., 1995). In this work, DFOB has been successfully immobilized to the industrially relevant polystyrene polymer for the chelation of Fe(III)-citrate, a physiologically and environmentally essential molecule, found in blood plasma, natural waters, plants and pathogenic bacteria (Ito, 2011).

The metal-binding ability of DFOB is primarily achieved by its hydroxamates groups, which coordinate the metal ion and allow the ligand to wrap around it, forming a stable octahedral

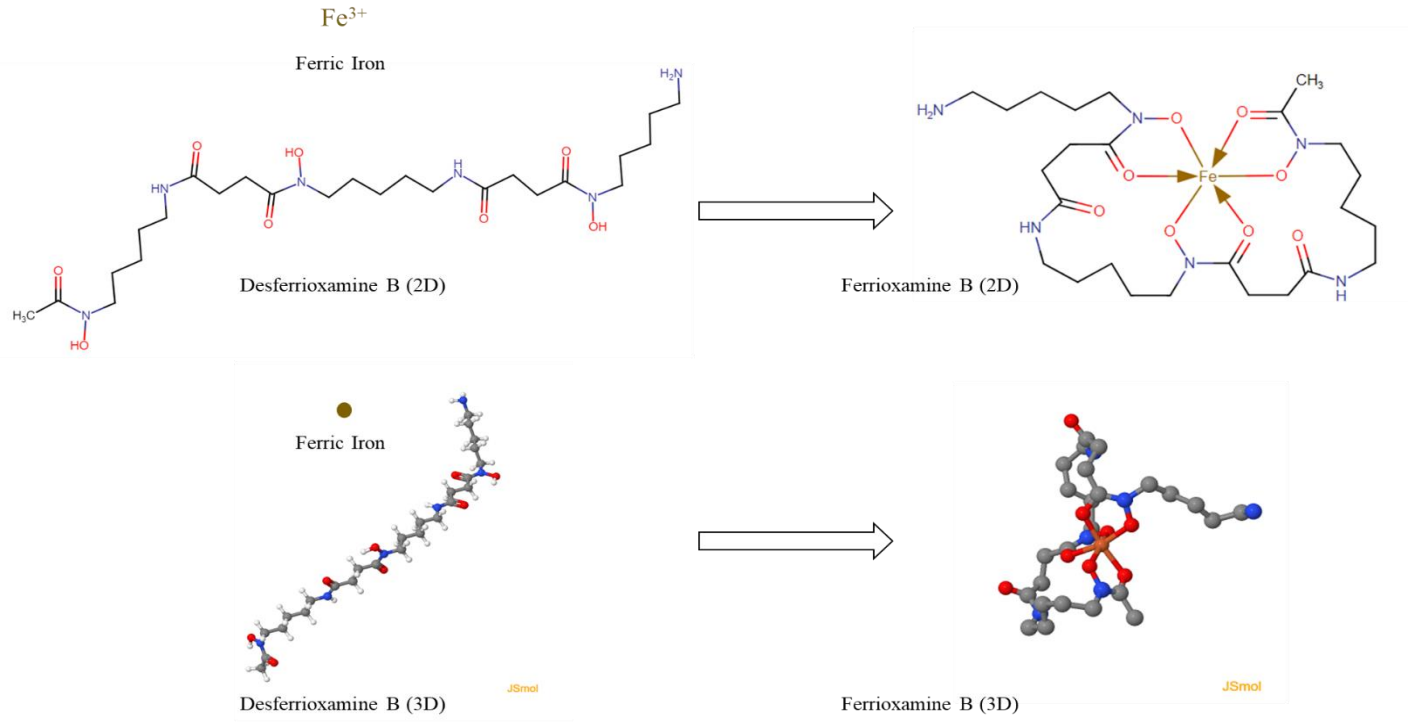

Figure 1.1 Desferrioxamine B complexation of Fe(III) forming Ferroxamine B (2D and 3D representations). Adopted from (chem.nlm.nih.gov)

complex with the ion on a 1:1 molar basis (Kiss et al., 1998; Enyedy, 1966)**. Figure 1.1** shows the complexation of Fe(III) by DFOB and the formation of the brick-colored ferrioxamine B complex.

Although DFOB binds most strongly to iron (III) (Kiss et al., 1998), previous studies have successfully used this siderophore, either in solution or anchored to a solid support, to chelate aluminum (III) (Anthone, 1995), zirconium (IV) (Takagai et al., 2007), vanadium (V) (Alberti et al., 2015), and gallium (Koizumi et al., 1988; Petrik et al., 2016), among other metals. Kiss et al. (1998) and Hernlem et al., (1995) reported the stability constants of DFOB's complexes with different trivalent and bivalent metals which illustrated the excellent chelating properties of DFOB and explained the versatile and wide-range applications of this molecule. As can be seen in **Table 1.1,** the high equilibrium stability constants Log β for the physiological complexes of DFOB with Fe(III) and Al(III), along other metals, justify the suitability of this chelator to capture different metals in physiological applications.

1.2 Immobilization of DFOB in the Literature

Given that the terminal amino group of DFOB does not participate in the complexation of metal ions as can be seen in **Figure 1.1**, previous studies have frequently adopted immobilization strategies that consisted of targeting this amino group to attach DFOB on different supports for various applications.

DFOB was immobilized on solid supports to address a number of medically relevant objectives. Biesuz et al. (2014) covalently bound DFOB on a self-assembled monolayer on mesoporous silica (SAMMS) to detect traces of Fe(III), which can be potentially used in studying chelation

therapy, measuring non-transferrin bound iron (NTBI) and investigating the half-life of drugs. Bhadra et al., (2018) created a miniature real-time biosensing platform that can selectively bind to living bacteria by covalently binding DFOB on gold coated microcantilever surface. Additionally, Su et al. (2011) developed a nanosensor for labile plasma iron (LPI) by immobilizing fluorescein–desferrioxamine on mesoporous silica. Moreover, Alberti et al. (2015) developed a simple colorimetric sensor able to detect iron(III) and vanadium(V) by functionalizing cellulose filter papers with DFOB. Alberti et al. (2014) were able to measure iron concentrations in urine samples using DFOB-functionalized mesoporous silica, while Ambrus et al. (1987) and Anthone et al. (1995) have immobilized DFOB on polysulfone hollow fibers to extract Fe(III) and Al(III) from blood, respectively. Wenk et al. (2001) coupled DFOB to cellulose for the chelation of Fe(III)-citrate in order to limit the increase of free iron and reactive oxygen species via the Fenton reaction, responsible for persistent inflammation, increased connective tissue degradation, in addition to lipid peroxidation. Finally, Hallaway et al. (1989) were able to attach DFOB to biocompatible materials such as dextran and hydroxyethyl-starch to increase the chelator's plasma half-life by more than 10-fold.

The benefits of immobilizing DFOB were not restricted to medical treatment and diagnostic applications. For example, Yehuda et al. (2012) and Yehuda et al. (2003) developed a slow-release fertilizing system for iron deficient crops by immobilizing DFOB on sepharose. Additionally, by attaching DFOB on nylon-6, 6, Tagakai et al. (2007) were able to selectively adsorb zirconium (IV), a high-valence metal ion relevant for the production of frontier materials.

1.3 Current Study: Aims and Objectives

This work presents the required protocols for the reversible and covalent immobilization of DFOB to aminated polystyrene beads and investigates the effectiveness, kinetics and sorption studies for Fe(III)-citrate adsorption on the developed chelator-polymer system under physiological conditions.

1.3.1 Reversible Immobilization of DFOB and Support Regeneration

The reversible covalent immobilization of molecules, peptides and enzymes on solid supports is highly desirable because it permits the detachment of surface species, thus allowing the regeneration of both the depleted molecules and the reuse of the polymeric support. This technical ability can prove economically and environmentally advantageous to both large-scale operations and small-scale devices such as microreactors and biosensors (Schilke, 2009; Mohamad et al., 2015; Fraas and Franzreb, 2017; Carlsson et al., 1975; Miyazaki, et al., 2004). Consequently, in this work, Pyridyldithiol-activated DFOB was reversibly linked to the polystyrene surface via disulfide bonds (S-S), which are readily cleavable upon reduction with dithiothreitol (DTT). It is worth noting that, to the best of our knowledge, no previous work in the literature on reversibly attaching DFOB to solid supports was found, despite the envisioned economic and environmental benefits of that process.

In addition to permitting the regeneration of the support via replacing the spent surface chelators with fresh ones, this immobilization technique can also allow for the regeneration of the Fe(III)-bound DFOB molecules and the restoration of the chelator via the aquation of ferrioxamine (Monzyk and Crumbliss, 1982) or its reduction (Alderman et al, 2009) which release the ion from the DFOB. Monzyk and Crumbliss (1982) investigated the aquation of ferrioxamine over a $[H^+]$ range of 0.03 – 1.0 M at 25 ˚C and an ionic strength of 2.0 ($NaClO_4/HClO_4$). They were

able to show that the dissociation reaction (2.1) is achieved through four kinetically different stages. The proposed dissociation mechanism was a stepwise unwrapping of DFOB from Fe(III) which starts from the N-O oxygen atom closer to the DFOB's protonated amine terminal. Alderman et al (2009) used the Fe(II) chelator 2,2'-bipyridine (bipy) to achieve the reduction of ferrioxamine B (FO) via ascorbate. The facilitation of the FO reduction by bipy was attributed to a mechanism that involves the formation of a ternary complex between the chelator, iron and bipy and a shift of the reduction potential of Fe(III) to a more positive value.

$$Fe(HDFOB)^{+} + 3H_{aq}^{+} \leftrightarrow Fe_{aq}^{+} + H_4DFOB^{+} \quad (2.1)$$

1.3.2 Selection of Polystyrene Support

Polystyrene (PS) was chosen based on its reported optical transparency, flexibility, relative low cost and stability, industrial relevance, in addition to its suitability for mass production compared to other microfluidic manufacturing materials such as glass, silicone and polydimethylsiloxane (PDMS) (Chin et al., 2011; Chan et al., 2014; Pandey et al., 2017; Yuen and DeRosa, 2011). This perceived aptness of PS in microfluidics manufacturing is further enhanced by the recent improvements on the injection molding process reported by Chin et al. (2011), along other technologies, such as soft lithography (Wang et al., 2011) and controlled perfusion (Tran et al., 2014). The suitability of Polystyrene for mass production of surfaces, biosensors and microfluidics devices can prove vital to the advancement of in-situ healthcare in distant areas without proper access to medical facilities (Chin et al., 2011). Additionally, this polymer has been successfully functionalized with different protein-repellant materials, such as Pluronic®, which constitutes a critical step to enhance the performance of biomedical devices (Hecker et al., 2018; Fry, 2010). All these attributes make polystyrene an attractive material for the

manufacturing of affordable microfluidics and lab-on-a-chip devices, dedicated to both diagnostic and therapeutic applications. Consequently, this work aimed at immobilizing DFOB on this highly versatile platform.

1.3.3 Selection of Fe(III)-Citrate Solution

Fe(III)-citrate was our compound of interest in this study since it is one of the most relevant iron complexes in both physiological and environmental milieus (Ito, 2015). The importance of this iron form arises from the critical role of the biosynthesized citrate in the transformation, availability, transportation and uptake of iron in blood plasma, natural waters, plants and pathogenic bacteria (Ito, 2011; Ito, 2015).

On a physiological level, individuals requiring frequent blood transfusions such as thalassemia patients, along with individuals having hemochromatosis iron disorder, or undergoing chemotherapy treatment, in addition to other iron overload patients, show increased levels of non-transferrin bound iron (NTBI) in their serum (Evans et al., 2008). Normally, Fe(III) circulates in the blood by attaching itself to transferrin. However, with transferrin saturation levels exceeding 70% in iron overload patients (Borgna-Pignatti and Marsella, 2015), NTBI will form and then circulate in the blood mostly as Fe(III) ions in concentrations of less than 10 μM (Pootrakul et al., 2004). These ions can be free or attached to small ligands proteins and other plasma components (Cabantchik et al., 2005). Moreover, NTBI in blood, which is not attached to large proteins can have cell-penetrating capabilities and accumulate in the heart, pancreas, liver and other organs, leading to organ dysfunction, in addition to producing harmful hydroxyl radicals via the Fenton reaction (Aruoma et al, 1988). This iron is a subset of NTBI and is referred to as labile plasma iron (LPI). It is worth noting that LPI consists of unbound iron and

iron attached to proteins having a molecular weights of less than 5000 g/mol. LPI is considered the most redox active and organ-damaging form of iron, thus the prime target of chelators such as DFOB (Cabantchik et al.,2005; Patel et al., 2012). Consequently, since different studies have suggested that Fe(III)-citrate is a major species in NTBI (May et al., 1977; Parkes et al., 1991; Evans et al., 2008), we were interested in investigating its chelation by our DFOB-activated polystyrene beads. **Figure 1.2** shows the structure of dimeric iron citrate ($FeCit_2$) which is a common specie of Fe(III)-citrate in NTBI under physiological conditions at citrate:iron ratio of 100:1 (Evans et al., 2008).

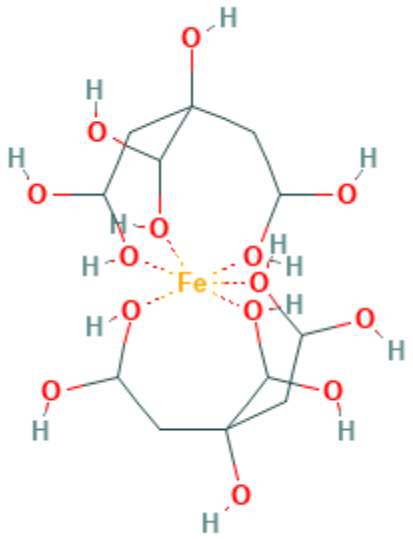

Figure 1.2 Structure of dimeric iron citrate ($FeCit_2$). Adopted from (pubchem.ncbi.nlm.nih.gov)

1.3.4 Potential Applications

For all the aforementioned reasons, developing a DFOB-polystyrene system and investigating its performance in citrate-bound Fe(III) has proved an interesting objective for this work. The potential applications of this system can include the chelation of iron, aluminum and other metals

from the serum of individuals with iron overload or metal poisoning, thus decreasing the adverse effects of introducing chelators in the human body. These side effects can include visual and oral neurotoxicity, ocular damage, renal failure, increased risk of infections, among other complications (Borgna-Pignatti and Marsella, 2015; Ambrus, 1987; Anthone S et al., 1995). Additionally, the immobilized chelator can be used for the rapid colorimetric determination of iron in serum, urine and environmental solutions due to the noticeable brick-color of the DFOB-iron complex ferrioxamine, which absorbs light most strongly in the range of 425 - 429 nm; λ_{max} = 425 nm, $\boldsymbol{\varepsilon}_{425}$ = 2700 M^{-} cm^{-} (Faller and Nick, 1994, Alberti et al., 2014; Alberti et al., 2015). In addition to that, this system can serve in the detection of living bacteria (Bhadra et al.,2018), the detection and extraction of heavy metals in environmental mediums (Tagakai et al., 2007), among other possible applications offered by the ability of DFOB to bind different metals.

1.3.5 Structure of Study

Chapter 2 presents the preparation protocols followed to reversibly and covalently immobilize DFOB on aminated polystyrene beads via disulfide bonds (S-S). Additionally, an examination of the parameters influencing the bioconjugation of that chelator on the surface was investigated. Finally, the polystyrene surfaces used for the chelation of Fe(III)-citrate were regenerated and used to process fresh batches of iron.

In Chapter 3, the kinetics and equilibrium studies for the Fe(III)-citrate adsorption on DFOB-activated beads at physiological pH levels are presented. The experimental data was analyzed in light of the relevant kinetics and sorption models, in addition to establishing the characteristics of the chelation mechanism which can prove helpful in designing future biomedical devices.

Finally, the effects of immobilizing DFOB on the reaction kinetics were also studied and compared to that of DFOB in solution.

In Chapter 4, the effects of serum proteins on the activity of DFOB-activated polystyrene beads are investigated. The tested proteins consist of albumin and plasma proteins such as fibrinogen, known to strongly and irreversibly attach to hydrophobic surfaces with detrimental effects on the performance of biomedical devices (Halperin, 1999; Unsworth et al., 2008; Schilke and McGuire, 2011). The findings of these studies can help in designing DFOB-functionalized devices that are better suited for operating in protein-rich biological fluids.

Table 1.1 Cumulative stability constants ($Log\ \beta$) for the physiological complexes of DFOB with trivalent and divalent metal ions (Kiss et al., 1998). With $\beta = \frac{[MLH]}{[M][LH]}$ and M: Metal, LH: Protonated DFOB ligand and MLH: Protonated DFOB ligand-metal ion complex

	Aluminum (III)	**Gallium (III)**	**Indium (III)**	**Iron (III)**	**Bismuth (III)**	**Lanthanum (III)**	**Ytterbium (III)**	
	34.93	38.96	31.39	41.39	34.40	21.90	27.00	
Magnesium (II)	**Calcium (II)**	**Strontium (II)**	**Cobalt (II)**	**Nickel (II)**	**Copper (II)**	**Zinc (II)**	**Lead (II)**	**Tin (II)**
14.66	13.25	13.20	21.33	19.71	23.98	20.40	20.89	32.01

2 REVERSIBLE COVALENT IMMOBOLIZATION OF DESFERRIOXAMINE B (DFOB) TO ALIPHATIC AMINE POLYSTYRENE BEADS AND SUPPORT REGENERATION

2.1 Abstract

The reversible and covalent immobilization of desferrioxamine B (DFOB) to aminated polystyrene beads was achieved by reacting pyridyldithiol-activated desferrioxamine to sulfhydryl-activated support, thus linking the chelator to the surface via covalent disulfide bonds. The following study has shown that from all the surface species, only DFOB was responsible for the observed iron chelation. Additionally, it was found that most of the active DFOB on the surface was covalently attached to the beads and not as a result of surface adsorption. Moreover, our experiments showed that the conjugation of DFOB to the surface was limited by the production of PDS-DFOB species given the fast hydrolysis of NHS esters at the working pH. Finally, comparing the iron chelation levels under fresh and regenerated beads, it was shown that both beads were able to chelate similar amounts of iron.

2.2 Introduction

In this chapter, the protocols followed to reversibly and covalently immobilize DFOB molecules on polystyrene beads for the chelation of citrate-bound Fe(III) is presented. This was achieved by linking the DFOB to the surface via disulfide bonds which allows for the DFOB's detachment after its complexation with the Fe(III), thus potentially permitting the regeneration of the support and the DFOB (Schilke, 2009; Fraas and Franzreb, 2017; Miyazaki, et al. 2004; Alderman et al, 2009; Monzyk and Crumbliss, 1982).

Additionally, this work aims at covalently binding DFOB to the latex beads via disulfide bonds while avoiding the adsorption of that siderophore on the surface. For that reason, we investigated the contribution of adsorbed DFOB on the levels of chelated iron. The adsorption of DFOB on the polymeric surface can be assigned to hydrophobic and electrostatic interactions (Carrasco et al., 2009). At pH 7.7 employed during the coupling of the beads to PDS-DFOB, the amine terminal group of DFOB in the coupling solution is mostly in its protonated and hydrophilic form ($-NH_3^+$) (pKa 10.01 – 10.84), while the chelator's pentyl chain is of hydrophobic nature (Carrasco et al., 2009). However, the hydrophobic interactions required to promote the adsorption of DFOB on the particles' surface were expected to be limited, given the hydrophilic nature of the aminated latex beads. On the other hand, given the fact that these particles are polystyrene-based, which leads them to retain some hydrophobic characteristics (Molecular Probes, 2004) and thus promote hydrophobic interactions, coupled with the possibility of having non-specific binding caused by charge-based interactions (electrostatic attraction of the positively charged DFOB molecules to the negatively charged surfaces) (Neubauer et al., 2000), have led us to investigate the adsorption of DFOB on the microspheres during the coupling of PDS-DFOB to the microspheres. It is worth noting that Carrasco et al. (2009) concluded that hydrophobic interactions are more important than electrostatic ones in determining the extent of DFOB surface adsorption on goethite in the presence of the surfactant sodium dodecyl sulfate (SDS).

Moreover, the reaction of SPDP and DFOB in the coupling solution was of particular interest **(Scheme 2.3)**, since unlike previous works linking PDS-activated species to thiolated surfaces (Neff et al., 1997), the PDS-DFOB was not separated from the unreacted SPDP due to the relative similar small sizes of both molecules. The existence of unreacted SPDP in the coupling

solution can lead to its undesirable competition on binding to the surface SH sites. Instead, we relied on adding an excess amount of DFOB in the coupling solution, thus minimizing the amount of unreacted SPDP during the coupling process. Consequently, it was critical to understand the effects of varying the amounts of DFOB and SPDP in the coupling solution on the formation of PDS-DFOB molecules and the existence of unreacted SPDP. In the literature, the reported dissociation constant (pK_a) of the DFOB's amine group varied from 10.01 (measured in 1 M KCl, 25˚ C) (Borgias et al., 1989), to 10.79 (measured in 0.1 M KCl at 25˚ C) (Evers et al., 1988), and up to 10.84 (measured in KCl solutions of ionic strength 0.1 mol/dm^3) (Farkas et al., 1999) **(Figure 2.1)**. Thus, in order to avoid the full protonation of the DFOB's terminal amine leading to the creation of the non-nucleophilic and non-reactive ($-NH_3^+$) species, and to maintain a sufficient presence of the non-protonated, nucleophilic and reactive ($-NH_2$), Koizumi et al. (1988) and Arano et al. (1990) coupled the amine terminal of DFOB to N-succinimidyl 3-(2-pyridyldithio) propionate (SPDP) and N-[[4-(2-maleimidoethoxy)-succinyl]oxy]succinimide (MESS) in 10 mM borate-buffered saline at a pH of 8.6 and 8.2, respectively. This working pH was chosen despite being higher than the usually recommended pH range of 7 - 8 for SPDP, which is used to avoid the rapid hydrolysis of NHS esters (SPDP) in aqueous solutions (NHS esters hydrolyze within hours at pH = 7 and minutes at pH = 9) (Hermanson, 2008). Moreover, working at pH ranges lower than the dissociation constant (pK_a) of the targeted amino group has also been performed by Sélo et al., (1996). In that work, NHS and Sulfo-NHS esters were preferentially reacted with the terminal ($-NH_2$) of the protein (pK_a = 8.9) and not the ε–amino group of Lysine (K) (pK_a = 10.5) by carrying out the reaction at a pH of 6.5. At that working pH, the ε–amino group of the Lysine (K) was much more protonated (thus less reactive) than the terminal ($-NH_2$) of the protein. For all the aforementioned variables, the

formation of PDS-DFOB molecules, which is the surface molecule responsible for iron chelation, was investigated under different DFOB and SPDP amounts in the coupling solution.

Although previous studies have successfully immobilized DFOB on a variety of different supports; mesporous silica (Biesuz et al., 2014; Su et al., 2011), gold coated microcantilever (Bhadra et al., 2018), cellulose (Alberti et al., 2015), (Wenk et al., 2001), Dextran and Hydroxyethyl-starch (Hallaway et al., 1989), a reversible covalent immobilization of DFOB that can potentially allow the regeneration of the support was not found in the literature. Consequently, we investigated the ability of regenerated beads coupled to fresh PDS-DFOB molecules to chelate iron and compared their performance to that of fresh activated beads. In order to regenerate the beads, DTT was added to cleave the disulfide bond linking the DFOB-Fe(III) complex (ferrioxamine) to the surface, which in turn regenerated the (-SH) sites on the beads **(Scheme 2.6).** Subsequently, this was followed by the addition of a fresh PDS-DFOB coupling solution to the restored thiolated particles **(Scheme 2.7)**.

Fe(III)-citrate was chosen since it is a dominant species in non-transferrin-bound iron (NTBI) (May et al., 1977), which is the main target for chelation in the plasma of iron overload patients (Evans et al., 2008; Bellanti et al., 2016). In this study, Fe(III)-citrate solutions were prepared at a physiological pH level of 7.4. A citrate: iron ratio of 100:1 was chosen for several considerations: 1) its clinical relevance in blood plasma knowing that the clinically observed citrate: iron ratios vary from approximately 10 to 100:1 (Evans et al., 2008; Tiffin, 1966), 2) its ability to significantly limit the precipitation of the insoluble ferric hydroxide species at pH=7.4 for at least 24 hours compared to lower citrate: iron ratios, thus rendering all the iron accessible to the DFOB (Evans et al., 2008; Rose and Waite, 2003) and 3) its ability to limit the predominant species in the solution at pH = 7.4 to both dimeric and mononuclear iron (Silva et

al., 2009; Evans et al., 2008), while avoiding the formation of oligomeric and polymeric iron species such as Fe_2Cit_2 and Fe_3Cit_3 which were found to slow down the iron access to chelator at lower citrate: iron ratios (Evans et al., 2008; Faller and Nick, 1994).

2.3 Materials and Methods

In order to reversibly and covalently attach pyridyldithiol-activated desferrioxamine (PDS-DFOB) to the microspheres via disulfide bonds, sulfhydryl (-SH) groups were created on the polymeric support. This was achieved by initially creating pyridyldithiol (-PDS) groups on the aminated beads via reacting the NHS's moiety of N-succinimidyl 3-(2-pyridyldithio) propionate (SPDP) with the ($-NH_2$) sites existing on the beads' surface **(Scheme 2.1)**. Subsequently, the disulfide bonds of the PDS groups were cleaved by the introduction of dithiothreitol (DTT) **(Scheme 2.2)**. After preparing the thiolated surface, the terminal amine groups of the DFOB were functionalized with pyridyldithiol (-PDS) by the addition of SPDP in a coupling solution **(Scheme 2.3).** Finally, the PDS-activated DFOB molecules in the coupling solution were added to the sulfhydryl (-SH) activated species, thus reacting the PDS and SH groups, which in turn linked DFOB to the surface by a cleavable disulfide bond **(Scheme 2.4).**

1 μm aliphatic amine latex beads (2% w/v) were purchased from Invitrogen™ (catalog # A37362, LOT # 1862713). The heterobifunctional crosslinker N-succinimidyl 3-(2-pyridyldithio) propionate (SPDP) was obtained from Thermo Scientific™ (catalog # 21857) and stored at -20˚ C. In order to avoid the condensation of moisture on the reagent and the hydrolysis of the N-hydroxysuccinimide (NHS) ester group, the bottle of reagent was opened after it was fully equilibrated to room temperature. The desferrioxamine mesylate salt used was acquired

from Sigma-Aldrich (≥92.5% (TLC), powder). Additionally, the disulfide reducing agent dithiothreitol (DTT) was obtained from Thermo Scientific™ (catalog # R0861) and stored at 4˚C. Dimethyl sulfoxide (DMSO) solvent was purchased from Sigma Aldrich (ACS reagent, ≥99.9%) to dissolve SPDP, while P2T (2-Mercaptopyridine, Sigma-Aldrich, ReagentPlus®, 99%) was used to experimentally determine the molar extinction coefficient of that compound at 340 nm. A Victor^3 plate reader (Perkin-Elmer, Waltham, MA) was used to spectrophotometrically determine the concentrations of P2T, ferrioxamine and iron. Fe(III) chloride (Alfa Aesar, Anhydrous, 98%) and citric acid (Alfa Aesar, Anhydrous, 99.5%) were used for the preparation of iron solutions, while iron concentrations were determined using a QuantiChrom™ Iron Assay Kit (Bioassay Systems, Hayward, CA). All the buffers and solutions in this work were prepared using HPLC-grade water.

The following sections detail the different experimental procedures followed in this chapter.

2.3.1 Preparation of the Aliphatic Amine Latex Beads

1 μm aliphatic amine latex beads were suspended by vortexing the containing bottle for 30 seconds and 10 mg aliquots (0.476 mL) were immediately withdrawn and pipetted into 1.5 mL microcentrifuge tubes. The tubes were centrifuged for 5 minutes at 13.2 RCF to separate the beads from their de-ionized water medium. Subsequently, the beads were equilibrated by washing twice with 1 mL of phosphate-buffered saline (PBS) (20 mM sodium phosphate, 150 mM NaCl, pH=7.5) at room temperature. After each wash, the tubes were centrifuged for 5 minutes at 13.2 RCF and the supernatant was carefully decanted. After the second wash, the beads were resuspended in 0.5 mL of PBS buffer in preparation for SPDP coupling in the subsequent step.

2.3.2 N-succinimidyl 3-(2-pyridyldithio) propionate (SPDP) Coupling to the Aliphatic Amine Latex Beads

Immediately before use, SPDP was dissolved in DMSO at a concentration of 40 mM. Subsequently, an appropriate volume of SPDP-DMSO solution was added to the aminated latex beads already suspended in 0.5 mL PBS (20 mM sodium phosphate, 150 mM NaCl, pH=7.5). The small amount of DMSO used did not affect the beads' stability. The molar ratio of NHS: Surface amine ($-NH_2$) was maintained at 15:1 for all the aliquots, while the reaction was allowed to proceed for 1 hour at room temperature under gentle end-over-end mixing. At the end of the reaction, the tubes were centrifuged for 5 minutes at 13.2 RCF, then the SPDP-PBS-DMSO supernatant was carefully decanted and the beads were washed twice with 1 mL PBS buffer. At the end of this procedure the beads were partially pyridyldithiol (-PDS)-activated. **(Scheme 2.1)** presents the modification of the amine groups on the latex beads by the SPDP.

2.3.3 Sulfhydryl (-SH)-Activation of Latex Beads via Dithiothreitol (DTT)

Just before use, DTT was added to PBS (20 mM sodium phosphate, 150 mM NaCl, pH=7.5) at a concentration of 50 mM. Subsequently, 1 mL of this DTT-PBS solution was added to each tube and the reaction was allowed to proceed for 1 hour at room temperature under gentle end-over-end mixing. At the end of the reaction, the supernatant was collected in order to measure the pyridine-2-thione (P2T) liberated following the reduction of the disulfide bonds. The details of the spectrophotometric measurement of P2T are presented in a Section 2.3.6. After performing the required steps to measure the P2T concentration in the supernatant, the tubes were washed twice with PBS buffer. At the end of this procedure, the beads were partially SH-activated.

Scheme 2.2 shows the reduction of the disulfide bonds of the PDS group on the latex beads and the formation of sulfhydryl groups.

2.3.4 Preparation of Pyridyldithiol-Activated Desferrioxamine (PDS-DFOB) in Borate-Buffered Saline (BBS)

In this work, desferrioxamine mesylate salt was dissolved in borate-buffered saline (BBS) (20 mM sodium borate, 150 mM NaCl, pH = 8.5) according to the desired DFOB: SPDP molar ratio. Just before use, SPDP was dissolved in DMSO at a concentration of 40 mM. Subsequently, a convenient volume of SPDP-DMSO solution, corresponding to the needed PDS: Surface (-SH) molar ratio, was added to the DFOB-BBS mixture and the reaction was allowed to proceed for 30 minutes at room temperature under gentle end-over-end mixing. The pH of the solution was registered at the end of the reaction. After this procedure, a portion of the desferrioxamine's terminal amine has been modified by reacting with the SPDP's NHS group. **Scheme 2.3** shows the preparation of PDS-DFOB from DFOB and SPDP, while **Scheme 2.9** presents an overall explanation of the PDS-DFOB coupling procedure. It is very important to note that, unlike previous studies concerned with coupling small PDS-activated peptides to SH-functionalized surfaces (Neff et al., 1997), no attempts were made in this work to separate the unreacted SPDP from the PDS-DFOB due to the similar small sizes of both molecules. However, we opted for an approach that used an excess amount of DFOB relative to SPDP to ensure the progress of the reaction, thus minimizing the amount of unreacted SPDP in the coupling solution, and consequently limiting the SPDP's competitive binding to the thiolated surface, favoring the attachment of PDS-DFOB.

2.3.5 Coupling of Pyridyldithiol-Activated Desferrioxamine (PDS-DFOB) to the Sulfhydryl (-SH)-Activated Latex Beads

After creating sulfhydryl (-SH) groups on the surface of the latex beads and the preparation of PDS-DFOB in borate-buffered saline, the coupling of the chelator to the beads can be initiated. Since the coupling of sulfhydryl (-SH) and pyridyldithiol (-PDS) groups occurs optimally at a pH range of 7 - 8 (Carlsson J. et al., 1978), the pH of borate-buffered saline solution containing the PDS-DFOB was decreased (if needed) to a value of 7.7 (± 0.05) and subsequently, a 0.5 mL volume of this solution was added to each microcentrifuge tube. The coupling of the PDS-DFOB and the SH-activated beads proceeded for 14 hours at room temperature under gentle end-over-end mixing. At the end of the reaction, the supernatant was collected in order to measure its pyridine-2-thione (P2T) concentration as will be detailed in Section (2.3.7) and its pH was recorded. Finally, the beads were washed 4 times with PBS buffer. After the final PBS wash and prior to the introduction of the iron solutions, the tubes were centrifuged for 12 minutes at 13.2 RCF and the supernatant was thoroughly decanted. Alternatively, the beads were stored at 4˚ C in PBS buffer (20 mM sodium phosphate, 150 mM NaCl, pH=7.5) containing 0.02% sodium azide (NaN_3) and washed twice with PBS buffer prior to use. **Scheme 2.4** shows the coupling of PDS-DFOB and SH-activated latex beads.

2.3.6 Spectrophotometric Measurement of Pyridine-2-Thione (P2T) after Reduction of Pyridyldithiol (-PDS)-Activated Latex Beads via Dithiothreitol (DTT)

Following the reduction of the disulfide bonds of the PDS groups on the surface of the latex beads, the concentration of the reporter molecule pyridine-2-thione (P2T) in the supernatant

(released on a 1:1 molar basis) can be spectrophotometrically determined to calculate the degree of sulfhydryl (-SH) coverage on the beads **(Scheme 2.2)** (λ_{max} = 343 nm, $\boldsymbol{\varepsilon}_{343}$ = 8060 M^{-} cm^{-}) (Li J-T et al., 1996). In our work, a Victor^3 plate reader was used to monitor the absorbance of the P2T compound. After adding known amounts of P2T to both PBS and HEPES, while taking these buffers as blanks, we calculated a molar extinction coefficient of 7318 M^{-} cm^{-} at 340 nm.

In order to measure the P2T absorbance following the SH-activation of the latex beads, the tubes were centrifuged for 10 minutes at 13.2 RCF and the top 0.5 mL layer of the DTT-PBS-P2T supernatant mixture (out of the originally introduced 1 mL DTT-PBS volume) was collected while avoiding the extraction of the microspheres. Subsequently, the extracted volume of this P2T-contaning supernatant was also centrifuged for another 10 minutes at 13.2 RCF. Finally, the absorbance of a 100 μL volume of the treated supernatant and the original DTT-PBS solution (blank) was measured in a 96-well plate. On the other hand, in order to account for any possible interference on the absorbance caused by unintentionally extracted beads in the DTT-P2T-PBS supernatant, the beads were washed once with 1 mL of PBS, then 1 mL of DTT-PBS solution (blank) was added to the beads. This was followed by vortexing the tubes for 30 seconds, and the same centrifugation steps carried out for the original supernatant were repeated (10 minutes centrifugation for the beads and another 10 minutes for the blank supernatant at 13.2 RCF). Comparing the absorbance at 340 nm of the DTT-PBS solution (blank), the DTT-P2T-PBS and the DTT-PBS supernatants, showed that the microspheres did not significantly interfere with the measurements.

2.3.7 Spectrophotometric Measurement of Pyridine-2-Thione (P2T) after Coupling of Pyridyldithiol-Activated Desferrioxamine (PDS-DFOB) to the Sulfhydryl (-SH)-Activated Latex Beads

The amount of pyridyldithiol-containing molecules (i.e. PDS-DFOB and unreacted SPDP) coupled to the SH-activated latex beads can be determined by measuring the concentration of P2T in the supernatant liberated during the process on a 1:1 molar basis **(Scheme 2.4)**. Thus, after the end of the 14 hours coupling period, the tubes were centrifuged for 10 minutes at 13.2 RCF, the top 0.3 mL layer of the supernatant was extracted (out of the originally introduced 0.5 mL volume), and the supernatant was further centrifuged for another 10 minutes at the same speed of rotation. Subsequently, the absorbance of a 100 μL of the treated supernatant and blank solution consisting of DFOB-SPDP in BBS-DMSO (centrifuged for 24 minutes) were measured in a Victor^3 plate reader at 340 nm. In order to account for any possible interference on the absorbance caused by unintentionally extracted beads in the supernatant, blank solutions were reintroduced in the tubes and a procedure similar to the one denoted in the previous section was achieved. It is worth noting that in most cases, the recorded absorbance was higher than 1, requiring a 10-fold dilution of the samples with borrate-buffered saline. However, despite diluting the samples, this method did yield inconsistent measurements, especially when operating under high SPDP and DFOB amounts.

2.3.8 Fe(III)-Citrate Solution Preparation under Physiological pH

Fe(III)-citrate is a dominant species of non-transferrin-bound iron (NTBI) (May et al., 1977), which is the main target for chelation in the plasma of iron overload patients (Evans et al., 2008;

Bellanti et al., 2016). In this study, Fe(III)-citrate solutions were prepared to a total final volume of 40 mL at a physiological pH level of 7.4. The preparation method employed in this study had similarities, but was not identical, to the ones reported by Evans et al. (2008), Ito et al. (2011) and Ito et al. (2015).

A 17.9 mM stock solution of acidic Fe(III) was prepared by dissolving Fe(III) chloride in aqueous 1% HCL thus avoiding the precipitation of Fe(III). Moreover, a 0.67 M stock solution of citric acid solution was also prepared by dissolving citric acid in HPLC-grade water. The pH of the citrate solution was raised to pH = 8 (± 0.05) to avoid a significant change of pH when the buffer is added. Finally, a HEPES buffered saline solution (2 mM HEPES, 150 mM NaCL, pH = 7.4) was also prepared to maintain a physiological pH level of 7.4 for the Fe(III)-citrate solution. The prepared stock solutions were stored at 4˚ C in the dark when not in use. After preparing the stock solutions, a convenient volume of citrate solution was added to acidic Fe(III) yielding the desired Fe(III) concentration and citrate: iron ratio. Subsequently, a portion of the HEPES buffer was added. After adjusting the pH of the Fe(III)-citrate-buffer mixture to 7.4 (± 0.05), the remaining amount of the HEPES buffer was added to a total final volume of 40 mL. The prepared Fe(III)-citrate solutions were directly introduced to the beads after preparation.

2.3.9 Spectrophotometric Measurement of Total Iron in Fe(III)-Citrate Solutions

Iron levels in Fe(III)-citrate-HEPES samples were detected by QuantiChrom™ Iron Assay Kit using a Victor^3 plate reader. This method consists of adding 200 µL of the kit's working reagents to 50 µL of iron samples in 96-well plates. Fe(III) is subsequently reduced to Fe(II) and the chromogen develops a blue colored complex with Fe(II) that is detectable at 510 nm - 630 nm

(peak absorbance at 590 nm, we used 595 nm) after incubation for 40 minutes at room temperature. The assay's linear detection range is 4.8 μM to 179 μM of iron, which covers the experimentally tested concentrations in this work. Finally, the suitability and repeatability of the assay in measuring iron in Fe(III)-citrate-HEPES solutions were tested and confirmed and the required standard curves were developed (with 15 μM iron increments).

Moreover, in order to extract the 50 μL Fe(III) samples after a given reaction time, the microcentrifuge tubes were centrifuged for 5 minutes at 13.2 RCF. Subsequently, the extracted portion of the supernatant was centrifuged for another 10 minutes, before finally transferring the required iron volume to the 96-well plate for testing.

A secondary method of determining iron concentrations consisted of adding 10 μL of a DFOB-HEPES mixture to 100 μL of Fe(III)-citrate sample. The DFOB amount added corresponded to at least a DFOB: Fe(III) ratio of 10:1, which ensured a near total conversion of iron to ferrioxamine (FO) (stoichiometric ratio = 1:1). Subsequently, the concentration of FO was measured as described in Section 2.3.15, which in turn reflected the iron content of the solution. It is worth noting that the blank for this method was prepared by adding 10 μL of DFOB-free HEPES to100 μL of Fe(III)-citrate samples, while the required standard curves for FO were developed using Fe(III)-citrate solutions with known concentrations (with 15 μM iron increments).

2.3.10 Preparation of SH-activated Beads (Control)

After preparing the chelator-functionalized beads, the iron chelation levels under DFOB-activated beads were compared to those observed under a control consisting of SH-activated beads that were not coupled to the chelator **(scheme 2.5).** This experiment was performed in

order to assess the role of both the DFOB and the existing surface species on the level of iron chelation.

DFOB-functionalized beads were prepared by coupling PDS-DFOB molecules to SH-activated beads **(Scheme 2.4)**. Thus, SH-activated beads with no conjugated DFOB and having similar SH coverage to the DFOB-functionalized microspheres were used as controls. These control beads served to illustrate the role of immobilized DFOB on Fe(III) chelation. The DFOB-functionalized beads were prepared using a DFOB: SPDP molar ratio of 5:1 and a PDS: Surface SH molar ratio of 60:1. Both the DFOB-activated and control beads had a close percentage of SH coverage. Subsequently, 1 mL of 75 μM iron solutions were introduced in tubes containing either DFOB-functionalized or SH-activated beads. After 180 minutes of end-over-end rotation at room temperature, the remaining iron concentrations in the supernatants were recorded. **(Scheme 2.5)** shows the difference between DFOB-functionalized and the SH-activated beads.

2.3.11 Investigating DFOB Surface Adsorption on Latex Beads

This work aims at covalently binding DFOB to the latex beads via disulfide bonds **(Scheme 2.4)** while avoiding the adsorption of that siderophore on the surface. Consequently, two sets of experiments have been performed. In the first one, SH-activated beads were coupled for 14 hours to either PDS-DFOB in BBS (DFOB: SPDP = 15:1, PDS: Surface SH = 30:1, [DFOB] = 24 mg/mL) or DFOB in BBS having twice the DFOB concentration of the PDS-DFO solution (no SPDP, [DFOB] = 48 mg/mL). The concentration of the chelator in BBS (48 mg/mL) was chosen since it is close to the solubility limit of DFOB in water (50 mg/mL). After the coupling phase, 1

mL of 75 μM iron solutions were introduced in the containing tubes under end-over-end mixing, and the remaining iron concentrations were measured after 90 minutes

In the second experiment, SH-activated beads were coupled for 14 hours to either PDS-DFO in BBS (DFOB: SPDP = 5:1, PDS: Surface SH = 60:1, [DFOB] = 13 mg/mL) or DFOB in BBS having the same DFOB concentration as the PDS-DFO solution (no SPDP, [DFOB] = 13 mg/mL). In this experiment the concentrations of the remaining Fe(III) were measured after 180 minutes.

2.3.12 Effects of DFOB: SPDP Molar Ratios in the Coupling Solution on PDS-DFOB immobilization and Fe(III) Chelation

In this work, no attempts were made to separate the created PDS-DFOB molecules from the unreacted SPDP. However, a high molar ratio of DFOB: SPDP was used to minimize the amount of unreacted SPDP, thus limiting its competition with PDS-DFOB on binding to the SH-surface. Consequently, it was important to understand the effects of varying the DFOB: SPDP molar ratios on the formation and immobilization of PDS-DFOB and the resulting Fe(III) uptake. For that reason, latex beads having similar SH coverage were coupled to three different PDS-DFOB solutions. These PDS-DFOB coupling solutions were prepared using a varying DFOB: SPDP molar ratio of 5:1, 10:1 to 15:1 under the same SPDP concentration (corresponding to 30:1 PDS: Surface SH molar ratio). Finally, 1 mL of 75 μM iron solutions were introduced to the DFOB-functionalized beads, and the remaining iron concentration in each tube was measured after 30 minutes of end-over-end rotation at room temperature.

2.3.13 Effects of PDS: Surface SH Molar Ratios in the Coupling Solution on PDS-DFOB immobilization and Fe(III) Chelation

The effects of varying the PDS: Surface SH molar ratio on the immobilization of PDS-DFOB were studied by coupling SH-activated beads having similar SH coverage to different PDS-DFOB solutions. These coupling solutions were prepared using a constant concentration of DFOB of 23 mM or a constant DFOB: SPDP molar ratio of 5, while varying the SPDP amounts to have PDS: Surface SH molar ratios of 10:1, 30:1 and 60:1. Iron levels were also measured as described in the previous section.

It is worth noting that by fixing the DFOB concentration at 23 mM and varying the SPDP amounts, the resulting DFOB: SPDP ratios were 30:1, 10:1 and 5:1 for the solutions having 10:1, 30:1 and 60:1 PDS: Surface SH ratios, respectively.

2.3.14 Ferrioxamine (FO) Detachment from Latex Beads and Support Regeneration

The chelation of Fe(III) by the DFOB-activated beads led to the formation of a visible brick-colored ferrioxamine (FO) compound on the microspheres' surface **(Figure 2.3)**. Each FO molecule was linked to the latex surface via one disulfide bond**.** Consequently, in order to determine the quantity of FO existing on the particles, and to regenerate the latex beads via reintroducing SH sites in the place of the FO occupied ones, the FO molecules had to be detached from the surface by reducing the existing disulfide bonds with DTT. **Scheme 2.6** shows the cleaving of FO and the resulting regeneration of the support.

Experimentally, upon the conclusion of mixing Fe(III)-citrate with the DFOB-functionalized beads and the ensuing formation of FO, the containing tubes were centrifuged for 5 minutes at 13.2 RCF and the iron solution was thoroughly decanted. Subsequently, the beads were washed with 1 mL of HPLC-grade water under gentle vortexing. Later on, the particles were centrifuged for another 5 minutes and the water was extracted. After this step, a 1 mL volume of 50 mM DTT solution prepared in HEPES buffer (2 mM HEPES, 150 mM NaCL, pH = 7.5) was added to the beads, followed by an end-over-end mixing for 1 hour at room temperature. It is worth noting that PBS was avoided given its reported ability to precipitate/bind polyvalent cations (Biological Buffer Applichem, 2008; Ferreira et al., 2015). At the end of the mixing period, the tubes were centrifuged for 10 minutes and the FO containing DTT-HEPES solution was decanted to measure its FO content. The spectrophotometric measurement of ferrioxamine in this solution is detailed in Section 2.3.15. Finally, the tubes were washed twice with HEPES buffer (2 mM HEPES, 150 mM NaCL, pH = 7.5) before being recoupled to a fresh batch of PDS-DFO (recoupling procedure detailed in Section 2.3.18).

2.3.15 Spectrophotometric Measurement of Ferrioxamine (FO)

Ferrioxamine (FO) is formed when Fe(III) is bound to DFOB on a 1:1 molar basis. Previous studies have reported that FO absorbs light most strongly in the range of 425 - 429 nm; λ_{max} = 425 nm, $\boldsymbol{\varepsilon}_{425}$ = 2700 M^{-} cm^{-} (Faller and Nick, 1994); λ_{max} = 429 nm, $\boldsymbol{\varepsilon}_{425}$ = 2280 M^{-} cm^{-} (Rose and Waite, 2003). Moreover, Faller and Nick (1994) reported that the Fe-citrate does not absorb light significantly at wavelengths higher than 420 nm, while Ito et al. (2015) presented the absorbance spectra of FO which showed that the absorbance of that compound remains high at a wavelength of 450 nm. In this study, FO compounds were prepared by adding a 0.006 M of

DFOB solution in HEPES, corresponding to a DFOB: Fe(III) molar ratio of 10:1, to Fe(III)-citrate-HEPES solution under at pH of 7.4. The addition of the DFOB-HEPES raised the total volume to 40 mL. This large excess of DFOB ensured a near complete binding of Fe(III) ions. Subsequently, samples of this FO containing solution were introduced in 96-well plates and the absorbance was monitored by a Victor^3 plate reader, with the original Fe(III)-citrate solution serving as the blank. Subsequently, we measured the absorbance of FO at 450 nm and determined the molar extinction coefficient to be 2403.5 M^{-} cm^{-} ($\boldsymbol{\varepsilon}_{450}$ = 2403.5 M^{-} cm^{-}), which is close to the previously reported values.

In order to monitor the FO formation in Fe(III)-citrate solutions (as required in Chapter 3 - Section 3.4.4), a known volume of the FO solution was simply introduced in 96-well plates, while the original iron solution served as the blank.

On the other hand, determining the FO amount detached from the microspheres' surface via DTT was determined according to the following method; the FO-containing DTT-HEPES supernatant decanted from the tubes was centrifuged for 10 minutes at 13.2 RCF. Subsequently, 100 μL of this solution was transferred to 96-well plates and the absorbance of FO was measured at 450 nm. The blank consisted of 50 mM DTT in HEPES (2 mM HEPES, 150 mM NaCL, pH = 7.5). The final actual FO concentration was determined after taking into account the reduction percentage of disulfide bonds by DTT in HEPES (found to be 97% in a Section 2.4.5). Consequently, the following Equation (2.2) can be applied:

$$[FO]_{actual} = \frac{[FO]measured}{0.97} \quad (2.2)$$

2.3.16 Dithiothreitol (DTT) Reduction of Disulfide Bonds in PBS and HEPES Buffers

In this work, DTT was used for two main purposes; the first was to reduce the disulfide bonds of the PDS groups attached to the beads' surface, thus leading to the SH-activation of the beads **(Scheme 2.2)**. As denoted in a previous section, this step consisted of adding 1 mL of 50 mM DTT-PBS (20 mM sodium phosphate, 150 mM NaCl, pH=7.5) in the microtubes and gently mixing for 1 hour at room temperature. The second use of DTT aimed at breaking the disulfide bonds binding the ferrioxamine (FO) to the latex beads, thus enabling the measurement of FO and regenerating the surface **(Scheme 2.6)**. In this process, a 1 mL of 50 mM DTT-HEPES (2 mM HEPES, 150 mM NaCL, pH = 7.5) was employed.

Since the concentration of N-hydroxysuccinimide (NHS) reporter molecules liberated after activating the surface with PDS were not measured **(Scheme 2.1)**, it was important to approximate the percentage of disulfide bonds reduced by 50 mM DTT in PBS relative to the initial amount of PDS groups. By measuring the concentration of SH groups created by DTT, we can gain a better insight on the amount of initial PDS group existing on the beads, which will prove helpful in explaining the findings reported in the beads regeneration study (Section 2.4.7). For this purpose, 40 mM of SPDP in DMSO was added to PBS (20 mM sodium phosphate, 150 mM NaCl, pH=7.5) in an amount that corresponded to 77% and 15% of the initial NH_2 surface sites (9.847×10^{-5} M and 1.918×10^{-5} M of SPDP on 1 mL supernatant basis, respectively). Subsequently, DTT was added to the solution at a concentration of 50 mM. After an end-over-end mixing for 1 hour at room temperature, the concentration of the released P2T was measured at 340 nm, allowing us to calculate the percentage of reduced SPDP relative to its initial concentration.

Moreover, since DTT was used to release the ferrioxamine (FO) formed on the beads' surface, it was critical to have a good estimate of the percentage of FO released by the DTT relative to its actual amount attached to the surface. Consequently, 40 mM of SPDP in DMSO was added to HEPES (2 mM HEPES, 150 mM NaCL, pH = 7.5) in an amount that corresponded to 25% of the initial NH_2 surface sites (3.197×10^{-5} M SPDP on 1 mL supernatant basis). This number was chosen since it is close to the commonly calculated values of FO coverage on the surface. After adding 50 mM DTT to the SPDP in HEPES and allowing for a 1 hour reaction time at room temperature, we were able to compare the value of reduced SPDP relative to its initial concentration. Finally, it is worth noting that the blank used in both studies consisted of SPDP-DTT in PBS or HEPES which was also measured after 1 hour.

2.3.17 Dithiothreitol (DTT) Effect on Ferrioxamine (FO) Concentrations

Since DTT will be used to detach the ferrioxamine (FO) formed on the surface of the beads allowing for its spectrophotometric measurement, and given that the concentration of DTT at 50 mM is significantly higher than that of FO at around 37.5 μM, it was critical to investigate any effects of DTT on the stability of FO, which can possibly jeopardize the above proposed FO assay. The importance of this examination was further enhanced by the findings of previous studies (Netto and Stadtman, 1996; Fontecave et al., 1990) which showed that DTT oxidation is catalyzed by Fe(III), leading to its reduction to Fe(II). Although Fe(III) is firmly bound to the FO molecule ($K_{Fe(III)-DFOB} = 4 \times 10^{30}$), its possible reduction to Fe(II) can decrease the binding of the DFO to the metal ($K_{Fe(II)-DFOB} = 1.6 \times 10^{7}$) (Manning et al., 2009).

Consequently, we prepared a 37.5 μM Fe(III) in HEPES (2 mM HEPES, 150 mM NaCL, pH = 7.4) (as described in Section 2.3.8). However, no citrate was added to this solution since the detachment of FO from the beads occurs in a citrate-free environment (in addition to the fact that citrate can bind iron, thus possibly interfering with the experiment). Subsequently, a 0.006 M DFOB in HEPES solution was added to the iron mixture, yielding a DFOB: Fe(III) ratio of 1:1 and raising the total volume of the solution to 40 mL. After the produced FO reached a constant level, DTT was added to the solution at a concentration of 50 mM. Additionally, in order to assess the role of citrate in the medium, the same experiment was repeated with 100:1 citrate: iron addition to the initial iron solution. Finally, the change of FO absorbance immediately after adding DTT to both solutions was monitored at 450 nm for 3 hours. It is worth mentioning that 300 μL samples were introduced in the 96-well plates in order to minimize the effects of sample evaporation on the measurements.

2.3.18 Recoating Beads with Pyridyldithiol-Activated Desferrioxamine (PDS-DFOB) on Regenerated Latex Beads

This work aims at reversibly and covalently binding DFOB to the polystyrene surface via cleavable disulfide bonds (S-S). The main advantage of this approach is that it can allow the reuse of the polymeric thiolated support to immobilize fresh batches of molecules and enzymes, which can prove particularly advantageous in both large-scale industrial processes, and in small-scale microreactors and biosensors (Mohamad et al., 2015; Fraas and Franzreb, 2017; Carlsson et al., 1975).

Following the introduction of 1 mL Fe(III)-citrate on fresh DFOB-activated beads, the iron remaining in the supernatant was measured after 180 minutes of mixing. The produced ferrioxamine (FO) was cleaved from the surface by introducing 50 mM of DTT in HEPES to break the disulfide bonds (as described in Section 2.3.14). This allowed both the measurement of the surface FO amount and the regeneration of the surface by recreating thiol sites in-place of the cleaved FO **(Scheme 2.6)**. Later on, the regenerated beads were washed twice with HEPES buffer (2 mM HEPES, 150 mM NaCL, pH = 7.5), before being put in contact for 14 hours with a fresh batch of PDS-DFOB coupling solution (coupling solution preparation detailed in Section 2.3.4). Finally a second solution of iron was introduced to the regenerated DFOB-activated beads **(Scheme 2.7)**. It is worth noting that special care was given to avoid the loss of beads throughout the process.

The prepared first and second coupling solutions had a DFOB: SPDP molar ratio of 5:1 and a PDS: Surface SH ratio of 60:1, while the initial SH coverage of the beads was approximately 25%. Additionally, the ability of the regenerated beads to chelate iron was tested under 4 different iron solutions having a 100:1 citrate: iron ratio, and Fe(III) concentrations of 37.5, 75, 150 and 300 μM. A volume of 1 mL of iron-citrate was introduced to the beads in both runs, while the beads were mixed under end-over end rotation at room temperature and the metal concentration remaining was measured after 180 minutes.

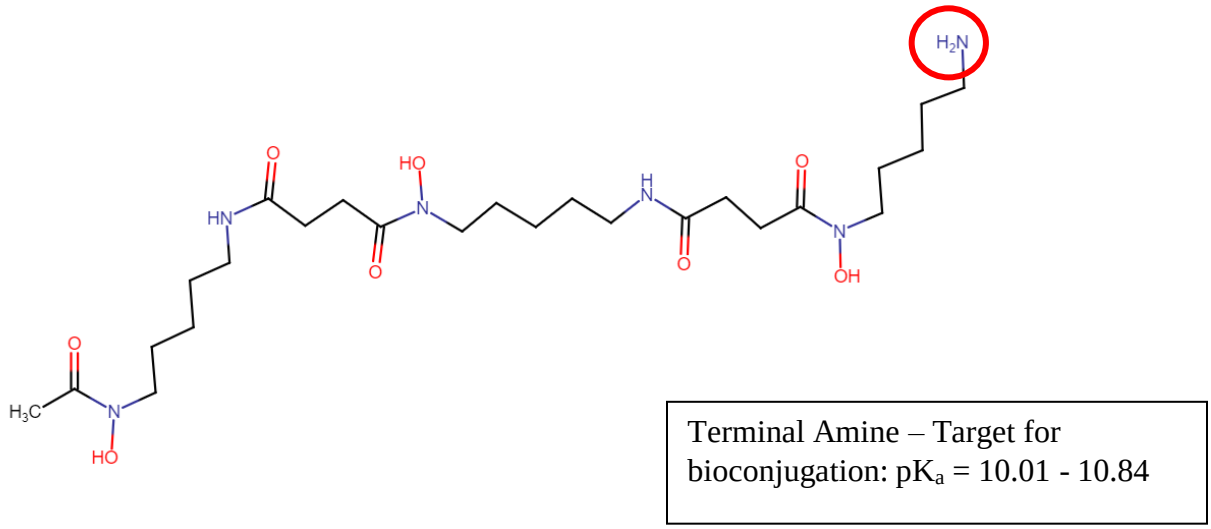

Figure 2.1 Desferrioxamine B molecule with terminal Amine and pK_a values

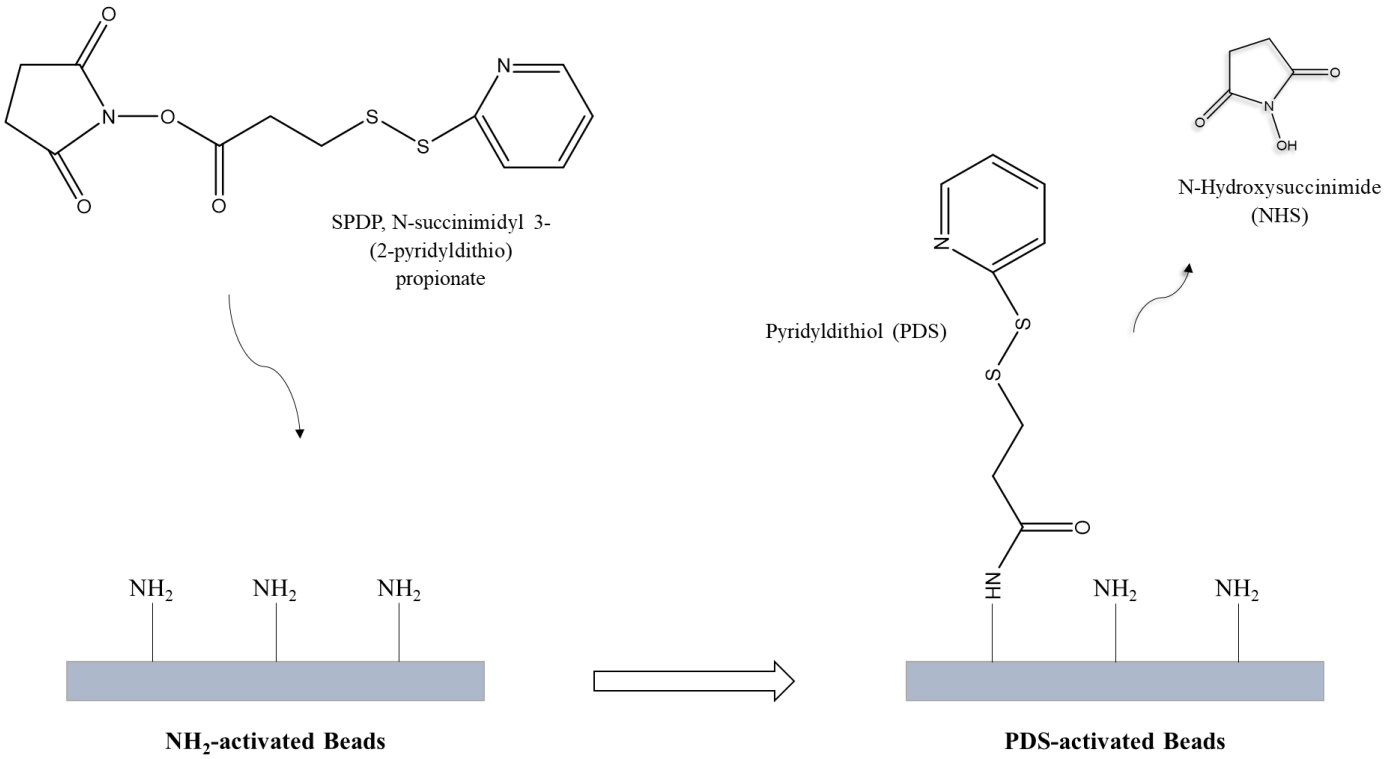

Scheme 2.1 Pyridyldithiol (-PDS) activation of Polystyrene beads

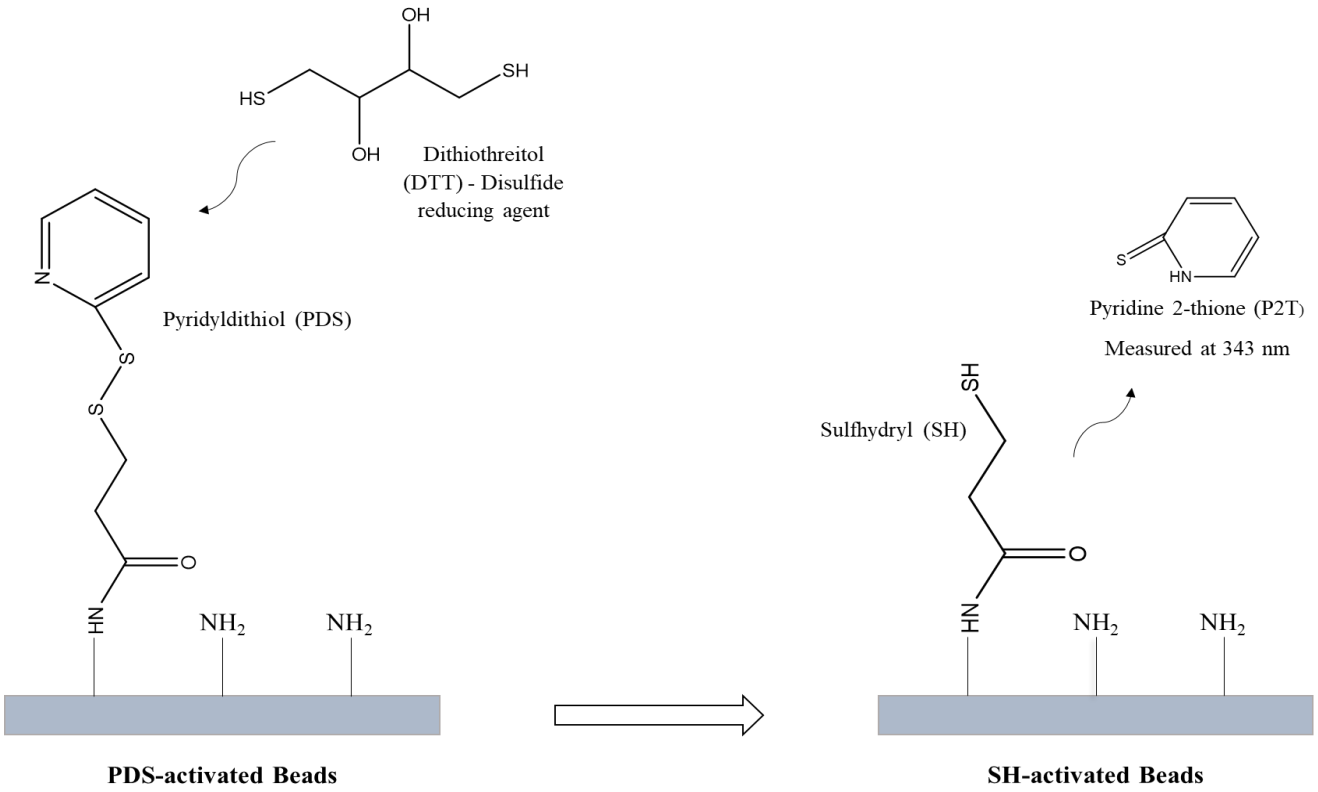

Scheme 2.2 Sulfhydryl (-SH) activation of Polystyrene beads

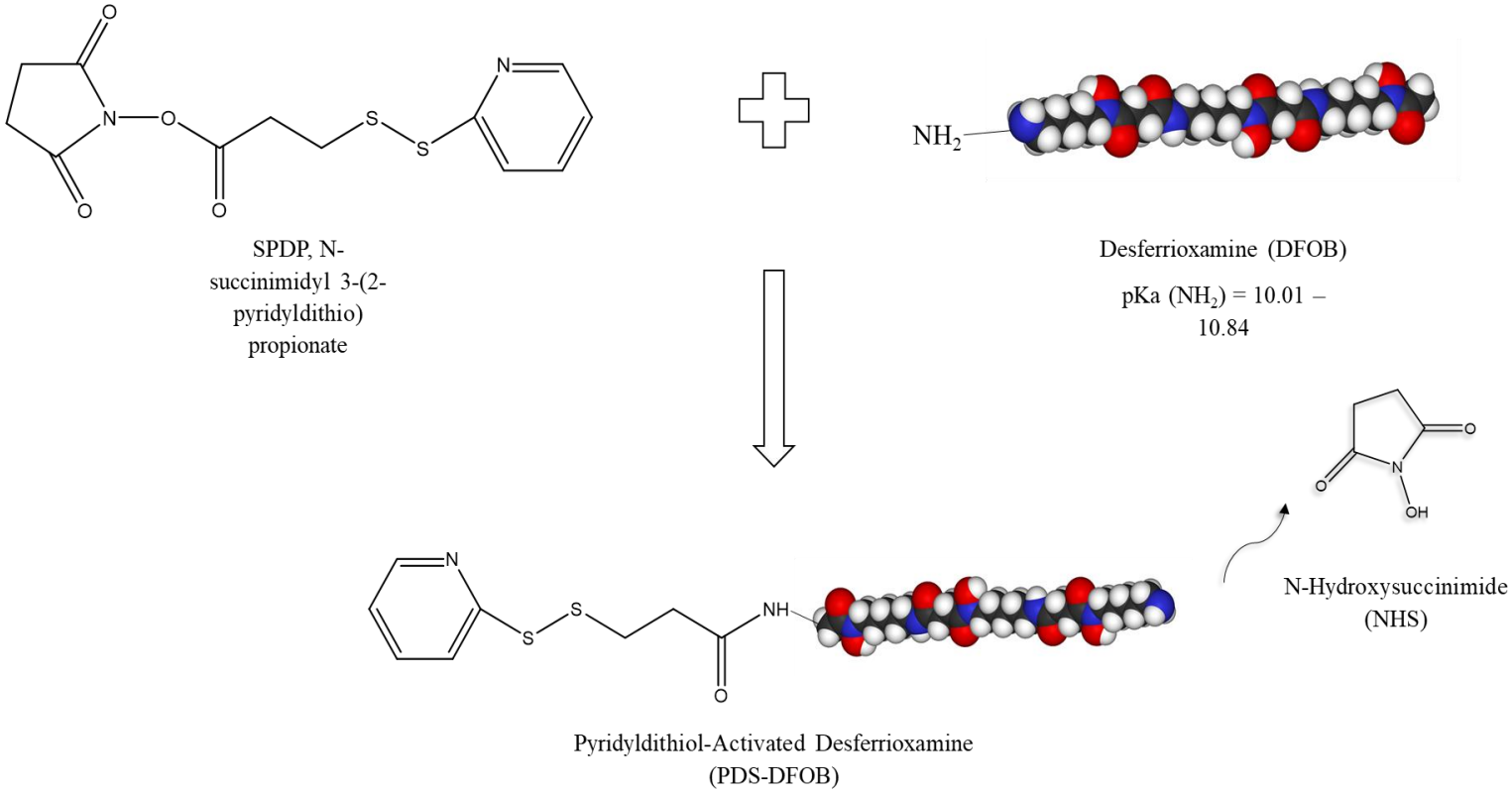

Scheme 2.3 Pyridyldithio (-PDS) activation of Desferrioxamine B in coupling solution

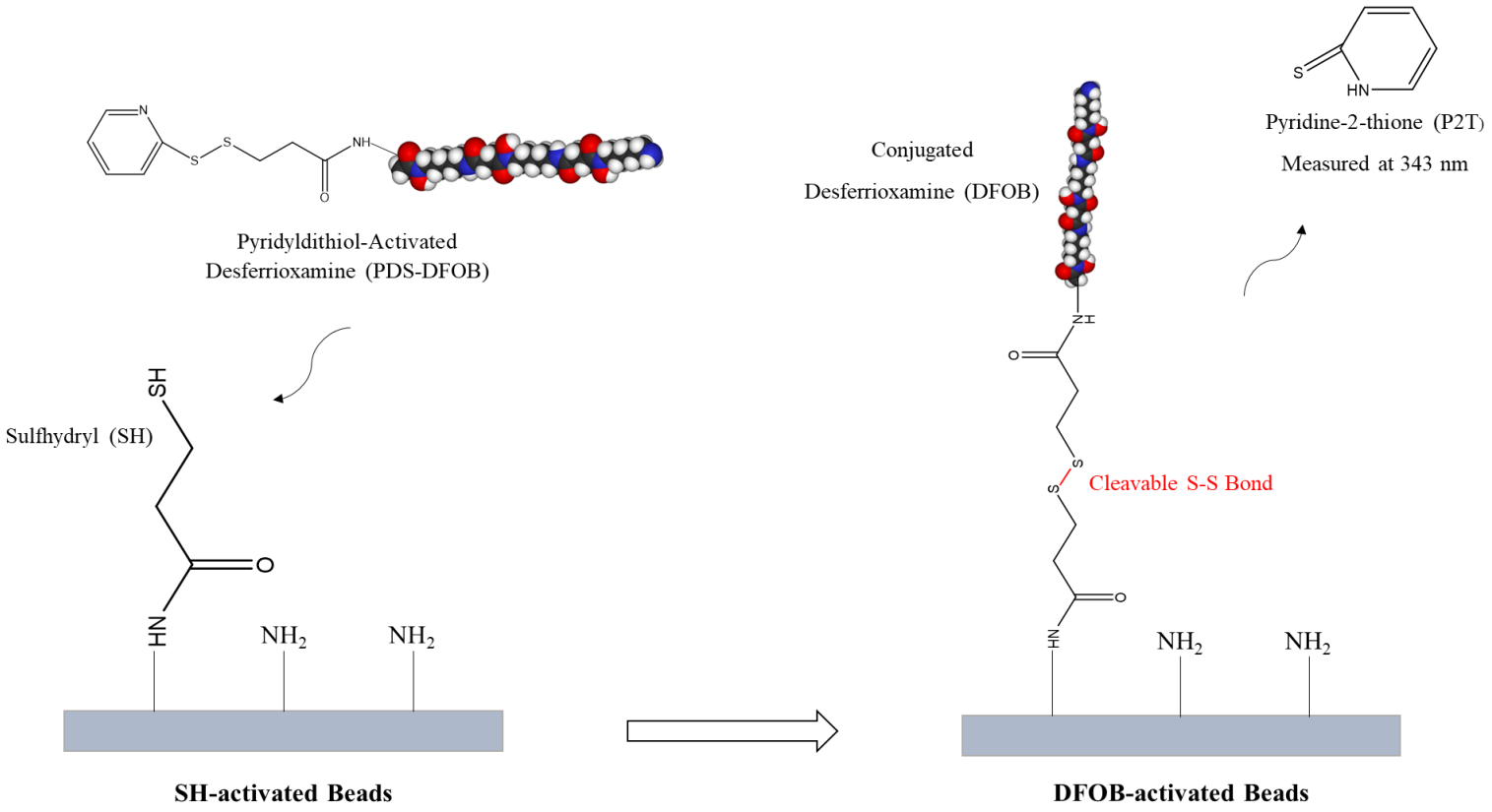

Scheme 2.4 Immobilization of PDS-DFOB on SH-activated Polystyrene beads

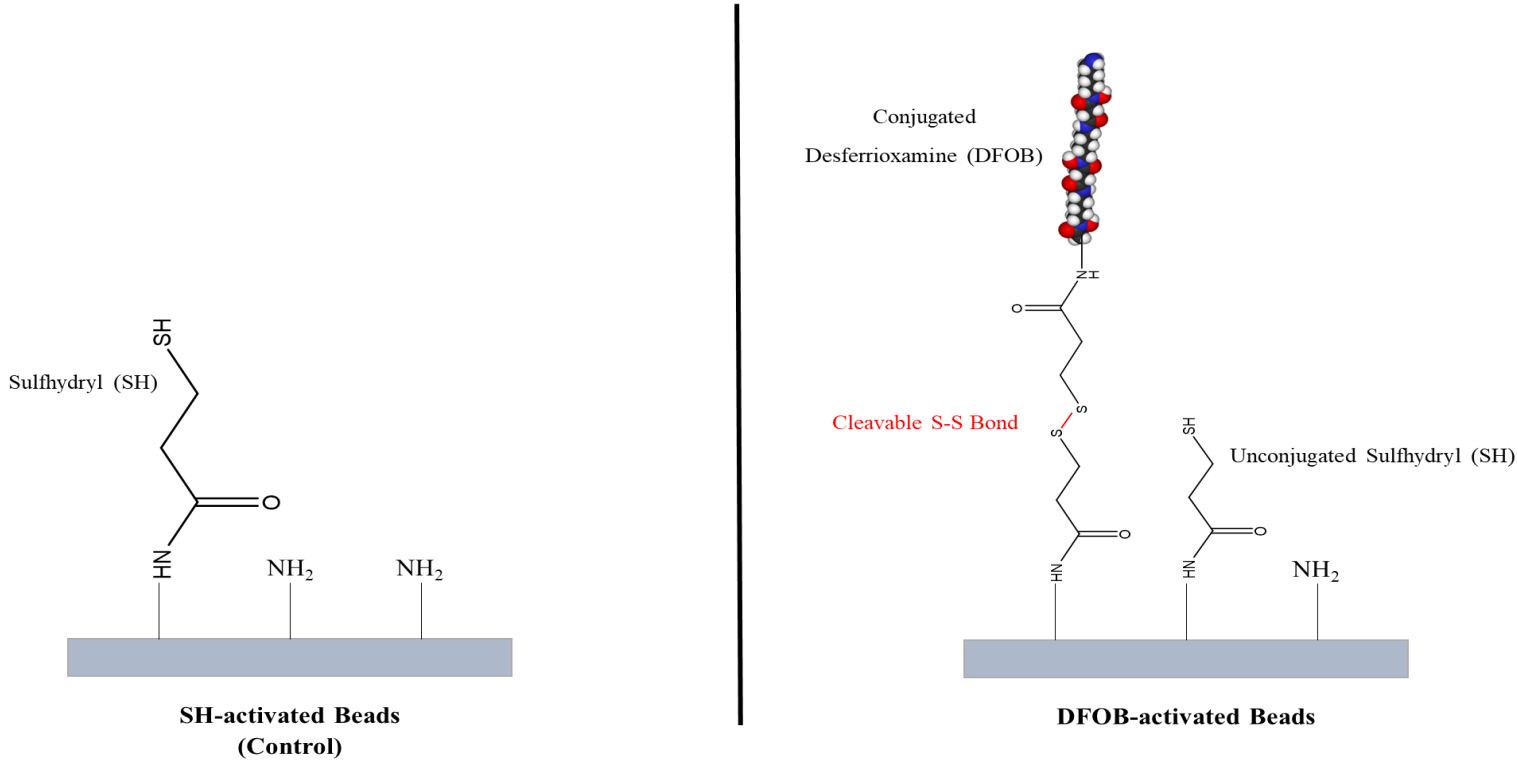

Scheme 2.5 Difference between SH-activated beads (control) and DFOB-activated beads

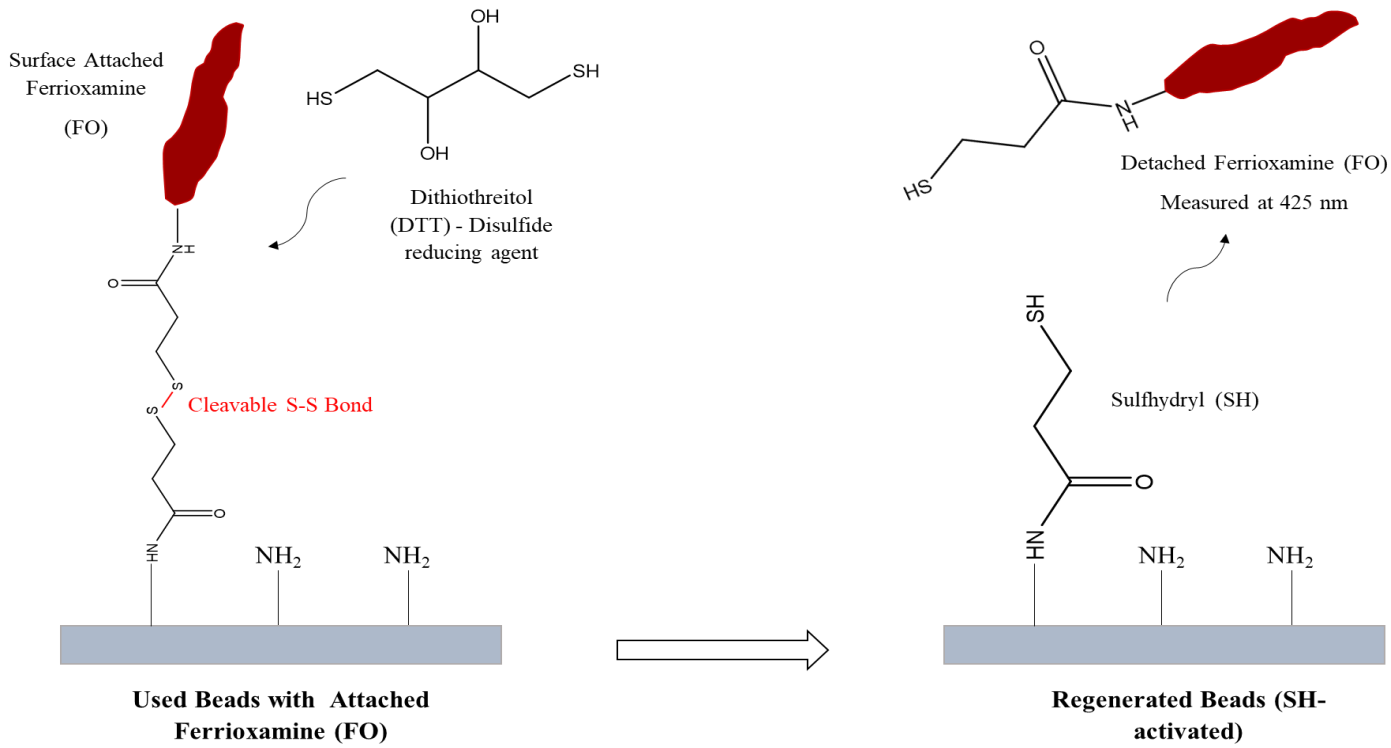

Scheme 2.6 Disulfide bonds cleavage to release Ferrioxamine and regenerate the beads by recreation of (-SH) sites

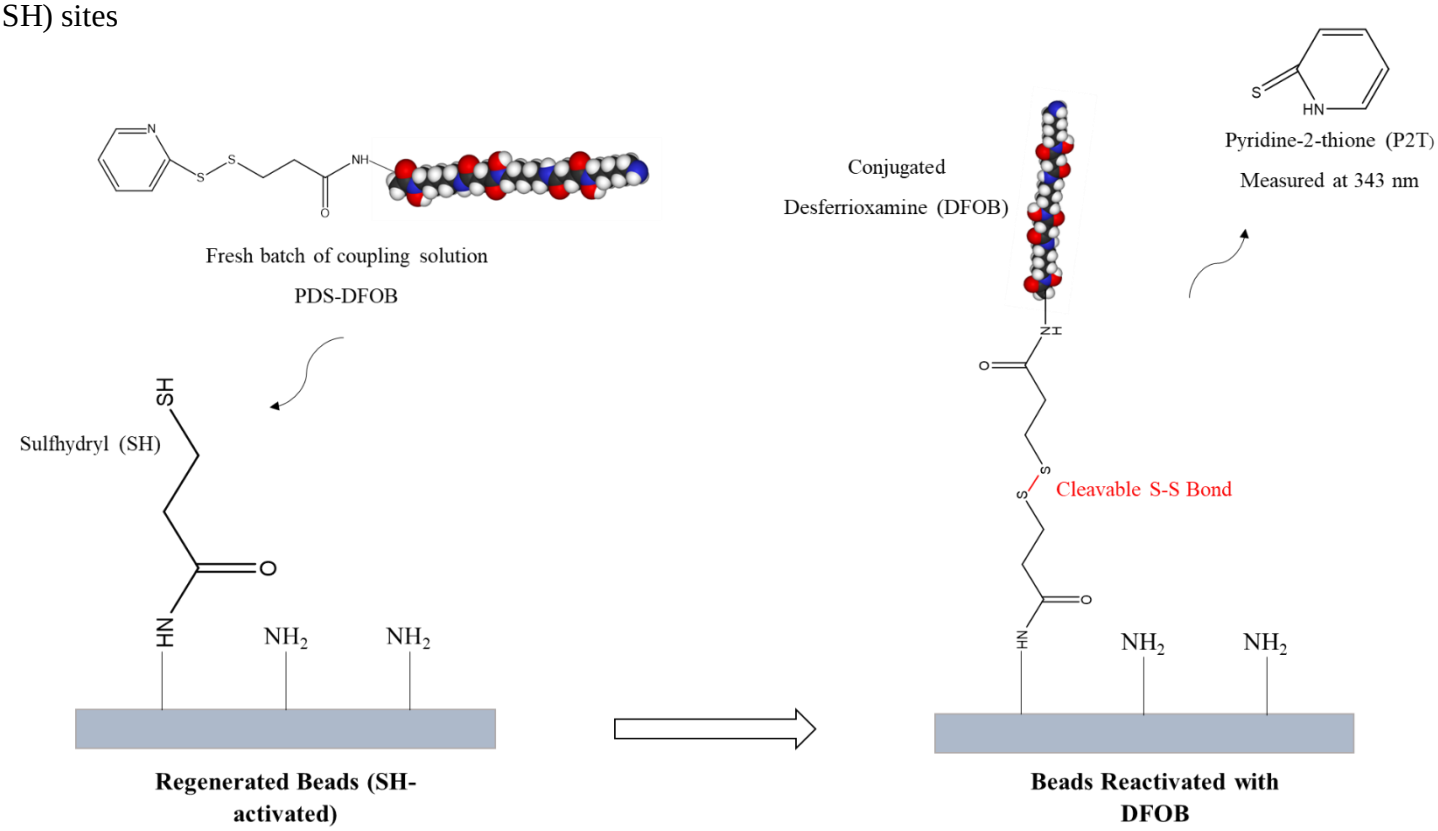

Scheme 2.7 Coupling of fresh PDS-DFOB on regenerated beads

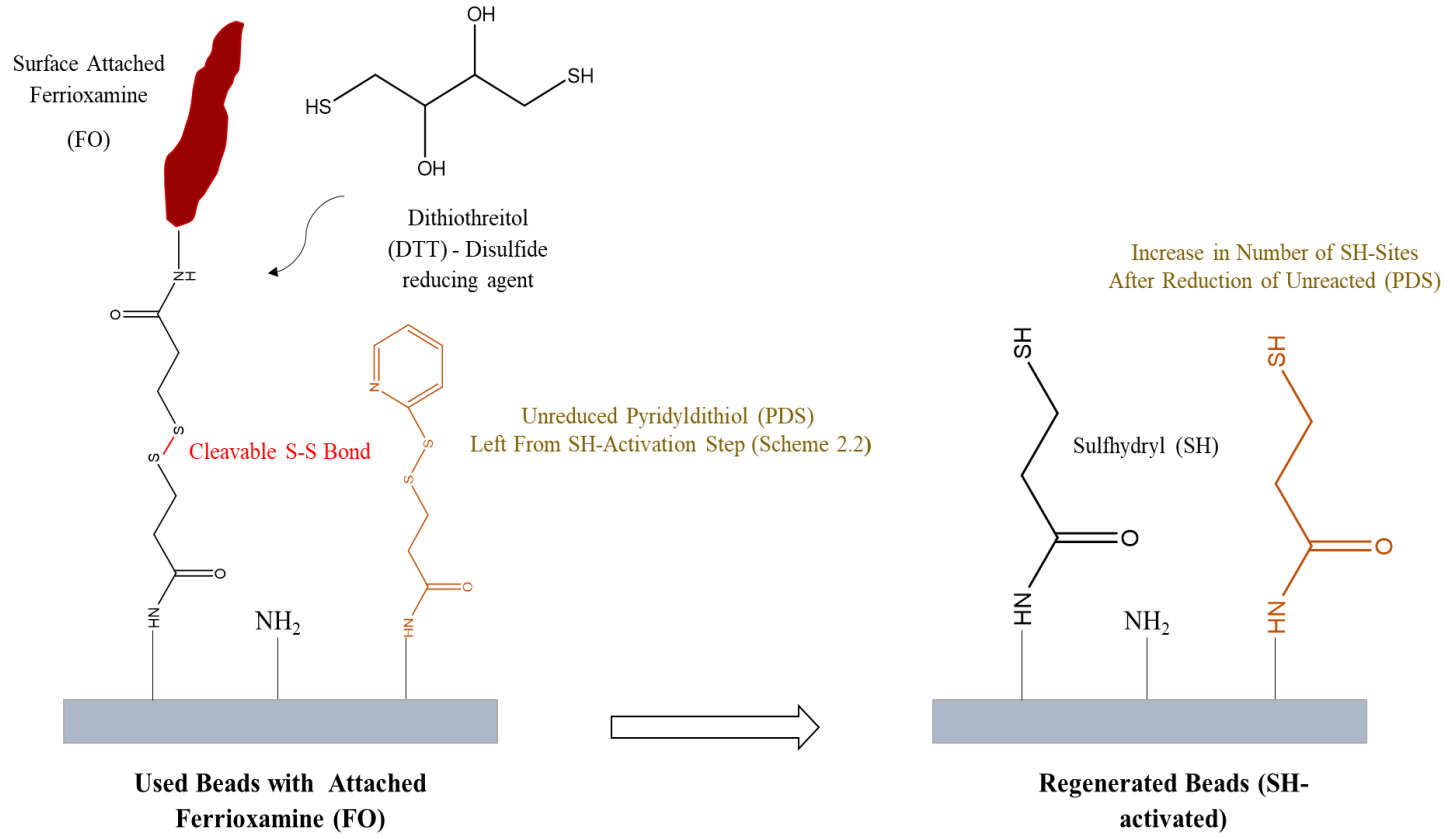

Scheme 2.8 Reduction of unreacted (-PDS) leading to creation of extra (-SH) sites

Step 1: Set DFOB: SPDP molar ratio

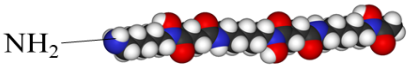

Desferrioxamine (DFOB)

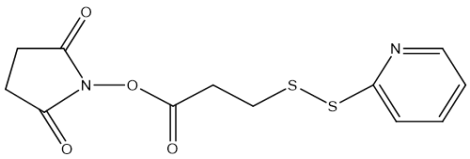

SPDP, N-succinimidyl 3-(2-pyridyldithio) propionate

Step 2: Set PDS: Surface (-SH) molar ratio

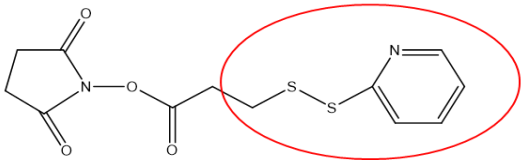

SPDP, N-succinimidyl 3-(2-pyridyldithio) propionate

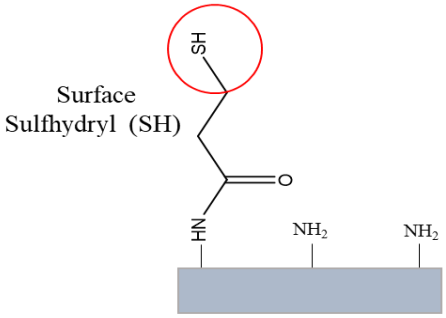

SH-activated Beads

Step 3: React DFOB and SPDP in coupling solution to create PDS-DFOB

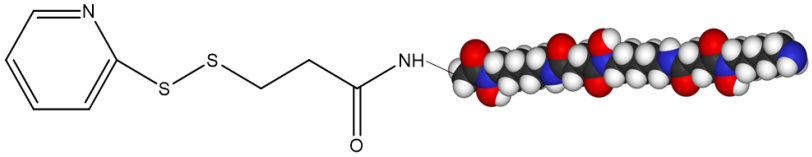

Pyridyldithiol-Activated Desferrioxamine (PDS-DFOB)

Step 4: Add coupling solution having PDS-DFOB to beads. NOTE: solution also contains unreacted SPDP and DFOB

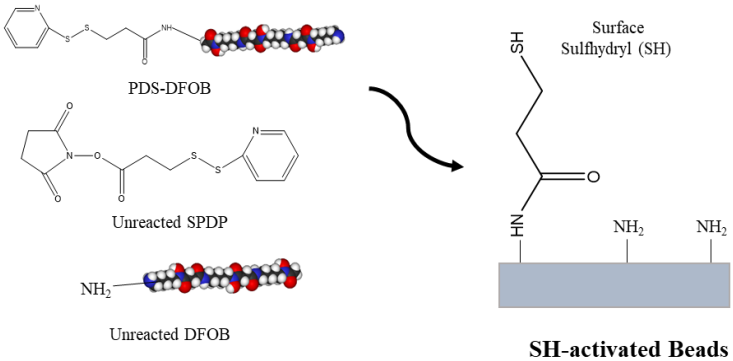

SH-activated Beads

Scheme 2.9 Steps of coupling PDS-DFOB to SH-activated beads

2.4 Results and Discussion

2.4.1 Comparison of Fe(III) Chelation by DFOB-Functionalized beads Vs Control Beads

Both DFOB-activated and SH-activated beads (control) had an approximate SH coverage value of 25%. As shown in **Figure 2.2**, after 180 minutes of introducing the 75 μM iron solutions to the DFOB-activated beads, the concentration of iron in the supernatant was reduced by 38 μM to a level of 37 μM. Conversely, the concentration of iron after the same contact time with the SH-activated beads (control) remained largely unchanged at 78 μM. Additionally, **Figure 2.3** shows the formation of the brick-colored ferrioxamine (FO) on the DFOB-activated particles and their absence on the control beads. Moreover, since the SH coverage on the particles was measured at approximately 25%, it can be deduced that none of the other species existing on the beads' surface (i.e. predominantly NH_2, with smaller amounts of unreduced PDS and COOH) contributed alongside the immobilized DFOB in chelating the iron from the citrate solution. These results strongly suggest that the DFOB molecules existing on the beads' surface were mainly responsible for the observed removal of iron.

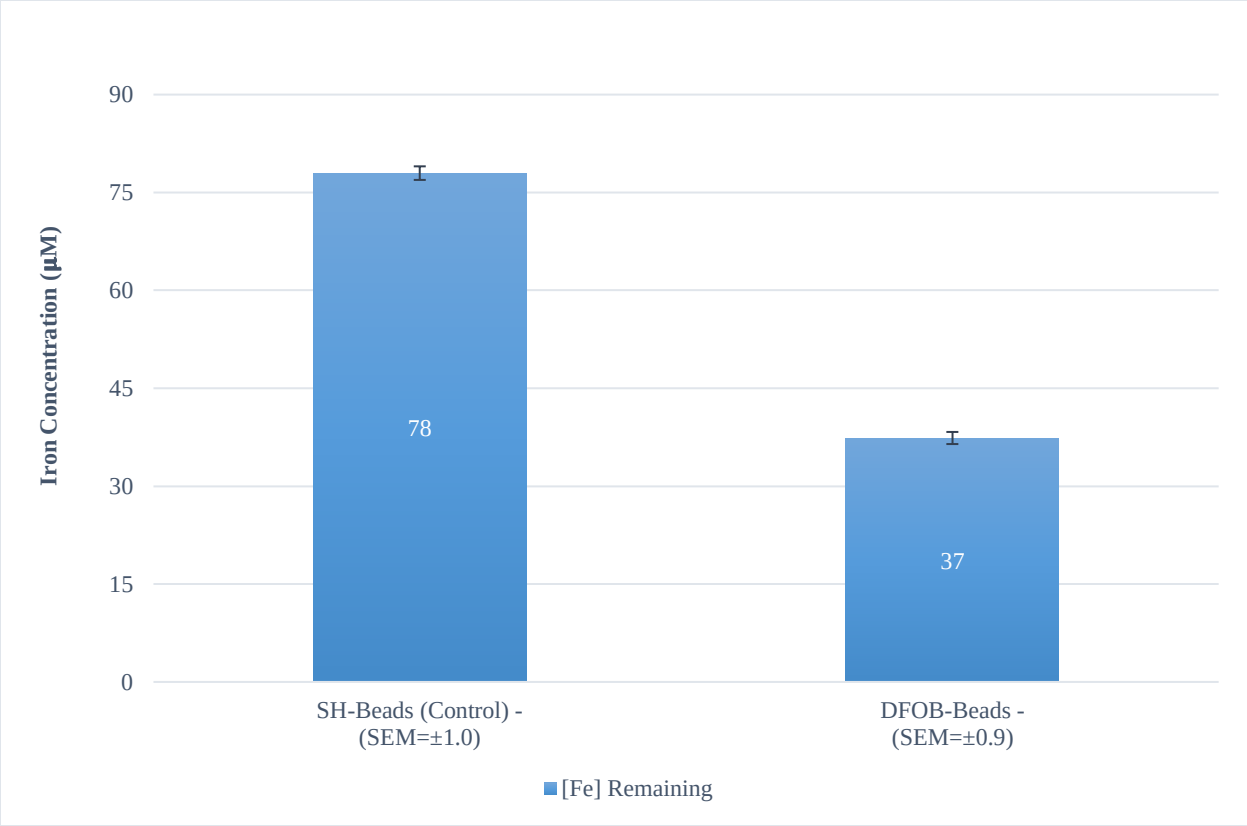

Figure 2.2 Remaining Fe(III) concentrations after 180 min of contact with SH-activated beads (control) and DFOB-activated beads at room temperature. Initial Fe(III) concentration=75 µM

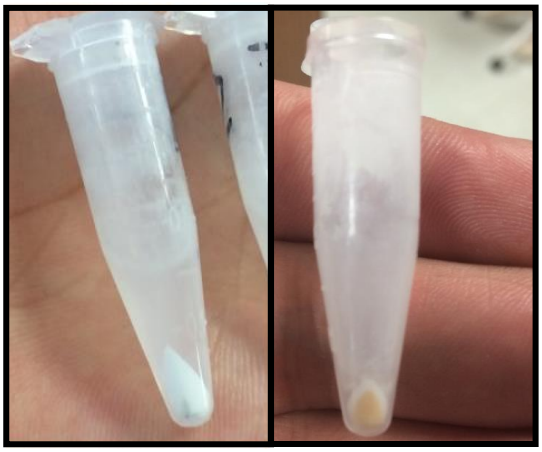

Figure 2.3 No ferrioxamine (brick color) on SH-activated beads (control-left) and its formation on DFOB-activated beads (right)

2.4.2 DFOB-Functionalized Beads: Covalent Bonding via Disulfide Bonds Vs Surface Adsorption

This work aims at covalently binding DFOB to the latex beads via cleavable disulfide bonds. After determining that DFOB siderophores are responsible for the Fe(III) chelation in the previous section, this part seeks to determine the nature of the DFOB binding to the latex beads and investigate whether the observed chelation of iron was due to the siderophore's covalent attachment to the beads, its adsorption on the surface, or both. For this reason, two sets of experiments have been performed. In the first one, SH-activated beads were coupled for 14 hours to PDS-DFOB molecules prepared by adding SPDP to DFOB (*Covalent solution*: Molar ratio of DFOB: SPDP = 15:1, PDS: Surface SH = 30:1, [DFOB] = 24 mg/mL). Other similar beads were put in contact for the same time period with a solution of DFOB without SPDP (*Adsorption solution*: no SPDP, [DFOB] = 48 mg/mL ≈ solubility limit of DFOB in water). As shown in **Figure 2.4**, after 90 minutes of introducing 1 mL of 75 μM iron solution in both tubes, a 37 μM reduction of the metal's concentration was observed under the beads coupled to PDS-DFOB, compared to only 6 μM for the beads mixed with DFOB. It is worth noting that this difference in iron uptake was achieved despite using twice the amount of chelator in the adsorption solution (48 mg/mL), which is also close to the compound's solubility limit in water (50 mg/mL).

In the second experiment, SH-activated beads were coupled for 14 hours to PDS-DFOB (*Covalent solution*: Molar ratio of DFOB: SPDP = 5:1, PDS: Surface SH = 60:1, [DFOB] = 13 mg/mL) or mixed with DFOB using no SPDP. The DFOB concentration was the same in both solutions (*Adsorption solution*: no SPDP, [DFOB] = 13 mg/mL). In this experiment the concentrations of the remaining Fe(III) were measured after 180 minutes. As can be seen in

Figure 2.5, 37 μM of iron remained in the iron solution under PDS-DFOB activated beads, while that value was substantially higher under the beads mixed with DFOB and no SPDP.

The results of both experiments indicate that the amount of Fe(III) chelated by the beads coupled to PDS-DFOB (covalent binding) was greater than under those mixed with DFOB only (no SPDP, surface adsorption). Consequently, two possible explanations can be put forward to justify the inability of the latter particles to chelate iron; the first is that DFOB did adsorb on the beads' surface, however this adsorption led to its deactivation. This possibility can be dismissed given the fact that different studies have shown that depositing DFOB on different surfaces did not lead to a significant decrease in its activity (CM Ambrus, 1987; Neubauer et al., 2000; Anthone S et al., 1995). Thus it can also be concluded that both the hydrophobic and electrostatic interactions were not important enough to induce a noticeable adsorption of DFOB on the polymeric support.

The second explanation, which is the most probable one, is that the adsorbed chelator remained active after its adsorption on the surface, however it did not deposit in sufficient amounts to induce a significant reduction of iron levels. Our findings that showed a slight increase of iron chelation levels under higher DFOB loading in the *adsorption solution* (**Figure 2.4 Vs 2.5**) further confirm this conclusion. Finally, it can be established that the active DFOB species responsible for the chelation of iron in our experiments are mostly covalently immobilized to the support via disulfide bonds and not the result of surface adsorption.

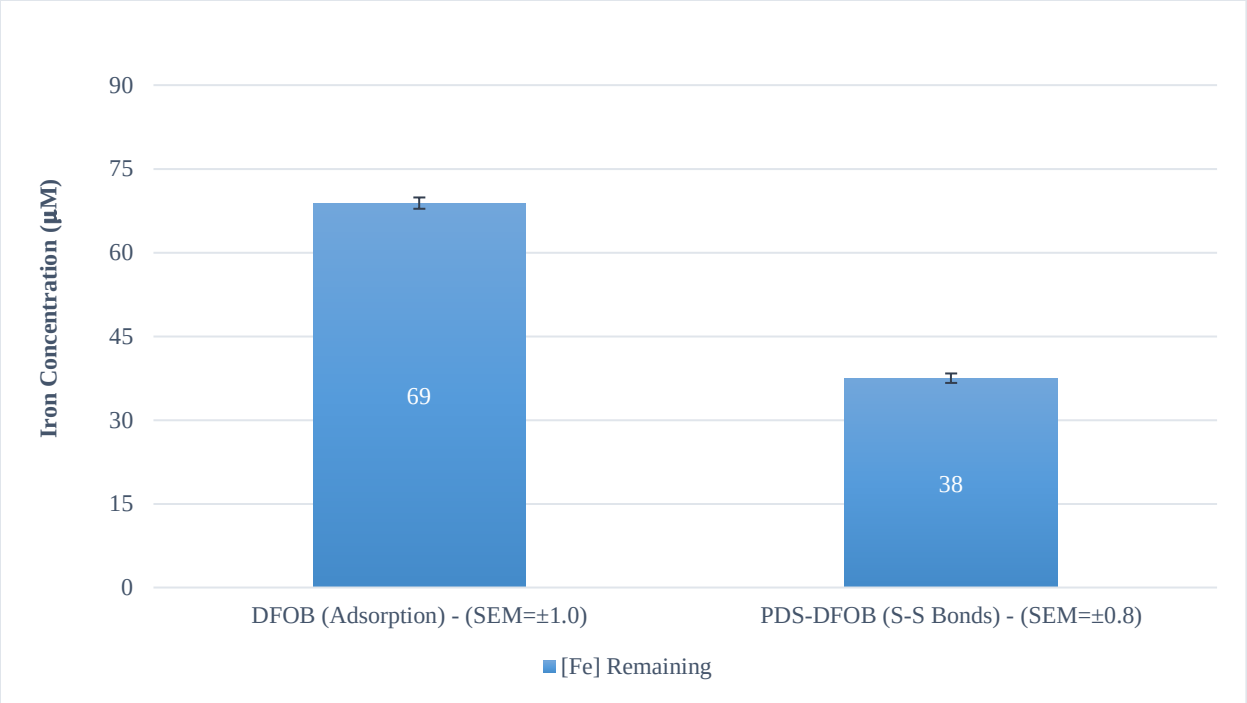

Figure 2.4 Iron concentrations after 90 min of contact with beads coupled to DFOB (no SPDP, [DFOB]=48 mg/mL) and PDS-DFOB (Molar ratio of DFOB: SPDP=15:1, PDS: Surface SH=30:1, [DFOB] = 24 mg/mL). Initial Fe(III) concentration=75 µM

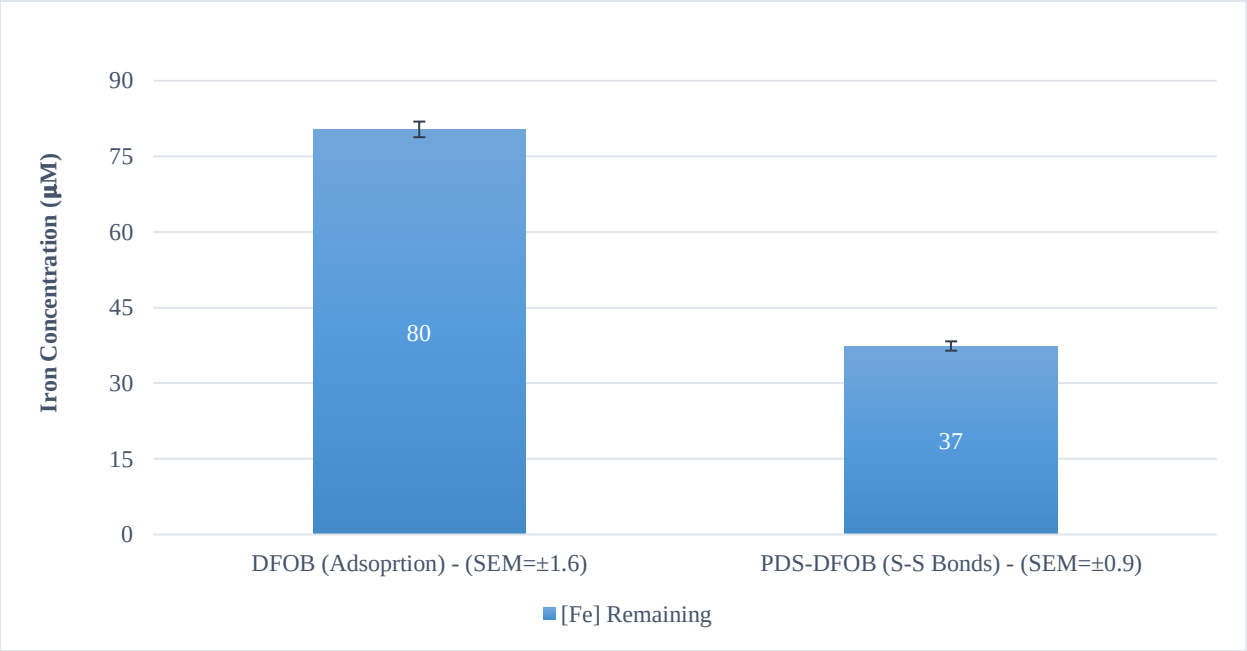

Figure 2.5 Iron concentrations after 180 min of contact with beads coupled to DFOB (no SPDP, [DFOB]=13 mg/mL) and PDS-DFOB (Molar ratio of DFOB: SPDP=5:1, PDS: Surface SH=60:1, [DFOB]=13 mg/mL). Initial Fe(III) concentration=75 µM

2.4.3 Effects of DFOB: SPDP Molar Ratios in the Coupling Solution on PDS-DFOB immobilization and Fe(III) Chelation

After establishing that covalently immobilized DFOB molecules are responsible for the observed chelation of Fe(III) in the previous sections, this part aims at investigating the effects of varying the DFOB: SPDP molar ratio on the immobilized amounts of that chelator and the resulting iron uptake (check **Scheme 2.9** for illustrations detailing the steps of PDS-DFOB coupling to the beads).

This study is especially important given that the targeted terminal amine of the DFOB has a reported dissociation constant (pK_a) of 10.01 – 10.84 (Borgias et al., 1989; Evers et al., 1988; Farkas et al., 1999), which is higher than the pH level of 8.5 employed for the coupling of DFOB and SPDP, leading the DFOB's amino group to mostly exist in its unreactive protonated form ($-NH_3^+$). Additionally, since unreacted SPDP (Mw = 312.36 g/mol) was not separated from PDS-DFOB (Mw = 774.00 g/mol) (as performed in previous studies dealing with small peptides (Neff et al., 1997)), an excess amount of DFOB had to be added to minimize the amount of unreacted SPDP, thus limiting its competition with the PDS-DFOB to attach on the beads' SH sites. For these reasons, it was important to understand the effects of DFOB: SPDP in the coupling solution on the overall immobilization of DFOB and the consequent Fe(III) chelation.

Figure 2.6 shows the iron levels remaining in the supernatants after 30 minutes of contact with beads coupled to PDS-DFOB solutions having different DFOB: SPDP molar ratios of 5:1, 10:1 and 15:1 and a constant amount of SPDP (corresponding to PDS: Surface molar ratio of 30:1). Knowing that all the tested beads had similar SH coverage of approximately 30%, increasing the DFOB: SPDP ratio in the coupling solutions did increase the calculated amount of Fe(III) chelated by the beads; from 13 μM for DFOB: SPDP ratio of 5:1 to 29 μM for DFOB: SPDP

ratio of 15:1. Additionally, as shown in **Table 2.1**, PDS-activated species (PDS-DFOB and Unreacted SPDP) did attach to the beads' SH sites when low DFOB: SPDP ratios were employed, which was confirmed by spectrophotometrically measuring the released P2T molecules. This was expected since the same concentration of SPDP was employed in all the coupling solutions. Based on these findings, we can conclude that employing high DFOB: SPDP molar ratios did convert a substantial portion of the SPDP to PDS-DFOB, which lowered the amount of unreacted SPDP in the coupling solution and subsequently translated to higher levels of iron removal. Conversely, when using lower amounts of DFOB, an important quantity of unreacted SPDP seemed to remain in the coupling solution, which competitively attached to the beads' SH sites and resulted in lower PDS-DFO binding, resulting in reduced iron uptake. Moreover, as presented in **Table 2.1**, we can notice that comparing the calculated amount of iron chelated by the beads (DFOB: SPDP molar ratio of 5:1), to the maximum theoretical amount that can be chelated based on the coverage of surface SH sites (assuming all SH sites are occupied by DFOB), we can conclude that at least 31 % of the SH sites were occupied by PDS-DFOB molecules. This 31% value assumes that all the SH-bound DFOB molecules were involved in Fe(III) chelation on a 1:1 molar basis. It is worth noting that higher DFOB occupancy percentages of SH sites were found for the beads prepared with higher DFOB: SPSP molar ratios (check **Table 2.1)**. These numbers seem satisfactory, especially when compared to the findings of Neff et al. (1997), which reported an 11% efficiency of coupling small PDS-activated GRGDSY to SH sites, despite separating the PDS-activated peptides from the unreacted SPDP via ion exchange chromatography.

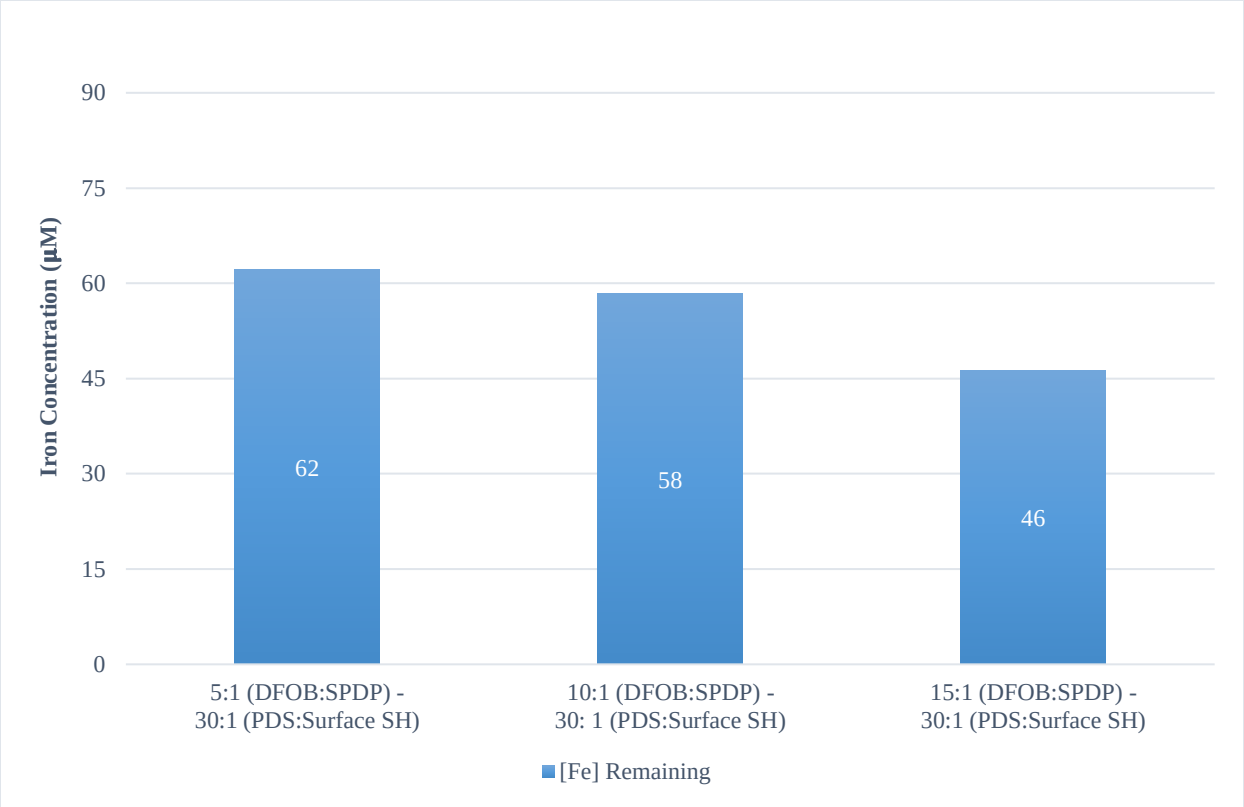

Figure 2.6 Iron concentrations after 30 min of contact with DFOB-activated beads coupled to solutions having constant PDS: Surface SH molar ratio of 30:1 and varying DFOB: SPDP ratios of 5, 10 and 15:1. Initial Fe(III) concentration=75 µM

Table 2.1 Properties of beads used to study *Effects of DFOB: SPDP Molar Ratios in the Coupling Solution on PDS-DFOB immobilization and Fe(III) Chelation* (Section 2.4.3)

	SPDP amount in Coupling Solution (mg/mL)	DFOB amount in Coupling Solution (mg/mL)	Maximum Possible PDS-DFOB Amount in Coupling Solution (mg/mL)	Sulfhydryl (-SH) Coverage % (Based on P2T Measurements)	PDS-Activated Species Coverage % (Based on P2T Measurements)	Maximum Theoretical [Fe] Removal (Based on SH Coverage %) (μM)	Maximum Theoretical [Fe] Removal (Based on PDS-Species Coverage %) (μM)	Calculated [Fe] Removal = Initial [Fe] - Measured [Fe] Remaining (μM)	Percentage of Calculated [Fe] Removed of Maximum Theoretical Amount (Based on SH Coverage %)	Percentage of Calculated [Fe] Removed of Maximum Theoretical Amount (Based on PDS-species Coverage %)
5:1 (DFOB: SPDP)- 30:1 (PDS: Surface SH)	0.72	8.17	1.78	33	28	42	36	13	31	36
10:1 (DFOB: SPDP)- 30: 1 (PDS: Surface SH)	0.72	16.34	1.78	33	18	42	23	17	40	74
15:1 (DFOB: SPDP)- 30:1 (PDS: Surface SH)	0.72	24.52	1.78	31	5	40	7	29	73	414

2.4.4 Effects of PDS: Surface SH Molar Ratios in the Coupling Solution on PDS-DFOB immobilization and Fe(III) Chelation

After investigating the effects of varying the DFOB: SPDP molar ratio in the coupling solution on the immobilization of PDS-DFOB in the previous section, this part examines the outcomes of varying the PDS: Surface SH fraction under a constant DFOB concentration **(Figure 2.7)** and DFOB: SPDP ratio **(Figure 2.8)**. (Check **Scheme 2.9** for illustrations detailing the steps of PDS-DFOB coupling to the beads)

As shown in **Figure 2.7**, increasing the initial amount of SPDP (i.e. PDS: Surface SH ratio) in the coupling solution under a constant concentration of DFOB (23 mM) led to higher iron chelation levels; for a 10:1 PDS: Surface SH ratio 7 μM iron were removed from the supernatant, while 17 and 26 μM were chelated under 30 and 60:1 ratios, respectively. Additionally, the spectrophotometric measurements of the released P2T shows that the surface coverage of PDS-species (PDS-DFOB and Unreacted SPDP) was similar on all the beads, despite the difference in the initial SPDP amounts **(Table 2.2)**.

Consequently, given that smaller iron amounts were chelated when lower PDS: SH molar ratios were used, coupled with the fact that a similar amount of PDS-activated species (PDS-DFOB and Unreacted SPDP) were attached to all the beads, lead us to conclude that smaller amounts of PDS-DFOB were conjugated to the beads prepared using lower amounts of SPDP in the coupling solution (lower PDS: Surface SH ratios).

These findings seem to be counter-intuitive at first, given the fact that the same concentration of DFOB was used in all the coupling solutions, which should stoichiometrically favor the formation of PDS-DFOB when lower amounts of SPDP were used: A constant DFOB

concentration of 23 mM yields a 30:1 DFOB: SPDP molar ratio for 10:1 PDS: Surface SH, a 10:1 DFOB: SPDP molar ratio for 30:1 PDS: Surface SH and 5:1 DFOB: SPDP molar ratio for 60:1 PDS: Surface SH.

One possible explanation for these results is the accelerated hydrolysis of the SPDP's NHS ester moiety at our coupling pH level of 8.5. NHS is the amine-reactive portion of the SPDP, which is responsible for binding the amine terminal of the DFOB to the PDS, creating the critical PDS-DFOB molecule **(Scheme 2.3)**. According to ThermoFisher's Crosslinking Reagents Technical Handbook, the hydrolysis of the NHS ester competes with the primary amine reaction, and the hydrolysis rate increases with the buffer's pH, reducing the half-life of NHS esters from 4 to 5 hours at pH 7 and 0°C to 10 minutes at pH 8.6 at 4°C. In fact, this rapid hydrolysis of NHS ester under our coupling pH level prevented us from accurately measuring its concentration post the 30 minutes reaction time, which would have allowed us to determine the amount of PDS-DFOB produced (Klykov and Weller,2015; G-Biosciences Application Note, n.d.).

Thus, it is expected that when low SPDP amounts were used, the fast hydrolysis reaction severely decreased the NHS levels in the solution, thus limiting the production of PDS-DFOB despite the stoichiometric advantage of the SPDP reaction with DFOB. Conversely, employing high SPDP amounts meant that NHS species were still available for binding with the amine groups despite the competing hydrolysis reaction.

Additionally, our proposed explanation does not contradict the fact that all the beads had a similar amount of PDS-species (PDS-DFOB and Unreacted SPDP) on their surfaces, since we expect that although the amount was similar, the distribution of these PDS-functionalized molecules on the beads was different, with higher ratios of unreacted SPDP (having hydrolyzed NHS moiety) expected on the beads prepared with lower SPDP amounts.

These findings show that the iron chelation capacity of the beads were mainly governed and limited by the progress of the DFOB reaction with SPDP, and not the attachment of PDS-species to the surface. While the DFOB and SPDP reaction seemed to produce sufficient PDS-DFOB amounts under adequate reaction conditions, the efficiency of this reaction was hindered by two opposing factors that forced a design trade-off; the first is the high pK_a value of the DFOB's terminal amine (10.01 - 10.84), which required working at a relatively high pH level (pH = 8.5) to maintain a sufficient presence of the reactive (-NH_2) species. The $\frac{[NH_2]}{[NH_3^+]}$ ratio is determined by the highly pH-sensitive Henderson–Hasselbalch Equation (2.3):

$$pH = pK_a + log_{10}\frac{[NH_2]}{[NH_3^+]} \quad (2.3)$$

The second factor is the high sensitivity of NHS to any increase in pH levels, which significantly decreases its half-life at higher pH due to hydrolysis, thus requiring more reactants to achieve satisfactory PDS-DFOB yields.

This trade-off can be illustrated by the following case: for a pK_a value of 10.5, carrying out the coupling reaction at pH = 8.5 will result in a $\frac{[NH_2]}{[NH_3^+]}$ ratio of 10^{-2}, with a NHS ester half-life of few minutes. However at pH = 7.5, $\frac{[NH_2]}{[NH_3^+]}$ will decrease by a factor of 10 to 10^{-3}, while the NHS half-life will increase to hours. On the other hand, **Figure 2.8** shows the effect of increasing PDS: Surface SH molar ratio under a constant DFOB: SPDP ratio of 5:1. We can notice that increasing the SPDP amount led to higher iron chelation, which is consistent with the above discussion. Finally, although satisfactory iron chelation levels were achieved under both 30:1 PDS: Surface SH / 15:1 DFOB: SPDP and 60:1 PDS: Surface SH / 5:1 DFOB: SPDP molar ratios, the latter

ratios will be used to prepare the remaining tubes due to operational considerations (inability to store SPDP-DMSO solutions).

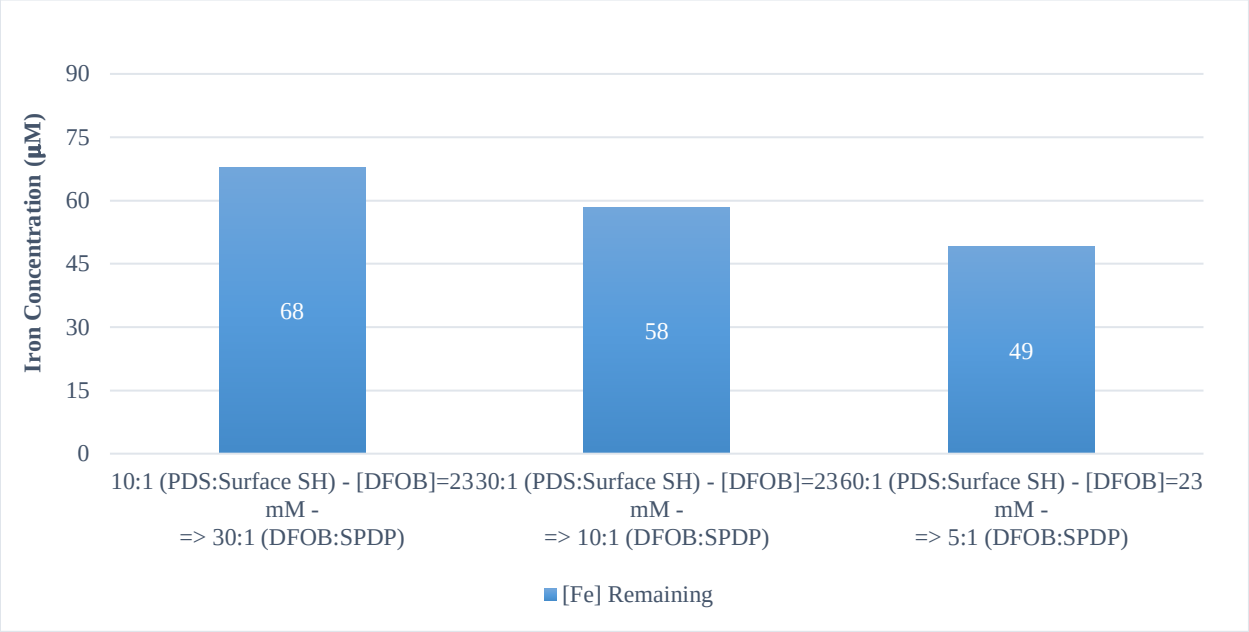

Figure 2.7 Iron concentrations after 30 min of contact with DFOB-activated beads coupled to solutions having constant DFOB amount ([DFOB]=23 mM) and varying PDS: Surface SH molar ratios of 10, 30 and 60:1. Initial Fe(III) concentration=75 µM

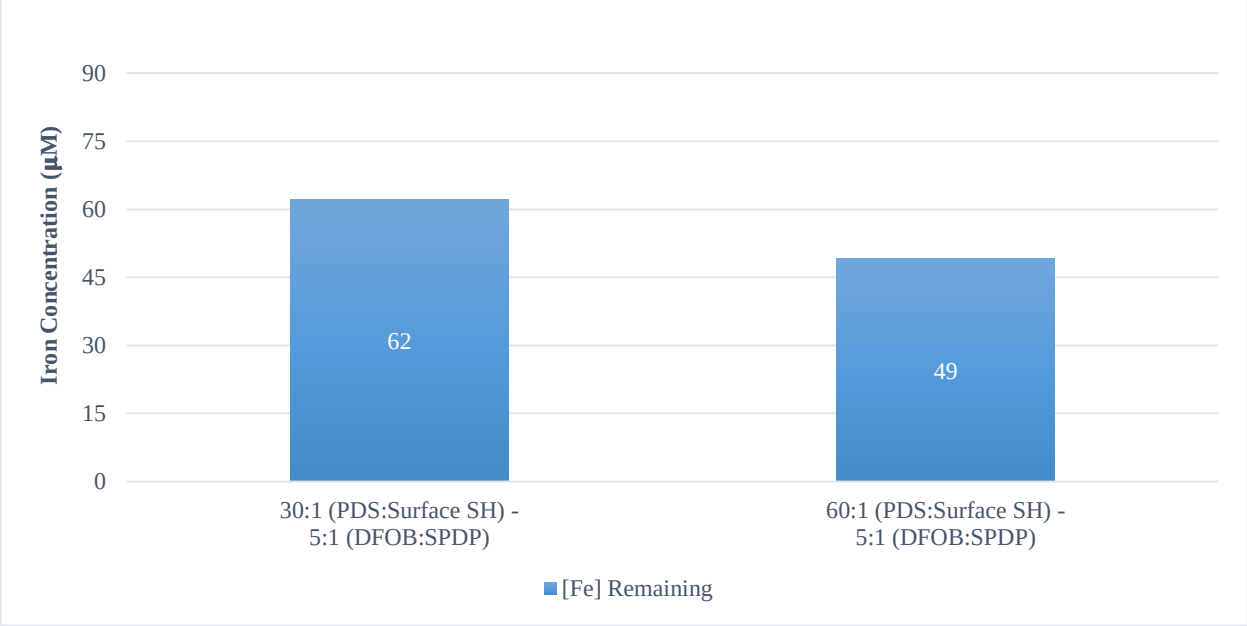

Figure 2.8 Iron concentrations after 30 min of contact with DFOB-activated beads coupled to solutions having constant DFOB: SPDP molar ratio of 5:1 and varying PDS: Surface SH molar ratios of 30 and 60:1. Initial Fe(III) concentration=75 µM

Table 2.2 Properties of beads used to study *Effects of PDS: Surface SH Molar Ratios in the Coupling Solution on PDS-DFOB immobilization and Fe(III) Chelation* (Section 2.4.4)

	SPDP amount in Coupling Solution (mg/mL)	DFOB amount in Coupling Solution (mg/mL)	Maximum Possible PDS-DFOB Amount in Coupling Solution (mg/mL)	Sulfhydryl (SH) Coverage % (Based on P2T Measurements)	PDS-Activated Species Coverage % (Based on P2T Measurements)	Maximum Theoretical [Fe] Removal (Based on SH Coverage %) (µM)	Maximum Theoretical [Fe] Removal (Based on PDS-Species Coverage %) (µM)	Calculated [Fe] Removal = Initial [Fe] - Measured [Fe] Remaining (µM)	Percentage of Calculated [Fe] Removed of Maximum Theoretical Amount (Based on SH Coverage %)	Percentage of Calculated [Fe] Removed of Maximum Theoretical Amount (Based on PDS-species Coverage %)
10:1 (PDS:Surface SH) - [DFOB]=23 mM - => 30:1 (DFOB:SPDP)	0.24	16.34	0.59	36	22	46	28	7	15	25
30:1 (PDS:Surface SH) - [DFOB]=23 mM - => 10:1 (DFOB:SPDP)	0.72	16.34	1.78	33	18	42	23	17	40	74
60:1 (PDS:Surface SH) - [DFOB]=23 mM - => 5:1 (DFOB:SPDP)	1.44	16.34	3.56	34	22	44	28	26	59	93

2.4.5 Dithiothreitol (DTT) Reduction of Disulfide Bonds in PBS and HEPES Buffers

Examining the effectiveness of 50 mM DTT solutions in reducing the disulfide bonds of surface PDS groups **(Scheme 2.2)** and detaching Ferrioxamine (FO) from the beads **(Scheme 2.6)** was required to explain the results of the beads regeneration experiments and to accurately determine the FO concentration on the beads.

Figure 2.9 shows the percentages of disulfide bonds cleaved by 50 mM DTT prepared in PBS and HEPES buffers after 1 hour reaction time at room temperature under different SPDP concentrations. As can be seen, DTT in PBS, used to reduce the PDS surface groups during the beads SH-activation, was able to cleave 92 and 88% of the initial SPDP's S-S bonds. SPDP was added in concentrations that corresponded to 77 and 15% of the bead's surface amine sites (on 1 mL supernatant basis).

Additionally 50 mM DTT in HEPES, used to detach the ferrioxamine (FO) species formed on the beads' surface, was able to reduce 97% of the initial SPDP's disulfide bonds, which was added in an amount that corresponded to 25% of the total sites, a frequently calculated value of FO coverage in this work.

These high percentages agree with the findings of Iyer and Klee (1973). In that work, a 50 mM DTT solution in 8 M urea was able to reduce more than 90% of the disulfide bonds of bovine α-lactalbumin, bovine serum albumin (BSA) and bovine pancreatic ribonuclease in less than 70 minutes.

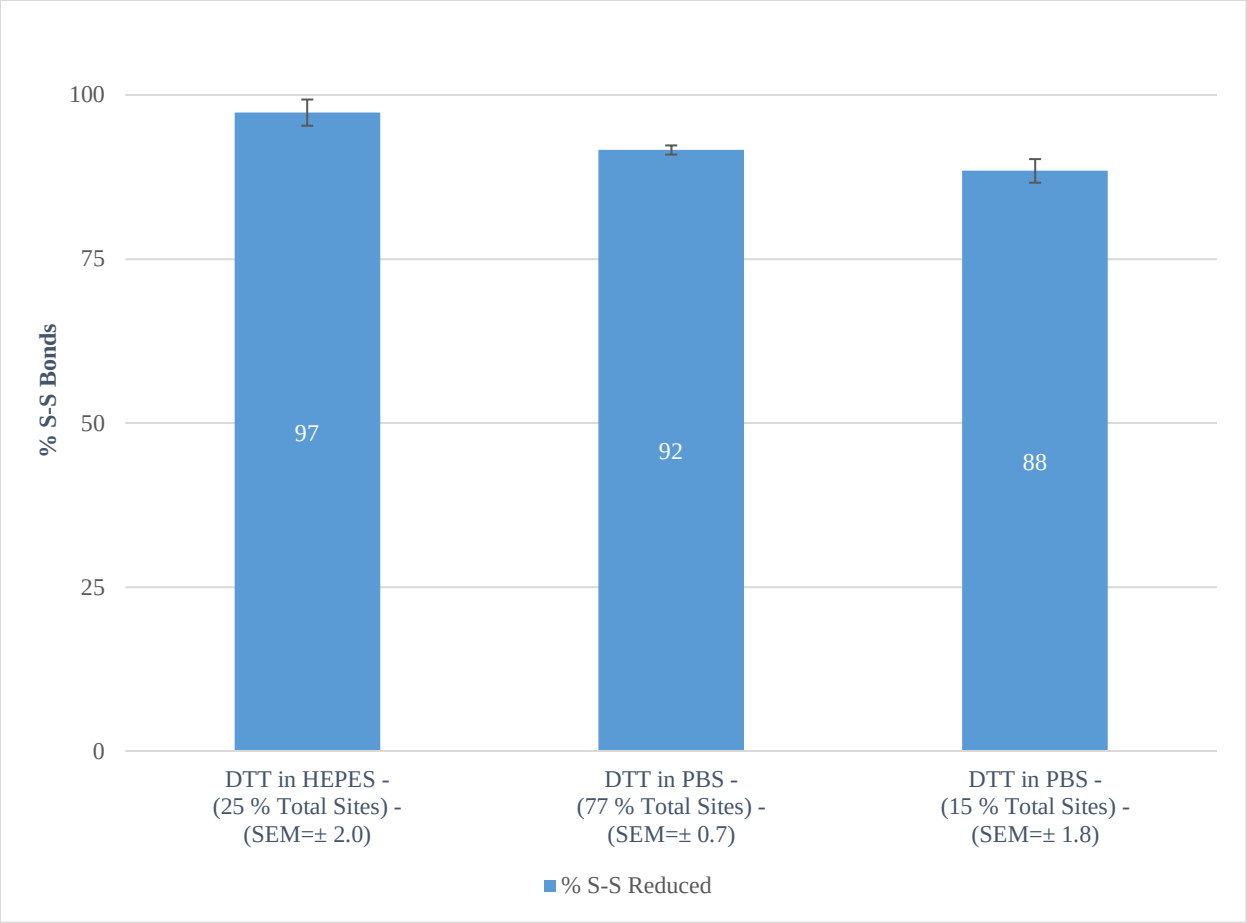

Figure 2.9 Percentage of reduced disulfide bonds by 50 mM DTT in PBS (initial [SPDP] = 77% and 15% total sites) and HEPES (initial [SPDP] = 25% total sites). Reaction conditions: 1 hour, room temperature, pH=7.5.

2.4.6 Dithiothreitol (DTT) Effect on Ferrioxamine (FO) Concentrations

In this work, DTT was used to detach FO from the bead's surface, allowing for the measurement of FO concentration and support regeneration. Knowing that DTT (50 mM) was used in an excess amount with respect to FO (≈37.5 μM) for a contact time of approximately 90 minutes, coupled with the findings of Netto and Stadtman (1996) and Fontecave et al. (1990) which showed that DTT oxidation is catalyzed by Fe(III), leading to its reduction to Fe(II), we were interested in determining the effects of prolonged exposure to DTT on the stability and concentration of FO. This was particularly important, given that Fe(II)-DFOB complex is significantly less stable than Fe(III)-DFOB ($K_{Fe(II)-DFOB}$ = 1.6 x 10^7 Vs $K_{Fe(III)-DFOB}$ = 4 x 10^{30}) (Manning et al., 2009)).

(Figure 2.10) shows the concentration change of ferrioxamine (FO) with time after the addition of 50 mM DTT. The FO solutions were prepared using 37.5 μM Fe(III)-citrate solutions under 100:1 and 0:1 citrate: iron ratios. The 0:1 citrate: iron solution was prepared to mimic the no-citrate environment of the FO surface detachment via DTT. As can be seen, the addition of DTT did not have any measurable effect on the FO concentration throughout the three hours measurement period, suggesting that Fe(III) was firmly bound to the DFOB molecules. Knowing that DTT will be mixed with FO for 1 hour to detach it from the surface, followed by a centrifugation and FO measurement time of approximately 30 minutes, we expect that this exposure to DTT will not have any effects on the FO's stability and concentration throughout the FO assay period. Finally, it can be seen that the FO solution prepared under 100:1 citrate: iron had a higher FO content than the one prepared with no citrate. This can be explained by the precipitation of Fe(III) at physiological pH when no citrate was used, which in turn decreased the Fe(III) amount that can be chelated by DFOB (Evans et al., 2008; Rose and Waite, 2003).

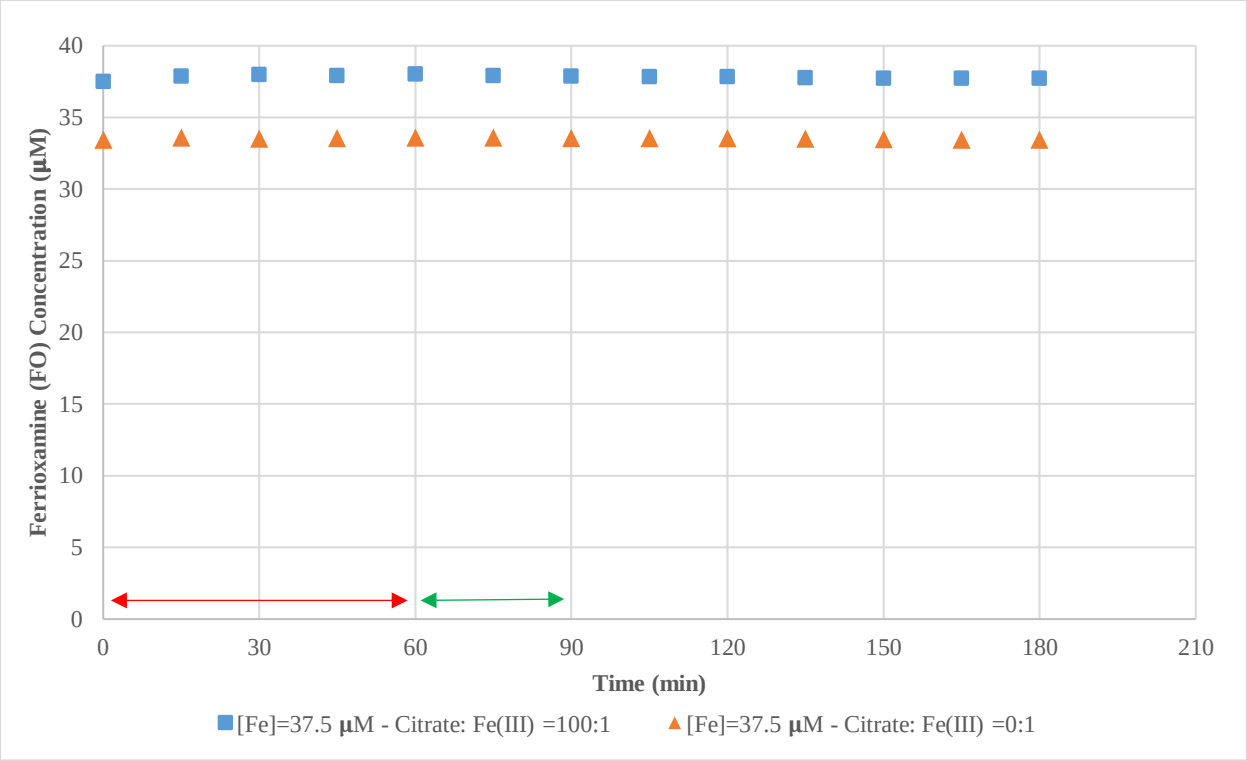

Figure 2.10 Ferrioxamine (FO) concentration change with time after addition of 50 mM DTT. FO solutions were prepared using 37.5 µM Fe(III)-citrate solutions under 100:1 and 0:1 citrate: iron ratios. Red arrow: FO detachment reaction time - Green Arrow: Centrifugation time during FO measurement

2.4.7 Regeneration of Latex Beads via Reduction of Disulfide Bonds and Recoating with Pyridyldithiol Activated Desferrioxamine (PDS-DFOB)

The reversible covalent binding of DFOB to the polystyrene surface via cleavable disulfide bonds (S-S) may allow the reuse of the polymeric thiolated support to immobilize fresh batches of PDS-DFOB. This strategy may prove economically and operationally advantageous to small and large-scale applications (Mohamad et al., 2015; Fraas and Franzreb, 2017; Carlsson et al., 1975).

In order to test the ability of regenerated beads to chelate iron, 1 mL of Fe(III)-citrate having iron concentrations of 37.5, 75, 150 and 300 μM were introduced to 4 sets of DFOB-activated beads and allowed to react for 180 minutes at room temperature (1st run - fresh beads). The beads were subsequently regenerated by DTT cleavage of FO **(Scheme 2.6)**, coupled to fresh PDS-DFOB batches **(Scheme 2.7)**, followed by a second addition of iron-citrate (2nd run - regenerated beads).

Figures 2.11 shows the iron amounts chelated by fresh and regenerated beads starting from initial Fe(III) concentrations of 37.5 and 75 μM, while **Figure 2.12** presents the chelation levels seen under 150 and 300 μM of iron. Additionally, **Table 2.3** shows the SH and PDS species coverage % on fresh beads, the PDS species coverage % on regenerated beads, all obtained via measuring the released P2T, among other information. As previously stated, the measurement of PDS-species coverage % via measuring the released P2T did yield widely inconsistent results when high SPDP amounts were present in the coupling solution. Additionally, as can be seen in **Table 2.3**, the measured iron (and FO) concentrations chelated by the beads frequently exceeded the theoretical maximum amount calculated from the SH coverage %. Consequently, it is possible that the SH coverage determination via P2T measurement consistently reflected lower values than the actual ones.

As can be noticed in both **Figure 2.11** and **Figure 2.12,** for all Fe(III) concentrations, except 300 μM, the amounts of iron remaining at the end of the 2nd run (regenerated beads) were lower than those observed in the 1st one (fresh beads). It is worth noting that under 37.5 and 150 μM, a respective increase of 28 and 49% in the amount of chelated iron was observed under the regenerated beads, while this percentage drops to 5% under 75 μM. As for the 300 μM iron concentration, we observed a decrease of 6 μM in the concentration of iron chelated under the regenerated beads, corresponding to 15%.

These findings show that the regenerated beads were generally able to chelate higher amounts of iron than their fresh equivalents, which may indicate the existence of higher amounts of DFOB on the regenerated surfaces. Since the used beads were washed twice with HEPES buffer before recoupling to fresh PDS-DFOB batches, it is expected that most adsorbed DFOB molecules from the first coupling solution were removed by the washing buffer. Consequently, an accumulation of adsorbed DFOB molecules cannot explain the increase in iron chelation levels seen under the regenerated beads.

Moreover, since our previous experiments showed that Fe(III) is firmly bound to FO in DTT solutions, coupled with the fact that approximately 97% of surface FO were expected to be detached during the surface regeneration process, we can conclude that a Fe(III) release from undetached FO molecules (i.e. regeneration of DFOB) cannot explain the possible increase of iron uptake observed under the regenerated beads.

One possible hypothesis that can partially explain these findings is that the introduction of DTT in HEPES during the FO detachment and surface regeneration step, did also reduce the disulfide bonds of the initially introduced PDS groups, thus creating more sulfhydryl (-SH) sites for the PDS-DFOB molecules in the second coupling solution to attach to **(Scheme 2.8).** As seen in a previous section of this chapter, a 50 mM DTT in PBS was able to reduce between 88 and 92% of the SPDP's disulfide bonds, thus leaving the remaining unreduced portion (between 8 and 12 %) available for reduction (SH activation) during the surface regeneration step. However, even if we assume that these additional SH sites can bind 12% more PDS-DFOB molecules, and to consequently increase the chelated iron amounts by the same percentage in the 2^{nd} run, the percent increase in iron chelation seen under the 37,5 and 150 μM test beads of 28 and 49%,

respectively, cannot be justified. Finally, errors in iron measurements that contributed in increasing the amounts of chelated iron under the regenerated beads cannot also be ruled out.

Although these effects clearly deserve further investigation, it is safe to assume that the regenerated beads were able to achieve a satisfactory level of iron chelation relative to the fresh ones.

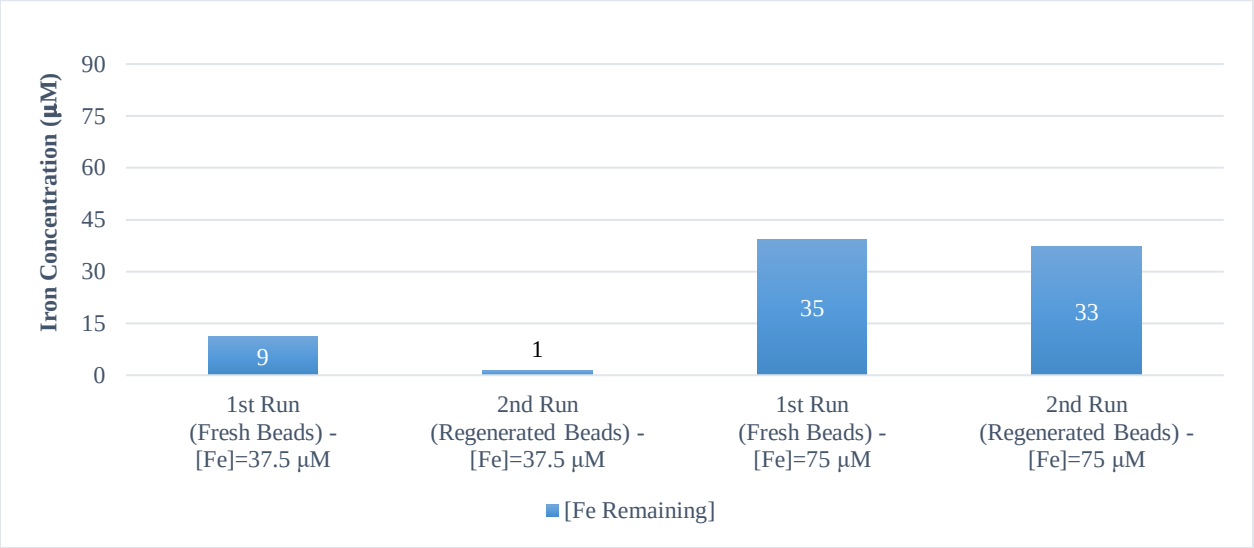

Figure 2.11 Iron chelation levels under fresh and regenerated beads for initial iron concentrations of 37.5 and 75 µM

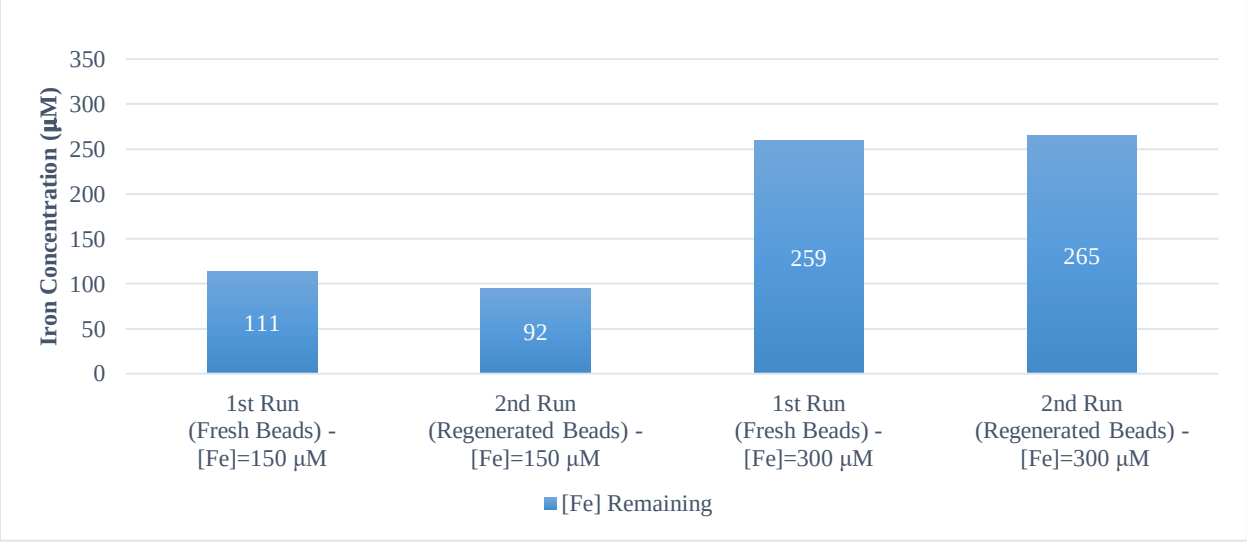

Figure 2.12 Iron chelation levels under fresh and regenerated beads for initial iron concentrations of 150 and 300 µM

Table 2.3 Properties of beads used to *Regeneration of Latex Beads via Reduction of Disulfide Bonds and Recoating with Pyridyldithiol Activated Desferrioxamine (PDS-DFOB)* (Section 2.4.7)

	DFOB: SPDP Molar Ratio in 1st and 2nd Coupling Solution	PDS: Surface SH Molar Ratio in 1st and 2nd Coupling Solution	Fresh Beads Sulfhydryl (SH) Coverage % (Based on P2T Measurements)	Fresh Beads PDS-Activated Species Coverage % (Based on P2T Measurements)	Maximum Theoretical [Fe] Removal (Based on Fresh Beads SH Coverage %) (μM)	Maximum Theoretical [Fe] Removal (Based on Fresh Beads PDS-Species Coverage %) (μM)	Calculated [Fe] Removal = Initial [Fe] - Measured [Fe] Remaining - 1st Run (Fresh Beads) (μM)	Percentage of Calculated [Fe] Removed of Maximum Theoretical Amount (Based on Fresh Beads SH Coverage %)	Percentage of Calculated [Fe] Removed of Maximum Theoretical Amount (Based on Fresh Beads PDS-species Coverage %)	Regenerated Beads PDS-Activated Species Coverage % (Based on P2T Measurements)	Maximum Theoretical [Fe] Removal (Based on Regenerated Beads PDS-Species Coverage %) (μM)	Calculated [Fe] Removal = Initial [Fe] - Measured [Fe] Remaining - 2nd Run (Regenerated Beads) (μM)	Percentage of Calculated [Fe] Removed of Maximum Theoretical Amount (Based on Regenerated Beads PDS-species Coverage %)
Beads - $[Fe]_0$ = 37.5 μM	5:1	60:1	22	5	29	6	28.5	98	475	23	29	36.5	126
Beads - $[Fe]_0$ = 75 μM	5:1	60:1	23	15	29	19	40	138	211	39	50	42	84
Beads - $[Fe]_0$ = 150 μM	5:1	60:1	22	11	29	14	39	134	279	31	40	58	145
Beads - $[Fe]_0$ = 300 μM	5:1	60:1	23	10	30	12	41	137	342	34	43	35	81

2.5 Conclusions

In this chapter, the reversible covalent immobilization of DFOB on polystyrene beads via disulfide bonds has been successfully achieved and the following conclusions and findings were made:

- Comparing the activity of DFOB-activated beads with SH-activated ones (control) showed that the immobilized DFOB was the sole surface species responsible for the observed iron chelation. Consequently, it was deduced that the remaining surface species in addition to sulfhydryl (-SH); i.e. amino groups ($-NH_2$), and smaller amounts of pyridyldithiol (-PDS) and carboxyl groups (-RCOOH) did not contribute in chelating Fe(III)-citrate.
- After measuring the iron chelated under both covalently immobilized and surface adsorbed DFOB, it was found that iron was predominantly chelated by covalently bound molecules. Although surface adsorbed chelators were able to complex a small portion of iron, this activity was only observed when using DFOB amounts close to the compound's solubility limit in water, which far exceeded the amounts used in our coupling solutions.
- After investigating the effects of varying the DFOB and SPDP amounts in the coupling solution on the levels of iron chelated by the beads, it was found that the bioconjugation of DFOB to the surface was limited by the formation of PDS-DFOB species in the coupling solution and not the binding of that molecule to the thiolated surface.
- Our studies showed that under a constant DFOB concentration in the coupling solution, fewer PDS-DFOB molecules were produced when lower SPDP amounts were used despite the stoichiometric advantage. We expected that the fast hydrolysis of the SPDP's

NHS moiety (responsible for binding PDS to DFOB) at the working pH of 8.5 limited the creation of PDS-DFOB species.

- DFOB-activated beads used to chelate the iron were regenerated by cleaving the disulfide bonds connecting the formed DFOB-Fe(III) complexes (ferrioxamine) to the surface, which in turn created (-SH) sites in their places. After coupling the regenerated beads to fresh PDS-DFOB molecules, it was found that the amounts of iron chelated under the regenerated beads was on average higher than those observed under the fresh ones. A partial explanation for these surprising results was that the reduction of initially intact PDS groups during the ferrioxamine cleaving process, created new -SH sites for the fresh PDS-DFOB to attach to. Further investigation of these effects is warranted.

2.6 Future Directions

Despite the successful immobilization of DFOB on polystyrene beads and the similar iron chelation levels observed under both fresh and regenerated beads, the following suggestions can be made to improve the efficiency of the bioconjugation process:

- Reversibly attaching DFOB to the surface required the existence of a cleavable disulfide bond linking the chelator to the beads, which was achieved by using SPDP crosslinker. However it was shown that the reaction of SPDP with DFOB was hindered by the hydrolysis of NHS at the operational pH, which required using up to 6 times the recommended amounts of SPDP to yield satisfactory results (Hermanson, 2008). For that reason, it is suggested to employ another crosslinker that is cleavable, to ensure the reversibility of the immobilization, has an amine reactive moiety that is more stable than

NHS at the pH level required for coupling DFOB (pH=8.5), and possibly lower cost. Consequently, Wang and Richard's Reagent (DTBP) seems to be an appropriate substitution for SPDP. DTBP is an imidoesters, thiol-cleavable crosslinker that can ensure the reversibility of the immobilization. Additionally, having an amine reactive moiety of imidoester instead of NHS with a working pH range of 8-10, render this crosslinker more convenient to react with DFOB than SPDP given that a higher proportion of the chelator's terminal amine will be in its reactive ($-NH_2$) form under the higher operating pH of DTBP. Additionally, the cost of this homobifunctional crosslinker is at least ten times cheaper than the SPDP. One problem can arise with the use of DTBP and it is associated with its homobifunctional nature, which can lead to its non-specific binding to NH_2 surface sites. However, as stated by Hermanson (2008), this problem can be avoided by using an excess of DTBP, which should not lead to major drawbacks, since that excess can be retrieved from the beads and given the crosslinker's relative low cost. The steps of coupling DFOB molecules to ($-NH_2$) functionalized surfaces via DTBP is illustrated in **Scheme 2.10**. This DFOB immobilization technique consists of two steps only which are the imidoester-functionalization of the beads, followed by DFOB addition to the surface.

- Coupling DFOB to an amine reactive species on the surface (such as NHS or imidoesters) can simplify the immobilization procedure, since a separation of the crosslinker and DFOB in solution will not be required.
- In this work, the adsorption of Fe(III)-citrate on DFOB-activated beads has been investigated. In future studies, studying the effectiveness of the DFOB-polystyrene to chelate other ions such as calcium (II), magnesium (II), zinc (II), aluminum (III),

zirconium (IV), vanadium (V) and lead (II) along other metals can prove beneficial, given DFOB's ability to chelate these minerals and the associated potential biomedical and industrial applications (Kiss et al., 2008; Tagakai et al. 2007). Additionally, these studies can prove important given that iron overload patients receiving DFOB treatment can experience different adverse effects related to mineral ions deficiency, such as growth retardation, mainly caused by the DFOB's non-specific binding of metals (Genc et al., 2016).

- After successfully detaching the formed ferrioxamine and regenerating the support, a future work on the topic can consider the regeneration of the DFOB molecule itself by reducing the detached ferrioxamine (i.e. DFOB-Fe(III)) according to the mechanisms proposed by Alderman et al (2009), or the aquation of that complex proposed by Monzyk and Crumbliss (1982), which were both shown to restore the DFOB molecule after releasing the Fe(III) ion.
- In this work, aminated latex beads were used as a starting point for the immobilization of DFOB. Unlike non-functionalized polymeric supports, the aminated surface of the beads renders them receptive for bioconjugation reactions. Consequently, future studies can seek to functionalize the support itself via different strategies such as the adsorption and/or gamma irradiation of funtionalized triblocks on the surface (Hecker et al., 2018; Fry et al., 2010) or using silanization reactions to functionalize inert surfaces with reactive species (Schilke, 2009), among other methods.

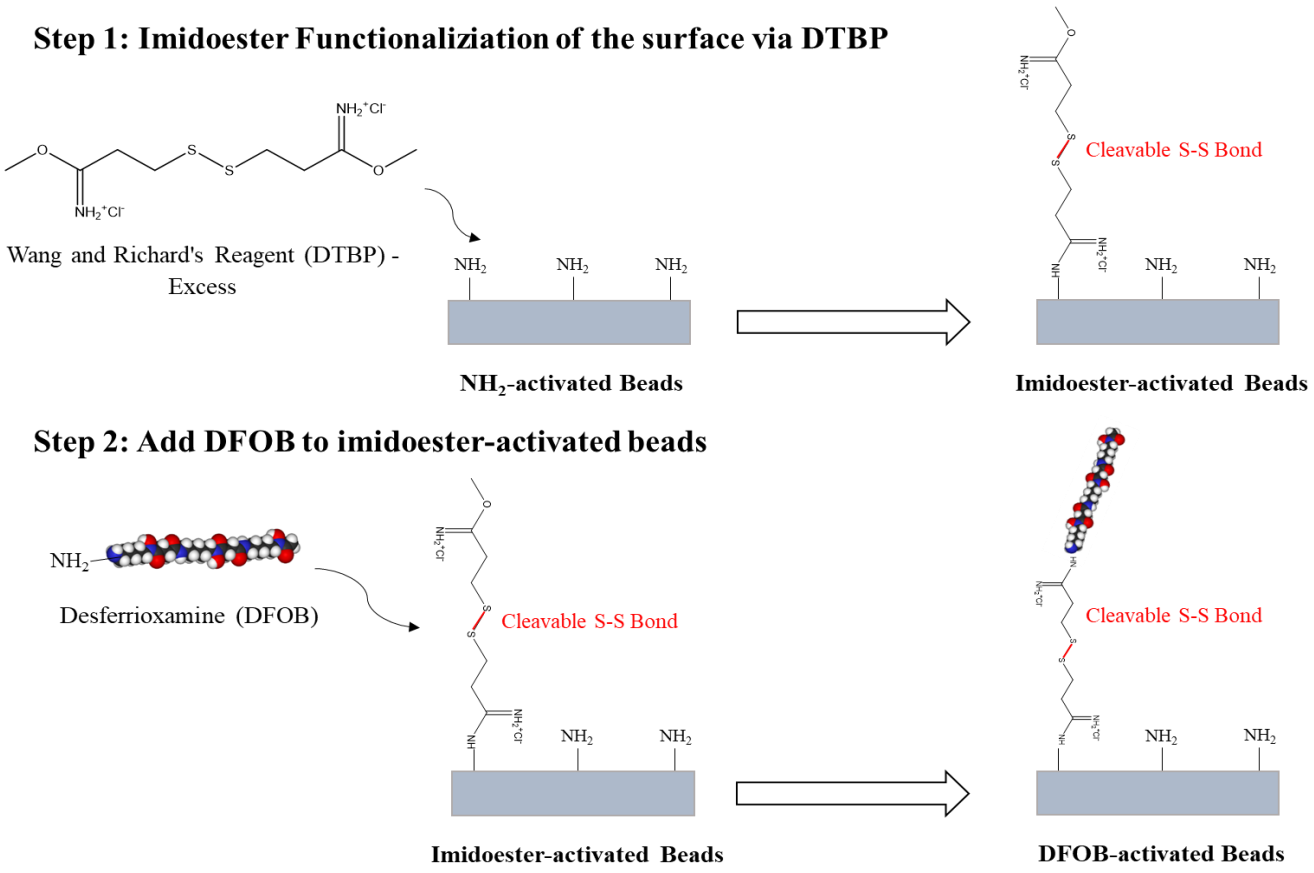

Scheme 2.10 Steps of coupling DFOB to NH_2-activated beads via DTBP

3 KINETICS AND EQUILIBRIUM STUDY FOR THE ADSORPTION OF CITRATE-BOUND FE(III) ON DESFERRIOXAMINE (DFOB)-FUNCTIONALIZED POLYSTYRENE BEADS

3.1 Abstract

A kinetics and equilibrium study for the adsorption of the physiologically and environmentally relevant Fe(III)-citrate on DFOB-activated beads has been achieved. Fitting the pseudo first-order, pseudo second-order and Elovich kinetics models to the experimental data did not conclusively determine the most suitable model given the similar correlation coefficients R^2. Studying the Langmuir and Freundlich models yielded relatively similar R^2 values of 0.992 and 0.953, respectively. However, knowing that the Langmuir physics closely matches that of the iron chelation by DFOB system, we expected that the Langmuir model offers a better description of the adsorption data, with a Langmuir constant K_L = 12.81 $(L/mg_{Fe(III)})$ and a maximum iron coverage q_{max} = 0.206 $(mg_{Fe(III)}/g_{adsorbent})$. Using the obtained K_L and q_{max} values to relate the pseudo first-order and pseudo second-order expressions via the Langmuir kinetics equation showed that for an initial iron concentration lower than 22 μM or higher than 68 μM, it was expected that the pseudo first-order model was the best fit for the kinetics data. However, for values close to 35 μM, the pseudo second-order model was expected to offer a more accurate description of the experimental data. Additionally, it was shown that 180 minutes were needed to reach equilibrium under immobilized DFOB, while 30 minutes were only needed for that chelator in solution. These results strongly reflect the negative effect of immobilization on the reaction rate of iron chelation, which can be attributed to a hindrance of the iron's citrate to DFOB exchange mechanism.

3.2 Introduction

In this chapter, a kinetics and equilibrium study for the adsorption of citrate-bound Fe(III) on DFOB-activated beads will be presented and the collected experimental data will be analyzed in light of the relevant adsorption kinetics and isotherm models. This study is important, especially that Fe(III)-citrate is a dominant species in the serum's non-transferrin bound iron (NTBI) which is the main target for chelation. The DFOB chelation of Fe(III) from citrate involves the transfer of iron from the citrate ligand to the DFOB. In solution, this exchange is kinetically determined by the citrate: iron ratio, the ionic strength and pH, along other parameters (Ito et al., 2011; Ito et al., 2015). Additionally, according to Evans et al. (2008), the speciation of iron citrate is also largely determined by the citrate: iron ratio. It was found that for a citrate: iron ratio of 100:1, which is a clinically relevant ratio used in our study, dimeric iron citrate complex species ($FeCit_2$) were the most dominant. It is important to note that in human serum, citrate: iron ratios vary from 10:1 to 100:1, However a 100:1 ratio was used in this work to avoid Fe(III) precipitation (Rose and Waite, 2003). Moreover, it was reported that the ability of DFOB to chelate iron-citrate in solution was found to be dependent on the species formed, with lower molecular weight citrate complexes (mono-citrate and di-citrate iron complexes formed at high citrate: iron molar ratios) being more easily chelatable than higher molecular weight ones (oligomeric and polymeric iron complexes formed at low citrate: iron molar ratios). Ito et al. (2011) proposed a kinetic model to describe the ligand exchange of Fe(III) from the citrate to the DFOB. This kinetic model was based on three possible mechanisms with the citrate: iron largely determining the probable mechanism. It was reported that for a citrate: iron ratio close to 100: 1, which is the ratio present in the blood and used in our work, the following mechanism of ligand exchange is favored: Starting from a dimeric iron citrate complex $FeCit_2$, one citrate molecule

dissociates from that complex. This is followed by an adjunctive association of DFOB to the remaining FeCit molecule. Subsequently, an intermediate complex of DFOB-Fe-citrate is formed, which later dissociates to leave DFOB-Fe(III) complex (i.e. ferrioxamine). This overall ligand exchanged reaction is expressed as:

$$FeCit_2 + DFOB \rightarrow FeDFOB + 2Cit \quad (3.1)$$

Additionally, the authors showed that under equimolar initial concentrations for DFOB and Fe(III) of 1 μM and a citrate: iron molar ratios of 500 to 5000:1, at pH = 8, the overall ligand reaction followed a second-order rate law, with rate constants $k_{overall}$ = 34 to 232 $M^{-} s^{-}$ for citrate: iron ratios of 500 to 5000:1, respectively.

Faller and Nick (1994) also investigated the kinetics of Fe(III)-citrate chelation by DFOB in solution at a physiological pH of 7.4. In their work, the citrate: iron ratio was set at 5:1. Starting with equimolar initial concentrations for DFOB and Fe(III) of 0.1 mM, the experimental data were well described by the second-order rate law, with a k_2 value of 1.58 x 10^{-3} $OD^{-} s^{-}$ (OD: measured absorbance). However, after increasing the initial concentration of DFOB to 1 mM, which corresponds to 10-fold that of iron, an observed shift of reaction rate law from a second-order to a pseudo first-order one was observed, with a rate constant k_1= 4 x 10^{-3} s^{-}. This effect can be ascribed to the use of excess initial DFOB concentration relative to iron, which leads the DFOB to maintain sufficiently stable concentration throughout the reaction that its amount can be considered as constant. This relatively unchanged concentration of DFOB allow the simplification of the rate formation equation of ferrioxamine (FO) from a second-order rate expression (3.2) that involves the concentrations of both DFOB and Fe(III), to a pseudo first-order one that is only based on the concentration of the changing Fe(III) (3.3).

Second-order Rate Equation:

$$\frac{dFO}{dt} = -k_2[DFOB][Fe(III)] \quad (3.2)$$

If [DFOB] used in excess => considered as constant => Pseudo first-order Rate Equation:

$$\frac{dFO}{dt} = -k_1\left[Fe(III)\right] \quad (3.3)$$

It is worth noting that second-order rate equation can be possibly simplified to pseudo first-order rate expression if any of the two reactants is used in large excess relative to the other (i.e. DFOB in excess relative to Fe(III) or vice versa) (Corbett, 1972), (Tinoco et al, 1995).

On the other hand, previous researchers have studied the kinetics and/or adsorption mechanisms of Fe(III) chelation by DFOB-activated supports (Alberti et al., 2015; Alberti et al., 2014; Alberti et al., 2014; Biesuz et al., 2014). Alberti et al. (2015) performed a kinetics and equilibrium study for the adsorption of Fe(III) in 0.1 M KNO_3 on DFOB-activated filter papers (pH = 2.5). Developing the kinetic profiles for the adsorption of Fe(III) in solution (V = 70 mL and C_{Fe} = 1.8 x 10^{-5} M) on 10 mg DFOB-papers, showed that the uptake of iron was best described by the pseudo first-order kinetic equation with rate constants $k_1 = 0.030$ and 0.23 min^- while equilibrium concentrations were reached within 150 or 30 minutes depending on the used support. Additionally, it was found that the Langmuir isotherm offered the best description of the adsorption data with a maximum coverage q_{max} of 0.04 mmoL Fe (III)/g adsorbent and Langmuir constant K_L of 23 L/mmoL. Moreover, Biesuz et al. (2014) investigated the kinetics and sorption profiles for the adsorption of Fe(III) in 0.1 M KNO_3 on DFOB immobilized on mesoporous silica (pH = 2.5). After performing a kinetic study for the adsorption of Fe(III) (V = 20 mL and C_{Fe} = 1.8 x 10^{-5} M) on 30 mg DFOB-SAMMS, it was shown that the pseudo first-

order model offered the best fit for the kinetics data with $k_1 = 0.048$ min^{-} and 0.043 min^{-} for MCM-41 and MSU-H types, respectively, while it was noted that the equilibrium was reached within 200 minutes. It is important to note that, according to the data presented in that work, it can be concluded that these kinetics experiments were carried out under high excess of DFOB relative to Fe(III). Finally, the sorption isotherms were best described by the Langmuir model, and a maximum coverage q_{max} of 0.33 mmoL Fe(III)/g adsorbent with a corresponding Langmuir constant K_L of 2.829 L/mmoL were achieved under optimized conditions.

In the literature, different authors sought to study the kinetic models of adsorption and explain their theoretical basis and applicability under different operational conditions (Azizian, 2004; Rudzinski and Plazinski, 2006; Liu and Shen, 2008; Moussout et al., 2018). Among the mostly used kinetic models to describe the adsorption of solutes from a solution onto solid surfaces are the pseudo first-order model or Lagergren's model (Lagergen, 1898) and the pseudo second-order model (Ho et al., 1996; Ho and McKay, 1999). According to Largitte and Pasquier (2016), the assumptions made in both models are similar (more details in Section 3.4.1), except that the solute uptake from the solution is governed by a second-order rate equation instead of a first-order one under Ho et al's model. Azizian (2004) developed a general analytical solution based on the Langmuir kinetics that reduces to the pseudo first-order model at high initial solute concentrations, and converts to the pseudo second-order model at low initial ones. Later on, Liu and Shen (2008) further elaborated on that conclusion by stating that the Langmuir kinetics equation can be transformed to a polynomial expression of varying-order rate, which under sufficient and required conditions (more details in Section 2.4.3), reduces to either the pseudo first-order or pseudo second-order rate equation. More importantly, Liu and Shen (2008) showed that the pseudo first-order model is possibly applicable not only when the initial concentration of

the solute is in large excess relative to the available sorption sites (like Azizian (2004) previously concluded), but also when the available sorption sites are in large excess relative to the solute (i.e. low solute concentrations). It followed that Lui and Shen (2008) defined two solute concentration parameters C_{0Low} and C_{0High}, showing that for a given solute concentration C_0, if C_0 is less than C_{0Low} or higher than C_{0High}, the Langmuir kinetics will reduce to the pseudo first-order model. However if C_0 falls between these two values and assuming the satisfaction of other conditions (more details in Section 2.4.3), the Langmuir kinetics (which combines both models) can be simplified to the pseudo second-order model.

In this work, we will investigate the kinetics and sorption profiles for the adsorption of Fe(III)-citrate on DFOB-polystyrene. This study can prove beneficial from a physiological point of view given that Fe(III)-citrate is a prime target for iron chelators in human serum at pH = 7.4, in addition to the fact that an assessment that take into consideration the iron transfer mechanism from citrate to DFOB on the adsorption kinetics and isotherms has not been sufficiently addressed in the literature. The kinetic data will be analyzed according to the relevant adsorption kinetic models; the pseudo first-order model or Lagergren's equation (Lagergen, 1898), the pseudo second-order model (Ho et al., 1996; Ho and McKay, 1999) and Elovich's model (Elovich and Larinov, 1962). Additionally, given the apparent importance of the initial solute amounts relative to the adsorption sites on the kinetic order of the reaction, the adsorption of iron on DFOB-polystyrene will be investigated under different initial Fe(III): surface DFOB concentration ratios. As for equilibrium studies, the Langmuir (Langmuir, 1918) and Freundlich (Freundlich, 1907) models will be used to describe the experimental data. The findings of these studies can potentially prove beneficial for the design of DFOB-based biomedical devices concerned with the detection or removal of iron from serum.

3.3 Materials and Methods

3.3.1 Developing the Kinetics Profiles and Sorption Isotherms for the Adsorption of Citrate-Bound Fe(III) on DFOB-Functionalized Beads

In order to obtain the kinetic data of citrate-bound Fe(III) adsorption on DFOB-activated latex beads, microspheres with a similar SH coverage of approximately 25% were coupled to PDS-DFOB solutions prepared under a constant DFOB: SPDP ratio of 5:1 and PDS: Surface SH ratio of 60:1 (DFOB activation of beads detailed in Chapter 2 - Sections 2.3.1 thorough 2.3.5 and **Scheme 2.9**). Moreover, Fe(III)-citrate solutions in HEPES (2 mM HEPES, 150 mM NaCL, pH = 7.4) were prepared using a constant citrate: iron ratio of 100:1 and different Fe(III) concentrations of 37.5, 75, 150 and 300 μM (Iron-citrate preparation detailed in Chapter 2 - Section 2.3.8). Later on, 1 mL of these iron solutions were introduced in the tubes, followed by an immediate suspension of the beads by vortexing. Each tube contained 10 mg of DFOB-activated beads, corresponding to a dosage of adsorbent X value of 10 g/L. The tubes were mixed under gentle end-over-end rotation at room temperature for the entirety of the experiments. Iron samples were collected from each tube after 15, 30, 60, 120 and 180 minutes of the start of the reaction. At each iron extraction time, the tubes were centrifuged for 5 minutes, then a 100 μL supernatant volume was withdrawn and the tubes were immediately vortexed and returned back to the end-over-end rotator. Given that centrifuging the beads limited their contact with the iron solution to the relatively small solid-liquid interface, the 5 minutes centrifugation time was not considered as part of the reaction time. The 100 μL supernatants were subsequently centrifuged for another 8 minutes, and 50 μL volumes were withdrawn for iron testing while the remaining portion was returned back to the tubes (details on iron measurement in Chapter 2 - Section 2.3.9). The amount of iron adsorbed on the beads was determined as the difference

between the initial total iron amount and that remaining in the supernatant. All the tubes were prepared in triplicates, except for the iron concentration of 150 μM due to the reasons presented in Section 3.4.1.

Although it was desirable to take more iron measurements at different time intervals, especially during the first minutes of the reaction, the complexities associated with centrifuging the beads and supernatants hindered that task. However, given the fact that equilibrium values were reached after 180 minutes or more, meant that the obtained data points were useful in developing the kinetic profiles.

On the other hand, developing the sorption isotherms of Fe(III) uptake on DFOB-activated beads was achieved by measuring the equilibrium coverage of iron on the beads' surface q_e ($mg_{adsorbate}/g_{adsorbent}$) after a sufficient contact time at room temperature. It is worth noting that iron was bounded to the surface as Ferrioxamine (FO), which we measured its concentration according to the assay described in (Chapter 2 - Sections 2.3.14 and 2.3.15). The same tubes and iron concentrations used to develop the kinetic profiles were employed to determine the equilibrium coverage at different iron concentrations (37.5, 75, 150 and 300 μM). Additionally, the equilibrium coverage under an initial iron concentration of 20 μM was also investigated.

Finally, the non-linear forms of the kinetics and adsorption models were used to analyze the experimental data and obtain the relevant parameters. This was achieved using the non-linear least squares method on MATLAB R2016b. The linearization of the models' equations was avoided given this method's perceived distortive effects on the experimental data (Kumar and Sivanesan, 2006; Lin and Wang, 2009; Moussout et al., 2018).

3.3.2 Fe(III) Chelation under Immobilized and Free (DFOB)

The effects of immobilizing DFOB on the rate of ferrioxamine (FO) formation was investigated by comparing it to that of free DFOB in solution. For that purpose, we prepared Fe(III)-citrate-HEPES (2 mM HEPES, 150 mM NaCL, pH = 7.4) solutions, having a citrate: iron ratio of 100:1 and different Fe(III) concentrations of 37.5, 75, 150 and 300 μM. Subsequently, a 0.006 M DFOB in HEPES solution was added to the iron mixture, yielding a 37.5 μM DFOB concentration and raising the total volume of the solution to 40 mL. This added DFOB amount was chosen since it is close to the amount of DFOB deposited on the beads surface (on 1 mL supernatant basis), while the iron concentrations were the same as those used in the kinetics and equilibrium study in the previous section. The absorbance of FO was immediately tracked at 450 nm after the addition of DFOB, while the different iron-citrate solutions were used as blanks.

3.4 Results and Discussion

3.4.1 Fitting of Kinetics Models to Experimental Data

The kinetic profiles for the citrate-bound Fe(III) adsorption on DFOB-activated polystyrene beads (initial SH coverage ≈ 25%, dosage of adsorbent X=10 g/L , DFOB: SPDP molar ratio of 5:1, PDS: Surface SH ratio of 60:1) were obtained under different initial iron concentrations of 37.5, 75, 150 and 300 μM at 15, 30, 60, 120 and 180 minutes. The developed experimental data were subsequently analyzed in light of the mathematical expressions relating the adsorbed amounts of solutes $q_t(mg_{Fe(III)}/g_{adsorbent})$ and time t (min) provided by the three widely used kinetic models of adsorption listed below. These models have been tested due to their extensive

use in literature to describe the kinetic profiles for the adsorption of solutes in liquids on solid adsorbents:

1. Pseudo first-order model or Lagergren's equation (Lagergen, 1898)
2. Pseudo second-order model (Ho et al., 1996, Ho and McKay, 1999)
3. Elovich's model (Elovich and Larinov, 1962)

Figure 3.1 presents the increase of the adsorbed amounts of Fe(III) on DFOB-activated beads ($q_t\ mg_{Fe(III)}/g_{adsorbent}$) with time ($t\ min$) under the initial iron concentrations of 37.5, 75, 150 and 300 μM. It can be noticed that the q_t values under 37.5 and 75 μM seemed to progress consistently with time. This was not case under higher initial iron concentrations (150 and 300 μM), with widely fluctuating and even physically impossible readings (negative q_t value at 15 min for 150 μM) at successive time intervals. Consequently, the kinetic profiles for 150 and 300 μM were not deemed adequate for our kinetic study, thus no further experiments on the 150 μM beads were performed, and our investigation was restricted to the 37.5 and 75 μM profiles (tubes were prepared in triplicates). We expect that the observed inconsistencies and "noise" in measuring high Fe(III) concentrations (150 and 300 μM) can be attributed to the inadequacy of the QuantiChrom™ Iron Assay Kit (Bioassay Systems, Hayward, CA) at providing reliable readings at those ranges.

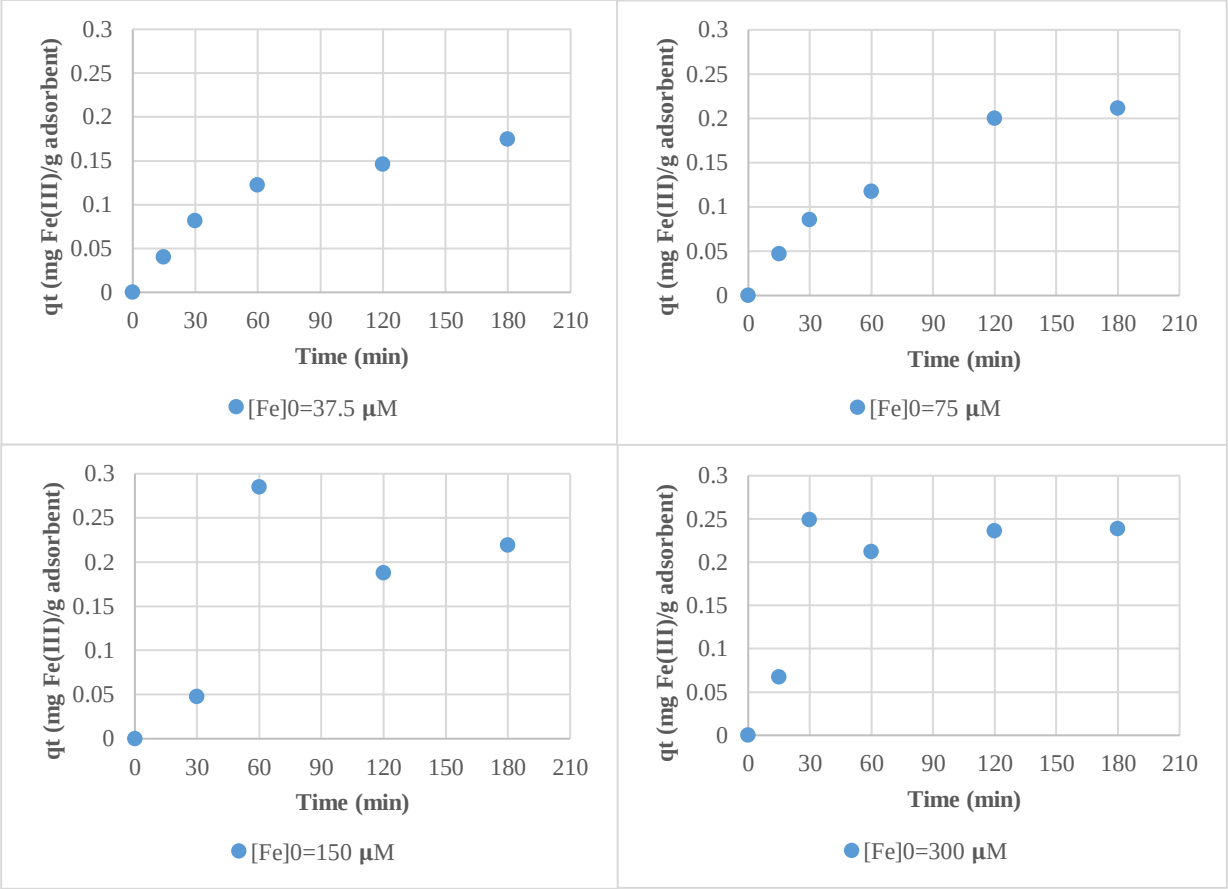

Figure 3.1 Experimental iron coverage of beads qt (mg Fe(III)/g adsorbent) in function of time (min) for 37.5, 75, 150 and 300 µM

Subsequently, the obtained kinetic data of 37.5 and 75 µM were studied in light of the three proposed models above. These kinetic studies can help in designing biomedical devices tailored for a specific therapeutic application based on the rate of iron removal from biological fluids. More particularly, if that DFOB-based biomedical device is developed for the purpose of the extracorporeal chelation of iron, knowing its rate of iron removal from biological fluids and studying it in light of the iron transport rate between the body's different iron pools (such as plasma iron and ferritin iron), can help physicians in determining its efficiency in targeting a particular iron source and the subsequent physiological implications of the new iron distribution (Ambrus et al., 1987; Anthone et al., 1995). Moreover, given the DFOB's non-selective binding

of metals and its resulting health risks (Genc et al.,2016), comparing the rate of iron chelation of a specific device to that of other metals, can possibly assist researchers in optimizing the design's parameters in a way that minimizes the chelation of non-iron metals. That study can also prove beneficial in developing iron-sensing or separation devices that operate in metal-rich environments.

In this study, the following kinetics models were investigated:

1. Pseudo first-order model or Lagergren's equation (Lagergen, 1898)

First introduced in 1898 (Lagergen, 1898), the Lagergen is the earliest known equation describing liquid-solid phase adsorption systems and relating the adsorption rate to the adsorption capacity (Ho, 2006). This equation has been extensively used in the literature to describe a wide range of sorption mechanisms, varying from Cr (VI) adsorption on fly ash/wollastonite (Panday et al., 1984), Fe(II) on wollastonite (Singh et al., 1998), to Ni (II) on China clay (Sharma et al., 1990).

As summarized by Largitte and Pasquier (2016), this kinetic model is based on the following assumptions:

a- Sorption of solutes occurs on specific localized sites.

b- No interaction between the sorbed solutes.

c- Maximum adsorption is defined by a saturated mono-layer of adsorbates on the adsorbent surface.

d- No dependency of adsorption energy on surface coverage

e- The concentration of the adsorbate is considered constant in the solution

f- The uptake of the solute on the adsorbent follows a first-order reaction rate

The Lagergen Equation is:

$$\frac{dq_t}{dt} = k_1(q_e - q_t) \text{ (3.4)}$$

With k_1 as the kinetic constant of the pseudo first-order adsorption (min^-), q_e and q_t in ($mg_{Fe(III)}/g_{adsorbent}$) representing the amounts of adsorbed Fe(III) on the beads at equilibrium and time t (min), respectively.

After integrating Equation (3.4) with the following boundary conditions:

$$t = 0, q_t = 0 \; and \; t = t, q_t = q_t$$

The linearized form of the Lagergen's equations can be obtained:

$$\ln(q_e - q_t) = lnq_e - k_1 t \text{ (3.5)}$$

While the non-linear equation relating q_t and t is:

$$q_t = q_e(1 - e^{-k_1 t}) \text{ (3.6)}$$

2. Pseudo second-order model (Ho et al., 1996), (Ho and McKay, 1999)

Developed in 1996 by Ho et al. (1996), the pseudo second-order model was able to accurately describe a broad range of liquid-solid adsorption systems such as Cd (II) adsorption on hydrous ferric oxide (Dzombak and Morel, 1986), Cr (VI) on peat (Sharma and Forster, 1993) and Pb (II) on peat (Ho and McKay, 1998).

The assumptions made in this model are almost the same as the ones presented above for the Lagergen's model, except that the solute uptake is governed by a second-order rate equation (Largitte and Pasquier, 2016).

The kinetic rate equation of the pseudo second-order model is:

$$\frac{dq_t}{dt} = k_2(q_e - q_t)^2 \quad (3.7)$$

With k_2 as the kinetic constant of pseudo second-order adsorption ($g/mg.min$), q_e and q_t in ($mg_{Fe(III)}/g_{adsorbent}$) representing the amounts of adsorbed Fe(III) on the beads at equilibrium and time t (min), respectively.

After integrating and rearranging equation (3.7), we obtain the linearized form of the equation:

$$\frac{t}{q_t} = \frac{1}{k_2 q_e^2} + \frac{t}{q_e} \quad (3.8)$$

While the non-linear equation relating q_t and t can be expressed as:

$$q_t = \frac{k_{q_e^2}2t}{1 + q_e k_2 t} \quad (3.9)$$

3. Elovich's model (Elovich and Larinov, 1962)

First established in 1934 by Zeldowitsch (1934) to model the adsorption (chemisorption) of carbon monoxide on manganese dioxide, the equation has been used in the following years to successfully describe the adsorption of pollutants from aqueous solutions on solid adsorbents (Fierro et al., 2008). Largitte and Pasquier (2016) presented the assumptions that this model relies on:

a- Sorption of solutes occurs on specific localized sites.

b- The sorbed solutes interact together.

c- The adsorption energy increases linearly with the surface coverage.

d- The concentration of the adsorbate is considered constant in the solution.

e- The solute uptake on the adsorbent is negligible before the exponential (i.e. the solute uptake is governed by a zero order rate equation).

The non-linear equation relating q_t and t can be expressed as:

$$q_t = \frac{1}{b}\ln(1 + abt) \quad (3.10)$$

In later years, Chien and Clayton (1980) simplified the equation by assuming $1 \ll abt$, thus obtaining:

$$q_t = \frac{1}{b}\ln(abt) \quad (3.11)$$

With a as the initial adsorption rate $(mg/g.min)$, and b in (g/mg) is the parameter related to the number of sites available for adsorption on the solid. As in the previous equations, q_t in $(mg_{Fe(III)}/g_{adsorbent})$ represents the amounts of adsorbed Fe(III) on the beads at time (min). **Figure 3.2** and **3.3** show the non-linear fitting of the pseudo first-order equation (3.6), pseudo second-order equation (3.9) and Elovich equation (3.10) relating q_t $(mg_{Fe(III)}/g_{adsorbent})$ and time (min) to the kinetic data at 37.5 and 75 μM. **Table 3.2** presents the values of the kinetic parameters and the corresponding correlation coefficients R^2 for the three different models.

As can be seen in **Table 3.2**, the correlation coefficients R^2 for all three models were very similar under the investigated initial iron concentrations of 37.5 and 75 **μ**M. Consequently, a firm conclusion regarding the suitability of a particular model cannot be statistically made based on these values (Liu and Wang, 2008). Moreover, it is worth noting that all three models have relatively high R^2 values under both investigated initial iron concentrations, indicating their convenient fitting to the experimental data. Despite the inconclusiveness of these kinetics

modelling results, the equilibrium isotherm study presented in Section 3.4.2 in which it is expected that the Langmuir isotherm model will offer the best description of the adsorption data, coupled with the mathematical models of Liu and Shen (2008) in Section 3.4.3, will allow us to relate the suitability of adsorption kinetics models (pseudo first and second-order models) to the system's parameters (such as: initial iron concentration, dosage of adsorbent and iron surface coverage). It is worth noting that some of the assumptions made in the Langmuir isotherm model, such as that the adsorption energy is constant and independent of the degree of sites' occupancy and that there are no interactions between the adsorbed molecules, are physically inconsistent with the assumptions presented in the Elovich kinetic model, but consistent with those put forward in the pseudo first and second-order models.

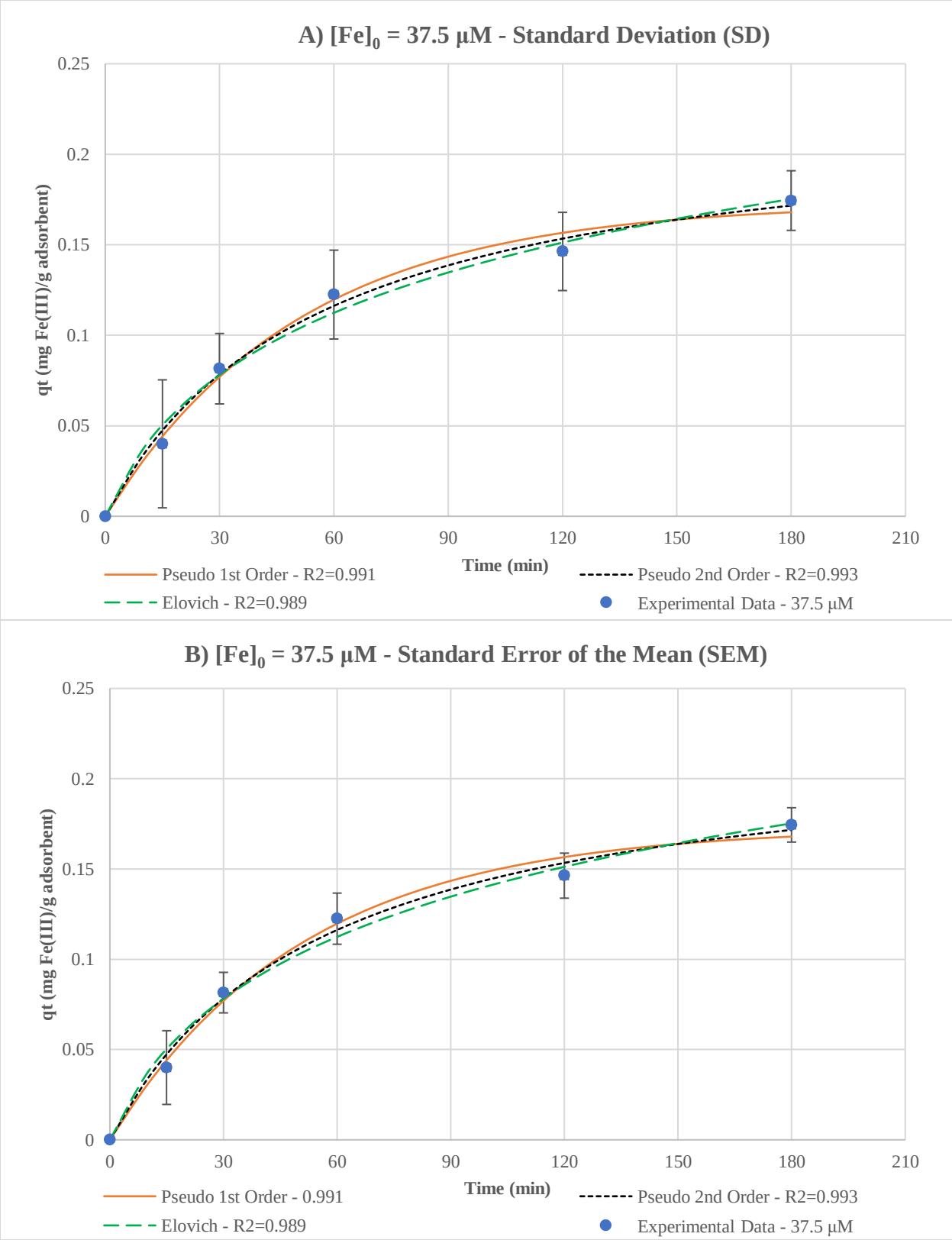

Figure 3.2 Iron coverage on beads qt (mg Fe(III)/g adsorbent) in function of time (min) for 37.5 µM as predicted by three different adsorption kinetics models. Number of samples (n=3)

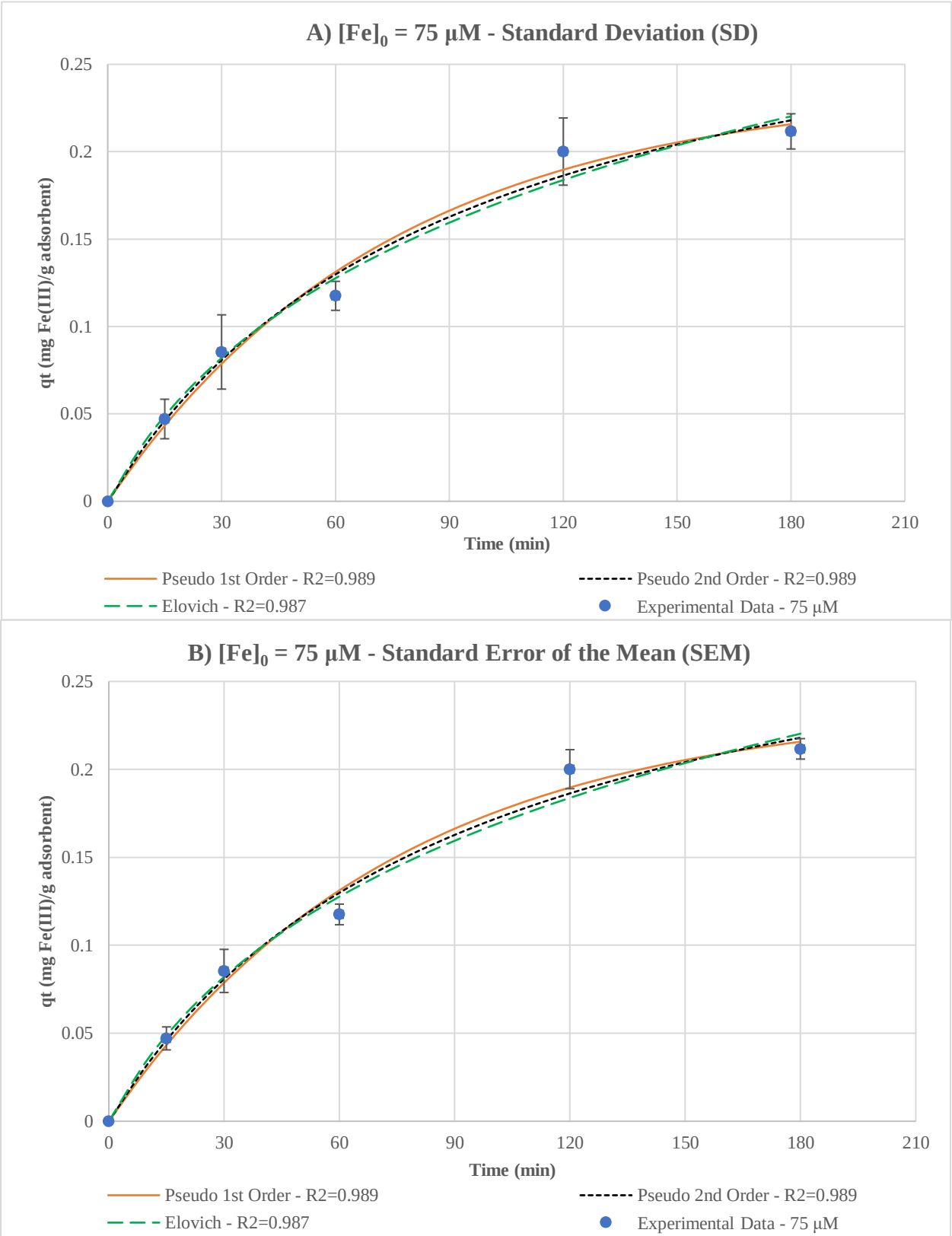

Figure 3.3 Iron coverage on beads qt (mg Fe(III)/g adsorbent) in function of time (min) for 75 µM as predicted by three different adsorption kinetics models. Number of samples (n=3)

Table 3.1 Kinetic parameters of the three investigated models

Pseudo First-order Model Parameters			**Pseudo Second-Order Model Parameters**			**Elovich Model Parameters**		
37.5 µM			**37.5 µM**			**37.5 µM**		
qe (mg/g)	**k_1 (min^-)**	**R^2**	**qe (mg/g)**	**k_2 (g/mg.min)**	**R^2**	**a (mg/g.min)**	**b (g/mg)**	**R^2**
0.173	0.020	0.991	0.225	0.079	0.993	0.005	15.5	0.989
75 µM			**75 µM**			**75 µM**		
qe (mg/g)	**k_1 (min^-)**	**R^2**	**qe (mg/g)**	**k_2 (g/mg.min)**	**R^2**	**a (mg/g.min)**	**b (g/mg)**	**R^2**
0.237	0.013	0.989	0.330	0.033	0.989	0.004	9.5	0.987

3.4.2 Fitting of Adsorption Models to Experimental Data

Developing the sorption isotherms of Fe(III) uptake on DFOB-activated beads (initial SH coverage ≈ 25%, dosage of adsorbent X=10 g/L , DFOB: SPDP molar ratio of 5:1, PDS: Surface SH ratio of 60:1) at room temperature was achieved by measuring the equilibrium coverage of iron on the beads' surface after a sufficient contact time at different iron concentrations of 20, 37.5, 75, 150 and 300 μM via the ferrioxamine detection method (Chapter 2 - Sections 2.3.14 and 2.3.15).

The developed sorption isotherms will be analyzed according to the adsorption models' non-linear equations relating the equilibrium coverage values q_e in $(mg_{Fe(III)}/g_{adsorbent})$ and the equilibrium concentration of the adsorbate in solution after adsorption C_e in $(mg_{Fe(III)}/L)$. Knowing the maximum amount of iron that can be adsorbed on the surface and the time scale of that iron chelation can dictate the engineering and design aspects of the DFOB-based biomedical device. These aspects can include the required surface size for a particular application, DFOB surface density, support manufacturing and bioconjugation strategies, among other considerations.

The investigated adsorption models are:

1. Langmuir Isotherm (Langmuir, 1918)
2. Freundlich Isotherm (Freundlich, 1907)

It is worth noting that according to Rudzinski and Plazinski (2007), most adsorption isotherm equations are based on modifications of the classical Langmuir equation.

1. Langmuir Isotherm (Langmuir, 1918)

According to Gimbert et al. (2008) and Fierro et al. (2008), the Langmuir isotherm make the following assumptions:

a- The adsorbed layer is a monolayer

b- Adsorption occurs on specific homogenous sites on the adsorbent

c- Every adsorption site can be occupied by one adsorbate

d- Adsorption energy is constant and independent of the degree of sites' occupancy

e- No interactions between the adsorbed molecules

f- The surface reaction is the limiting reaction step

g- The adsorbent is of homogenous structural nature

h- The adsorbent has a finite capacity for the adsorbate

The linear Langmuir equation is (3.12):

$$\frac{C_e}{q_e} = \frac{1}{K_L q_{max}} + \frac{C_e}{q_{max}} \quad (3.12)$$

With C_e in $(mg_{Fe(III)}/L)$ as the equilibrium concentration of the adsorbate Fe(III) in solution after adsorption, q_e in $(mg_{Fe(III)}/g_{adsorbent})$ as the equilibrium coverage value of Fe(III) on DFOB-beads, K_L as the Langmuir constant related to the adsorption energy $(L/mg_{Fe(III)})$ and q_{max} in $(mg_{Fe(III)}/g_{adsorbent})$ as the maximum uptake of Fe(III) on the DFOB-activated beads.

While the non-linear Langmuir equation relating q_e to C_e is:

$$q_e = \frac{q_{max} K_L C_e}{(1 + K_L C_e)} \quad (3.13)$$

2. Freundlich Isotherm (Freundlich, 1907)

The Freundlich isotherm assumes that the adsorption occurs on a heterogeneous surface, with a multilayer adsorption mechanism. Additionally, it is assumed that the adsorbed amount increases with the concentration following equation (3.14):

$$q_e = K_F\, C_e^{\frac{1}{n}} \quad (3.14)$$

With C_e in $(mg_{Fe(III)}/L)$ as the equilibrium concentration of the adsorbate Fe(III) in solution after adsorption, q_e in $(mg_{Fe(III)}/g_{adsorbent})$ as the equilibrium coverage values of Fe(III) on DFOB-beads, K_F as the Freundlich constant related to the adsorption capacity in $(mg/g.\left(\frac{mg}{L}\right)^n)$ and $(\frac{1}{n})$ as the heterogeneity factor.

The linear form of equation (3.14) can be written as (3.15):

$$log q_e = \log K_F + \frac{1}{n} log C_e \quad (3.15)$$

Figure 3.4 shows the non-linear fitting of the Langmuir equation (3.13) and the Freundlich equation (3.14) relating q_e $(mg_{Fe(III)}/g_{adsorbent})$ and C_e $(mg_{Fe(III)}/L)$ to the adsorption data. **Table 3.2** presents the values of the adsorption parameters and the corresponding correlation coefficients R^2 for both models.

It can be noticed from **Table 3.2** that the correlation coefficient obtained for the Langmuir isotherm model ($R^2 = 0.992$) is closely similar to that of the Freundlich model ($R^2 = 0.953$). Consequently, we can realize the need for more replicates to minimize the experimental variability of the data. Despite the similar R^2 values of both models, we can expect that the Langmuir model will offer the best fit for the data given that many of its underlying physical

assumptions are consistent with the physics governing the adsorption of Fe(III) on DFOB-activated beads:

a- The adsorbed layer (FO) is a monolayer *(expected)*

b- Adsorption occurs only on DFOB molecules *(expected)*

c- Every DFOB molecule can bind only one Fe(III) atom *(expected)*

d- Adsorption energy is constant and independent of the degree of sites' occupancy

e- No interactions between the adsorbed molecules

f- The surface reaction is the limiting reaction step

g- The adsorbent is of homogenous structural nature

h- The adsorbent has a finite capacity for the adsorbate *(expected)*

Additionally, as shown in **Table 3.2**, the obtained Langmuir parameters were K_L = 12.81 ($L/mg_{Fe(III)}$) and q_{max} = 0.206 ($mg_{Fe(III)}/g_{adsorbent}$), corresponding to 3.7 x 10^{-3} ($mmoL_{Fe(III)}/g_{adsorbent}$), 0.036 ($mg_{Fe(III)}/m^2_{adsorbent}$), 6.5 x 10^{-4} ($mmoL_{Fe(III)}/m^2_{adsorbent}$) or 37 (μM Fe(III)$/aliquot$) (on 1 mL supernatant basis).

The suitability of the Langmuir model to describe to adsorption data of Fe(III) on immobilized DFOB has been confirmed by Alberti et al. (2015) and Biesuz et al. (2014). Comparing the maximum iron coverage value q_{max} in this work of 3.7 x 10^{-3} $mmoL_{Fe(III)}/g_{adsorbent}$ to that reached by Alberti et al. (2015) after immobilizing DFOB to filter papers (q_{max} = 4 x 10^{-2} $mmoL_{Fe(III)}/g_{adsorbent}$) and those reported by Biesuz et al. (2014) after binding DFOB to SAMMMS (q_{max} = 1.4 x 10^{-1} and 6 x 10^{-2} $mmoL_{Fe(III)}/g_{adsorbent}$ for MCM-41 and MSU-H types, respectively), we can notice that our reported maximum iron coverage, per unit mass of adsorbent, is between 1 to 2 orders of magnitude lower than the values reported in literature.

However, this discrepancy can be upset once the iron coverage is assessed based on the surface area of the support; the non-porous polystyrene beads used in our work have a specific surface area of 5.7 $m^2/g_{adsorbent}$, while the porous supports used by Biesuz et al. (2014) have a reported surface area of 10^3 m^2/g for MCM-41 and 7.6 x 10^2 m^2/g for MSU-H. It follows that, calculating the maximum iron coverage based on unit area of support, we can deduce that the value of 6.5 x 10^{-4} $mmoL_{Fe(III)}/m^2_{adsorbent}$ reached in this work, favorably compares to those reported by Biesuz et al. (2014) at 1.4 x 10^{-4} $mmoL_{Fe(III)}/m^2$ for MCM-41 and 7.9 x 10^{-5} $mmoL_{Fe(III)}/m^2$ for less porous MSU-H. It is worth nothing that Biesuz et al. (2014) were able to optimize their immobilization process on MCM-41 and increase the maximum iron coverage to q_{max} = 3.3 x 10^{-1} $mmoL_{Fe(III)}/g_{adsorbent}$, which corresponds to 3.3 x 10^{-4} $mmoL_{Fe(III)}/m^2$ of support. Additionally, Wenk et al. (2001) coupled DFOB to different cellulose matrices for the chelation of Fe(III)-citrate and $FeSO_4$. The authors were able to bind 2 x 10^{-2} to 1 x 10^{-1} mmoL of DFOB to 1 gram of difference cellulose fabrics. These values corresponded to approximately 20 mmoL of DFOB per m^2 of cellulose dressing. Since more than 90% of the immobilized DFOB were able to chelate iron species after enough reaction time, we can deduce that the q_{max} values reached in that work, in terms of both adsorbent mass and surface area, are substantially higher than our reported values.

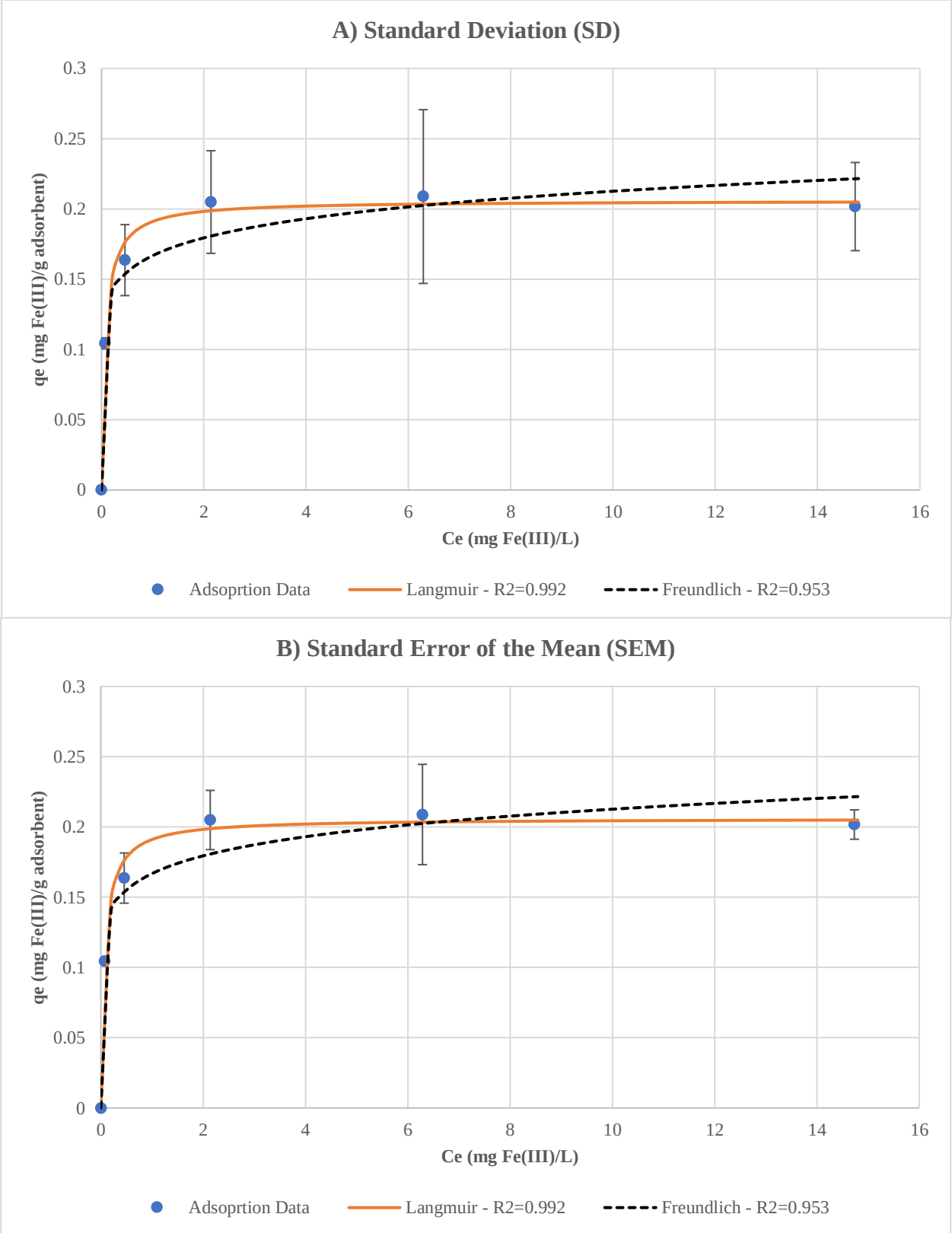

Figure 3.4 Equilibrium iron coverage on beads qe (mg Fe(III)/g adsorbent) in function of equilibrium iron concentration in solution (mg Fe(III)/L) as predicted by the Langmuir and Freundlich adsorption models

Table 3.2 Parameters of the Langmuir and Freundlich adsorption models

Langmuir Model			**Freundlich Model**		
qmax (mg/g)	**K_L (L/mg)**	**R^2**	**K_F (mg/g(mg/L)^n)**	**n**	**R^2**
0.206	12.81	0.992	0.167	9.483	0.953

3.4.3 Adsorption Kinetics and Dependency on Initial Fe(III) Concentrations

Our investigation of the adsorption kinetics of citrate-bound Fe(III) on DFOB-activated beads (initial SH coverage ≈ 25%, dosage of adsorbent X=10 g/L , DFOB: SPDP molar ratio of 5:1, PDS: Surface SH ratio of 60:1) in Section 3.4.1 did not yield a firm conclusion on the suitability of a particular adsorption kinetic model to describe the kinetics data. This was due to the similar values of the correlation coefficients R^2 for all three models.

In Section 3.4.2, it was expected that the Langmuir isotherm is the best fitting adsorption model for our liquid-solid system, with K_L = 12.81 (L/mg) and q_{max} = 0.206 $(mg_{Fe(III)}/g_{adsorbent})$ = 37 μM Fe$(III)/aliquot$ (on 1 mL supernatant basis). This conclusion was in agreement with that of Alberti et al (2015) and Biesuz et al. (2014).

Investigating the reaction order of Fe(III)-citrate chelation by DFOB in solution, Ito et al. (2011) reported that under equimolar initial concentrations for DFOB and Fe(III), the reaction followed a second-order rate law with rate constants $k_{overall}$ = 34 to 232 $M^{-} s^{-}$ for citrate: iron ratios of 500 to 5000:1, respectively. These findings were previously reported by Faller and Nick (1994); in their investigation of the kinetics laws governing the chelation of Fe(III)-citrate by DFOB in solution, and using a fixed citrate: iron ratio of 5:1, the authors found that under equimolar initial concentrations for DFOB and Fe(III), the experimental data were well described by the second-order rate law, with a k_2 value of 1.58 x 10^{-3} $OD^{-} s^{-}$ (OD: measured absorbance). However, after increasing the initial concentration of DFOB by 10-fold relative to that of iron, a shift of reaction rate law from a second-order to a pseudo first-order one was observed, with a rate constant k_1= 4 x 10^{-3} s^{-}. This can be ascribed to the fact that the concentration change of DFOB throughout the

reaction was negligible compared to that of Fe(III), thus the second-order rate equation governing the formation of ferrioxamine (3.2) can be simplified to a pseudo first-order one (3.3).

On the other hand, previous researchers have studied the kinetics of Fe(III) chelation by DFOB-activated supports. Alberti et al. (2015) showed that the uptake of iron in KNO_3 solution on paper-immobilized DFOB was best described by the pseudo first-order kinetic equation with rate constants $k_1 = 0.030$ and 0.23 min^{-}, while equilibrium concentrations were reached within 150 or 30 minutes, depending on the used support. Additionally, Biesuz et al. (2014) also showed that the chelation of Fe(III) in KNO_3 by DFOB-SAMMS followed the pseudo first-order model with $k_1 =$ 0.048 min^{-} and 0.043 min^{-} for MCM-41 and MSU-H types, respectively, while it was noted that the equilibrium was reached within 200 minutes. It is very important to note that, according to the data presented in that work, it can be concluded that these kinetics experiments were carried out under high excess of DFOB relative to Fe(III).

Given the apparent effect of the initial DFOB: Fe(III) concentration ratio on the order of the chelation reaction in solutions, coupled with the findings of Azizian (2014) and Liu and Shen (2008) which showed that the suitability of either the pseudo first or second-order models can largely depend on the initial solute concentration among other factors, we were interested in determining the effects of initial solute concentration (Fe(III) in citrate) relative to the adsorption sites (surface DFOB) on the adsorption kinetics and the suitability of a given model.

In their highly cited work titled "*From Langmuir Kinetics to First- and Second-Order Rate Equations for Adsorption*", Liu and Shen (2008) showed that the Langmuir kinetics, can be transformed to a polynomial expression of varying-order rate equation, which relates the rate equations of the pseudo first and pseudo second-order kinetic models. Subsequently, they

proceeded to show how the Langmuir kinetics equation can be simplified to one of the two models, and how that simplifications under a constant given dosage of adsorbent, is dependent on the initial concentration of the adsorbate (the Fe(III) in our case).

In the following section, we will briefly go through the mathematical and theoretical basis of Liu and Shen's work (details of the mathematical derivations can be found in Liu and Shen (2008)). Additionally, we will present the details of the perceived adsorption kinetics dependency of our system on the initial concentration of Fe(III).

Liu and Shen (2008) started their mathematical derivations from the Langmuir adsorption reaction:

$$A + B \leftrightarrow AB \quad (3.16)$$

With A as the solute (Fe(III) in our work), B as the adsorption site (DFOB on the beads) and AB as the formed surface complex (ferrioxamine (FO)). Additionally, they defined $k_a$and k_d as the adsorption and desorption rate constants, respectively.

Knowing that r_a and r_d are the rates of adsorption and desorption, respectively, while C_t is the concentration of the adsorbate at time t and θ_t is the proportion of the surface occupied by the solutes at time t, the Langmuir kinetics equation can be written as:

$$\frac{d\theta_t}{dt} = r_a - r_d = k_a C_t(1 - \theta_t) - k_d\theta_t \quad (3.17)$$

Subsequently, the authors transformed equation (3.17) to a polynomial expression of varying-order rate equations that combines the kinetic equations of the pseudo first (3.4) *(1st Term in 3.18)* and pseudo second-order (3.7) *(2nd Term in 3.18)* models. The transformed Langmuir equation is (3.18):

$$\frac{d\theta_t}{dt} = k_1(\theta_e - \theta_t) + k_2(\theta_e - \theta_t)^2 \quad (3.18)$$

With (θ_e) as the equilibrium coverage fraction of the solutes on the surface.

After transforming the Langmuir kinetics equation (3.17) to the polynomial equation (3.18) that relates the equations of both kinetic models, the authors showed that equation (3.18) can be reduced to either the pseudo first (similar to 3.4) or pseudo second (similar to 3.7) -order rate equation under sufficient and necessary conditions. The authors subsequently showed that the conditions to reduce the Langmuir kinetics to either models are governed by the relative magnitude of $\frac{k_1}{k_2}$ over $\theta_{e_{Theoratical}}$, according to the following rules:

- If $\frac{k_1}{k_2} > \theta_{e_{Theoratical}}$ or $\left(\frac{k_1}{k_2}\right) \approx \theta_{e_{Theoratical}}$ => The derived Langmuir kinetics equation (3.18) reduces to the pseudo first-order model rate equation (similar to 3.4).

  The physical significance is that under these conditions, the initial concentration of one reactant is high enough compared to the other, that it can be assumed as constant throughout the reaction, which allows for the simplification of the second-order rate equation (similar to 3.2 and 3.7) to a pseudo first-order one (similar to 3.3 and 3.4), thus the pseudo first-order model can offer a better fit to the kinetics data.

- If $\frac{k_1}{k_2} << \theta_{e_{Theoratical}}$ => The derived Langmuir kinetics equation (3.18) reduces to the pseudo second-order model rate equation (similar to 3.7).

  The physical significance is that under this condition, the initial concentrations of both reactants are comparable, thus the second-order rate equation must be applied since it strongly depends on both concentrations and cannot be reduced to the pseudo first-order

one. Consequently the pseudo second-order model can offer a better fit to the kinetics data.

- If neither conditions are satisfied, the derived Langmuir kinetics equation (3.18) cannot be simplified to one order or another, and has a varying reaction order of 1 – 2.

The authors then proceeded to calculate $\left(\frac{k_1}{k_2}\right)$ (3.19):

$$\frac{k_1}{k_2} = \frac{\sqrt{K_L^2(C_0 - q_{max}X)^2 + 2K_L(C_0 + q_{max}X) + 1}}{K_L q_{max} X} \quad (3.19)$$

And θ_e (theoretical) used for the conditions (3.20):

$$\theta_{e_{Theoratical}} = \frac{K_L(q_{max}X + C_0) + 1 - \sqrt{K_L^2(C_0 - q_{max}X)^2 + 2K_L(C_0 + q_{max}X) + 1}}{2K_L q_{max} X} \quad (3.20)$$

Since we experimentally obtained all the variables of equations (3.19) and (3.20) in Section 3.4.2, we can proceed to plot $\frac{k_1}{k_2}$ and $\theta_{e_{Theoratical}}$ in function of C_0 (initial Fe(III) concentration) and determine the ranges of applicability of the conditions defined above.

Figure 3.5 shows $\frac{k_1}{k_2}$ and $\theta_{e_{Theoratical}}$ in function of C_0 (concentrations will be presented in μM Fe(III) not mg Fe(III)/L for reading convenience). **Table 3.3** presents the values of $\frac{k_1}{k_2}$, $\theta_{e_{Theoratical}}$, $\theta_{e_{Experimental}}$ and $(\theta_{e_{Theoratical}} - \frac{k_1}{k_2})$ at different initial iron concentrations.

As seen in **Figure 3.5** and presented in **Table 3.3**, for an initial iron concentration of 300 μM, the value of $\frac{k_1}{k_2} = 7.18$ is substantially higher than $\theta_{e_{Theoratical}} = 0.99$. Thus the Langmuir kinetics equation can be reduced to the pseudo first-order reaction rate. This prediction seems reasonable, since the maximum experimental iron coverage on the beads was found to be q_{max} = 37 μM

$\mathrm{Fe}(III)/aliquot$ (on 1 mL supernatant basis), which indicates the original presence of 37 μM active DFOB$/aliquot$. (DFOB and Fe(III) react on 1:1 molar basis). It follows that, adding a 1 mL of 300 μM iron solution to the beads will lead to a large excess of Fe(III) relative to the immobilized DFOB. Consequently, it can be assumed that the concentration of iron will remain constant throughout the reaction, and the second-order rate equation governing the formation of ferrioxamine can be reduced to a pseudo first-order one that is solely dependent on the varying DFOB concentration.

The pseudo first-order model is also applicable when the DFOB on the beads exists in a relative excess to the amount of Fe(III) in solution. As can be seen in **Figure 3.5**, for very low initial iron concentrations (such as 3 μM), the value of $\frac{k_1}{k_2}$ is substantially higher than $\theta_{e\,Theoratical}$ and the DFOB amount is approximately 10-fold that of Fe(III). Consequently, the concentration of DFOB can be assumed as constant throughout the reaction, and the second-order rate equation of ferrioxamine formation (similar to 3.2) can be reduced to a pseudo first-order one that is only dependent on Fe(III) concentration (similar to 3.3). The suitability to approximate the ferrioxamine formation rate by a pseudo first-order equation under large DFOB to Fe(III) excess has been previously reported in solution by Faller and Nick (1994) and in liquid-solid adsorption systems by Biesuz et al. (2014) and Alberti et al (2015).

Conversely, for an initial iron concentration of 37.5 μM (similar to our kinetic experiments), which is almost identical to the amount of DFOB on an aliquot of beads (37 μM active DFOB$/aliquot$), we can notice from **Figure 3.5** that the value of $\frac{k_1}{k_2}$ is lower than $\theta_{e\,Theoratical}$ (0.39 Vs 0.83, respectively). This in turn suggests that, given the comparable concentrations of both species, the second-order rate equation cannot be reduced to a pseudo first-order one, since

it will depend on the concentrations of both DFOB and Fe(III) (similar to 3.2). Ito et al (2011) and Faller and Nick (1994) reported that the rate of iron chelation in solution was governed by the second-order rate law when initial equimolar amounts of DFOB and iron were reacted.

Moreover, it can be observed from **Figure 3.5** that for most initial concentrations, $\frac{k_1}{k_2}$ was larger or close to $\theta_{e\,Theoratical}$, suggesting that the pseudo first-order model can describe the adsorption kinetics of Fe(III) on our prepared DFOB-beads for most initial Fe(III) concentrations. It is very important to note that the developed $\frac{k_1}{k_2}$ and $\theta_{e\,Theoratical}$ values are specific to our prepared beads, and can change according to the dosage of adsorbent and DFOB loading on the beads.

The authors also presented the equations for the intersection points of $\frac{k_1}{k_2}$ and $\theta_{e\,Theoratical}$ and defined them as C_{0Low} and C_{0High} (shown on **Figure 3.5)**. It follows that if $C_0 \leq C_{0Low}$ or $C_0 \geq C_{0High}$, $\frac{k_1}{k_2}$ will be larger or equal than $\theta_{e\,Theoratical}$, thus the Langmuir kinetics equation can be reduced to the pseudo first-order model; In our work, we calculated $C_{0Low} = 22$ μM and C_{0High}= 68 μM, again confirming that 37.5 μM is not described by the pseudo first-order reaction model.

Moreover, the authors defined $(\frac{k_1}{k_2})_{min}$, $C_{0\,critical}$ and $\theta_{e\,critical}$, which show the minimum value of $\frac{k_1}{k_2}$, and presents its corresponding C_0 and $\theta_{e\,Theoratical}$. In our work, we calculated $(\frac{k_1}{k_2})_{min} =$ 0.39 and we found that $C_{0\,critical}$ = 35 μM, which is understandably very close to the experimental coverage of active DFOB on the beads = 37 μM/aliquot (on 1 mL supernatant basis).

Finally, we can see that the adsorption kinetics governing the uptake of citrate-bound Fe(III) on our prepared DFOB-beads are directly dependent on the initial iron concentrations used. It was

found that at initial iron concentrations lower than 22 μM or higher than 68 μM, the adsorption kinetics can be largely described by the pseudo first-order model. As for initial concentrations close to 35 μM, the pseudo second-order model can possible offer the best fit for the data. Thus, although our kinetics modelling efforts in section 3.4.1 did not allow us to determine the best fitting model, we can expect based on the findings above that for an initial iron concentration of 37.5 μM, the pseudo second-order model should offer a better description of the adsorption data than the pseudo first-order one, while that situation is expected to be reversed for an initial iron concentration of 75 μM. It is worth noting that the results presented are specific for these particular DFOB-beads. Consequently, changing the dosage of adsorbents or the beads characteristics may significantly alter the reported parameters.

These results, coupled with the calculated parameters of this kinetic transition, can prove very helpful in designing and optimizing different engineering applications for immobilized DFOB based on the iron concentration of interest. For example, if our DFOB-activated beads are to be used for the extracorporeal chelation of non-transferrin bound iron (NTBI), we can expect that the reaction will follow a pseudo first-order reaction given that the concentration of chelatable iron in the blood will be less than 10 μM (Evans et al., 2008). Moreover, assessing the rates of iron chelation from biological fluids can help physicians in determining the resulting iron distribution among the different iron pools (Ambrus et al., 1987; Anthone et al., 1995). Additionally, comparing the rates of iron chelation relative to that of other metals can help to mitigate the health risks arising for the DFOB's non-selective binding of metals.

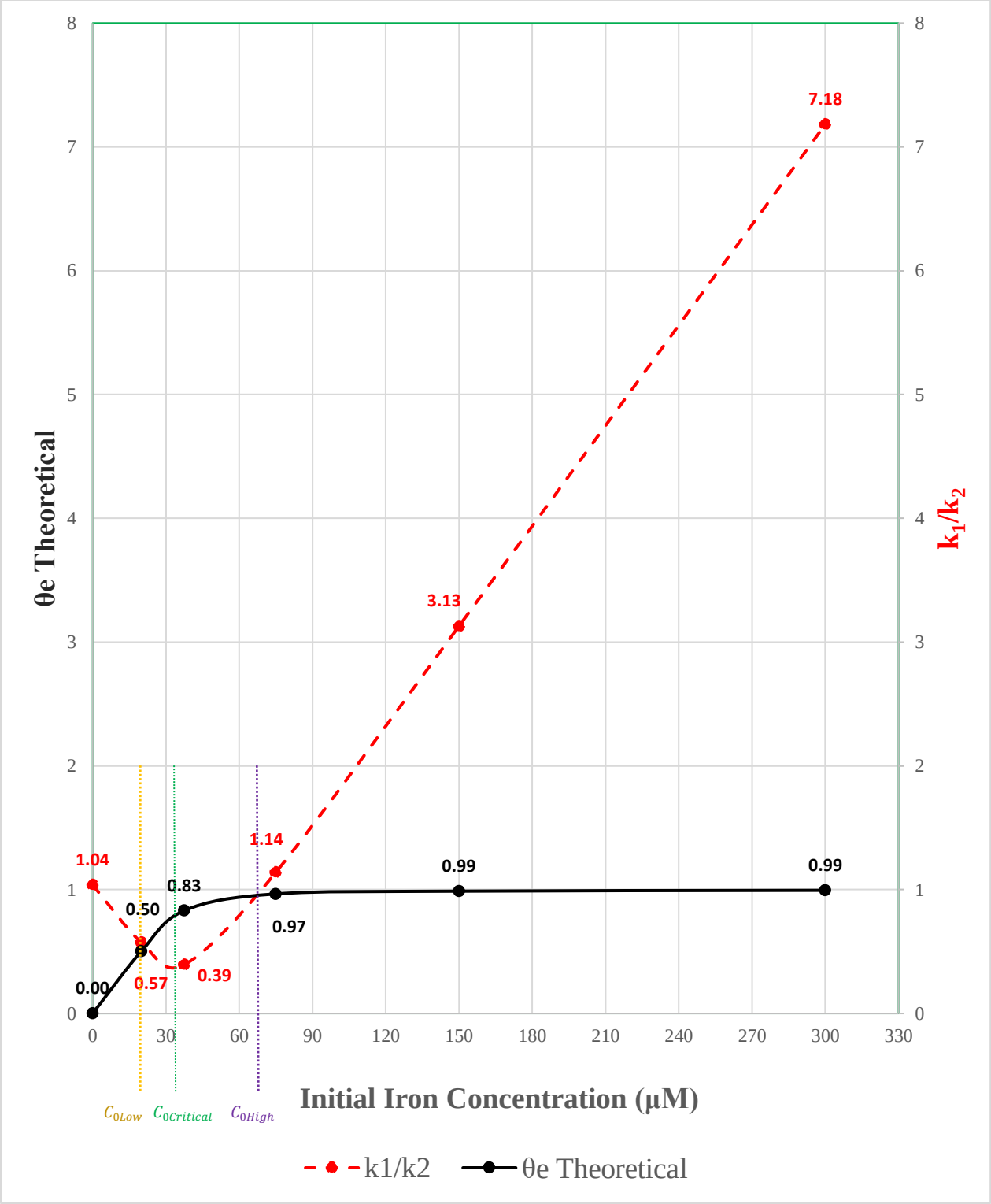

Figure 3.5 k_1/k_2 and θe Theoretical in function of initial iron concentration (µM) as predicted by equations (3.19) and (3.20), respectively. C_{0Low}, C_{0High} and $C_{0Critical}$ are shown on the graph.

Table 3.3 Parameters derived from the transformed Langmuir kinetics equation

Co (µM)	**θe Experimental**	**k_1/k_2**	**θe Theoretical**	**θ Theoretical - k_1/k_2**
0	0.00	1.04	0.00	-1.04
20	0.51	0.57	0.50	-0.07
37.5	0.79	0.39	0.83	0.44
75	0.99	1.14	0.97	-0.17
150	1.01	3.13	0.99	-2.14
300	0.98	7.18	0.99	-6.19
Co Critical (mg/l)	**θe Critical**	**k_1/k_2 min**	**Co Low (mg/L)**	**Co High (mg/L)**
2.0	0.91	0.39	1.2	3.8
Co Critical (µM)			**Co Low (µM)**	**Co High (µM)**
35			22	68

3.4.4 Fe(III) Chelation under Immobilized and Free (DFOB)

The effects of immobilizing DFOB on the rate of ferrioxamine (FO) formation was examined by comparing it to that of free DFOB in solution. **(Figure 3.6)** shows the formation of ferrioxamine (FO) with time under DFOB in solution with initial iron concentrations of 37.5, 75, 150 and 300 μM. Additionally, the figure shows the formation of FO under DFOB-activated beads for 37.5 and 75 μM iron concentrations. (DFOB-beads: Initial SH coverage ≈ 25%, DFOB: SPDP molar ratio of 5:1, PDS: Surface SH ratio of 60:1). It is worth noting that the kinetic profiles of FO under DFOB-activated beads for 150 and 300 μM were not included due to the fluctuating readings already discussed in previous parts of this chapter.

Comparing the kinetic profiles of FO formation under immobilized and free DFOB at 37.5 and 75 μM initial iron concentrations, we can easily notice that the equilibrium was reached significantly faster when DFOB in solution was used. Although under DFOB-activated beads (for $[Fe]_0 = 75$ μM,) the concentration of ferrioxamine eventually reached a value comparable to that achieved under DFOB in solution, the rate of formation was higher under free DFOB; 30 minutes were approximately needed for FO concentrations to reach equilibrium under DFOB in solution, while 180 minutes were needed under immobilized DFOB.

Consequently, we can conclude that immobilizing DFOB did not decrease the ability of the molecule to chelate iron, which was confirmed by the relatively high equilibrium value of ferrioxamine coverage on the beads. However, attaching the DFOB to the latex beads severely decreased the rate of iron chelation.

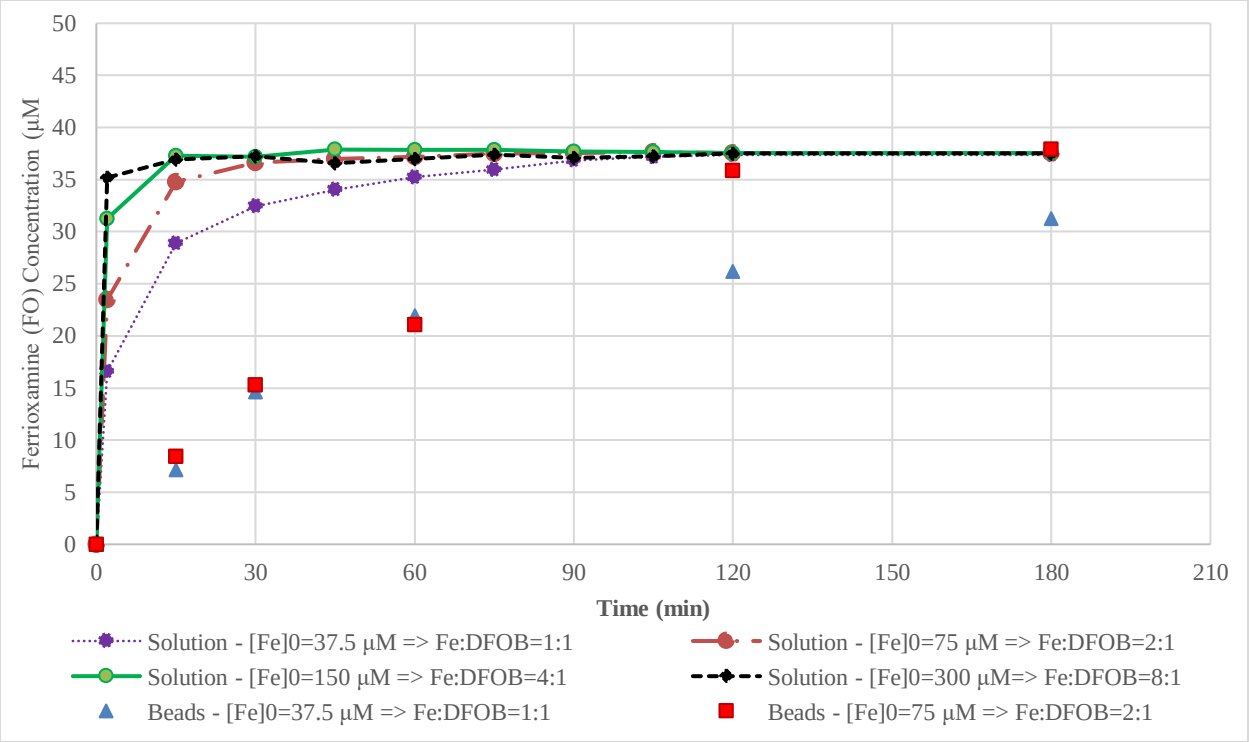

Figure 3.6 Rate of ferrioxamine formation in solution and on the beads for different initial iron concentrations corresponding to different DFOB: Iron ratios

Ito et al. (2011) proposed a mechanism for the citrate-DFOB ligand exchange by Fe(III) that is based on the following steps; one citrate molecule dissociates from a dimeric iron citrate complex FeCit2. Subsequently, an adjunctive association of DFOB to the remaining FeCit molecule occurs, which is followed by the formation of an intermediate complex of DFOB-Fe-citrate. Finally, the citrate dissociates to leave DFOB-Fe(III) complex (i.e. ferrioxamine). Consequently, it can be reasoned that the observed reduction of chelation rates can be the result of an imposed hindrance on the aforementioned mechanism. This can possibly arise from either a reduced diffusion of dimeric iron citrate complexes to the anchored DFOB, and/or an immobilization-induced physical obstruction of the chelator's hydroxamates groups preventing

them from wrapping around the Fe(III), thus delaying the formation of the critical DFOB-Fe-citrate intermediate complex.

It is worth noting that (Wenk et al., 2001) compared the performance of dissolved DFOB and cellulose-immobilized DFOB in chelating Fe(III)-citrate. The initial DFOB: iron molar ratio was 1:1 for both experiments. After 4 hours of exposure time, the authors concluded that the dissolved and immobilized DFOB had similar iron binding abilities. These findings do not contradict with our conclusion, since as shown in **Figure 3.6,** the ferrioxamine coverage at equilibrium is similar for both free and immobilized DFOB.

Finally, it is clear that a more thorough investigation of the effects of immobilizing DFOB on the rate of Fe(III)-citrate chelation is warranted.

3.5 Conclusions

In this chapter, the kinetics and sorption profiles for the adsorption of Fe(III)-citrate on DFOB-activated beads have been developed. The data were subsequently analyzed in light of the relevant kinetics and adsorption models with the following findings:

- Fitting the pseudo first-order, pseudo second-order and Elovich kinetics models to the experimental data did not offer a firm conclusion regarding the most convenient model given the similar correlation coefficients R^2.
- Comparing both the Langmuir and Freundlich models to our adsorption data, it was found that both models had similar correlation coefficients R^2 values of 0.992 and 0.953, respectively. However, since the Langmuir model's physical assumptions closely match

the physics of iron adsorption by DFOB, we can expect that the Langmuir model will offer the best fit for the sorption profile with K_L = 12.81 ($L/mg_{Fe(III)}$) and q_{max} = 0.206 ($mg_{Fe(III)}/g_{adsorbent}$). The q_{max} value obtained was compared to the ones reported for similar systems in the literature with varying favorability depending on the support used. It is important to note that more replicates are needed to minimize the experimental variability of the data.

- The dependency of adsorption kinetics on the initial iron concentration of Fe(III) relative to surface DFOB was established based on the transformed Langmuir kinetics equation (3.18); for an initial Fe(III) concentration lower than 22 μM or higher than 68 μM, the concentration of one reactant can be considered high enough relative to the other, that the adsorption kinetics can be described by the pseudo first-order kinetic model. As for initial concentrations close to 35 μM, the concentrations of the reactants are comparable and the pseudo second-order kinetic model is expected to offer the best fit for the kinetics data. It is worth noting that these parameters are specific to our DFOB-activated beads and change according to beads' properties and dosage of adsorbents.
- The reaction yield of ferrioxamine under immobilized DFOB was found to be similar to that of DFOB in solution, however the reaction rate was reduced for immobilized DFOB; Equilibrium was reached after approximately 30 minutes under DFOB in solution, while 180 minutes were needed for the immobilized DFOB. This can be explained by a hindrance of the citrate-DFOB ligand exchange mechanism by Fe(III), which can be caused by a lower diffusion rate of iron-citrate dimeric complexes to the immobilized chelator, and/or a physical obstruction of the DFOB's hydroxamates groups which

prevents them from binding iron. A more detailed investigation of this effect is warranted.

3.6 Future Directions

This study has investigated the kinetics and sorption profiles of Fe(III) adsorption on DFOB-activated beads. However different improvements can be made on this work:

- In order to increase the accuracy of the kinetics and adsorption data, a larger number of DFOB-activated tubes can be prepared and tested.
- Immobilizing DFOB on flat surfaces instead of beads can provide more reliable data since, unlike operating with microparticles, no centrifugation will be needed during the reaction to extract the samples. Additionally, decreasing the sample size relative to that of the solution from its current percentage of 5% can improve the measurements, especially when operating at low iron concentrations or when high number of samples are desired.
- Developing kinetics and adsorption studies of other DFOB-chelatable metals such as calcium (II), zinc (II), magnesium (II), aluminum (III), zirconium (IV), vanadium (V) and lead (II) along other metals can prove beneficial in designing DFOB-based sensors or other metal capturing devices (Kiss et al., 1998). Additionally, given the health risks associated with the DFOB's non-specific binding of metals (Genc et al.,2016), these studies can help in designing safer DFOB-based biomedical devices that limit the adverse effects of DFOB-induced mineral ions deficiency.
- In this work a citrate: iron ratio of 100:1 was adopted since it is physiologically relevant and prevents the formation of oligomeric iron citrate species which are less readily

available for DFOB chelation while also avoiding the ion's precipitation. However, given that human serum can have varying citrate: iron ratios ranging from 10:1 up to 100:1, a larger portion of oligomeric complexes will be expected in solutions having citrate: iron ratios lower than 100:1 (Evans, 2008). This in turn will lead to a less rapid chelation of Fe(III) from the citrate by the DFOB, which will possibly alter the kinetics and sorption profiles. Thus kinetics and sorption studies for iron solutions prepared with citrate to iron ratios lower than 100: 1 can be pursued.

4 EFFECTS OF SERUM PROTEINS SURFACE ADHESION ON THE ACTIVITY OF IMMOBILIZED DESFERRIOXAMINE (DFOB) ON POLYSTYRENE BEADS

4.1 Abstract

The effects of protein surface adhesion on the activity of DFOB has been investigated using bovine serum albumin (BSA) and equine plasma. It was shown that covering the beads' surface with washing in BSA-PBS solution for a total time of 30 minutes decreased the chelated iron amount by more than 50%. Additionally, 80% and 70% less iron were chelated from Fe(III)-citrate added to BSA and equine plasma, respectively. These results strongly reflect the detrimental effects of proteins surface adhesion on the activity of DFOB, suggesting that surface treatment such as copolymers immobilization is critical for a successful chelation in protein-rich fluids.

4.2 Introduction

Designing a DFOB-based biomedical device for the extraction or measurement of iron in serum must take into account the adhesion of blood proteins on hydrophobic surfaces and the subsequent effects on the activity of the attached molecules and the performance of the device (Hecker et al., 2018; Fry et al., 2010).

In order to minimize the adhesion of proteins on the hydrophobic supports, different researchers have successfully coated these surfaces with di-block or tri-block copolymers such as PEO-PPO-PEO or PEO-PBD-PEO to render them more hydrophilic and create a "brush" layer that repels large proteins and prevent their adhesion to the surface. (Li et al., 1996; Schilke, 2009; Heintz, 2012). The used Pluronic® triblock copolymers such as PEO-PPO-PEO **(Figure 4.1)** or other

custom made ones such as PEO-PBD-PEO **(Figure 4.2)**, are composed of a central hydrophobic polymer (PPO = polypropylene oxide or PBD=Polybutadiene) that get attached to the hydrophobic surface by adsorption and/or gamma-irradiation (Schilke and McGuire, 2011), with the hydrophilic tethers like polyethylene oxides (PEO) imposing a steric and entropic barrier that minimizes protein adhesion.

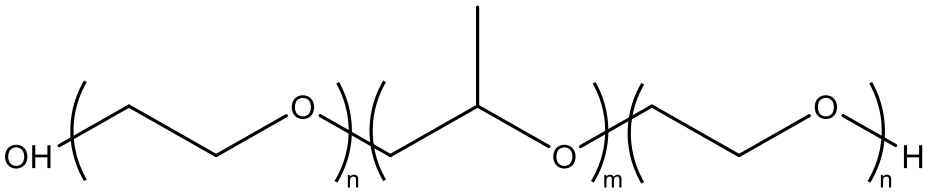

Figure 4.1 Chemical structure of Pluronic® F108 PEO-PPO-PEO triblock

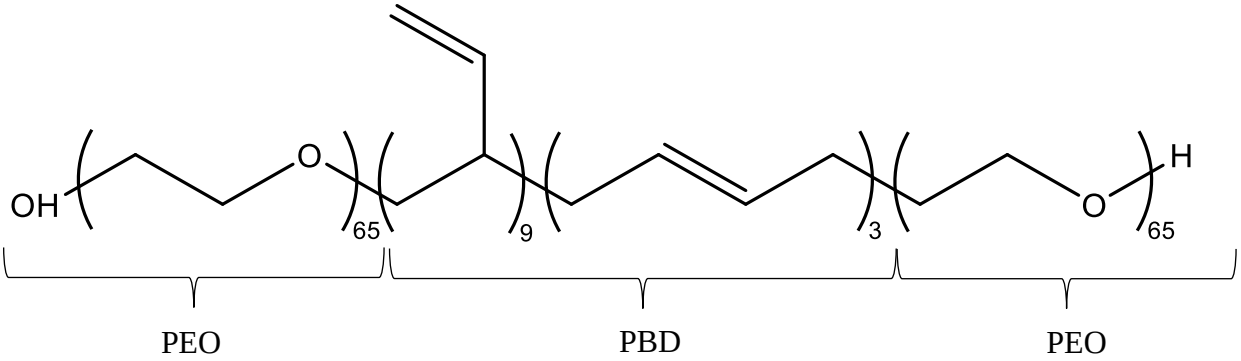

Figure 4.2 Approximate chemical structure of PEO–PBD–PEO triblock copolymer. The PBD centerblock is a random copolymer of 1,2- and 1,4-subunits. Adopted from (Schilke and McGuire, 2011)

Since this surface treatment has not been performed prior to attaching DFOB to the polystyrene surface, we were interested in investigating the effects of adding albumin and fibrinogen in the iron solution on the activity of the chelator. Both these proteins were known to strongly adsorb on hydrophobic surface (Nonckreman, 2010). Although the aminated latex beads used in this work had mostly hydrophilic properties, the fact that these particles are polystyrene-based, leads

them to retain some hydrophobic characteristics which can lead to noticeable surface adhesion (Molecular Probes, 2004).

Previous studies have shown that adding albumin at physiological concentration of 40 mg/mL to iron-citrate increased the amount of iron removed by the DFOB due to the possible creation of rapidly chelatable iron-citrate species, while it was also noted that albumin was loosely bound to Fe(III)-citrate (Evans et al., 2008). Conversely, the existence and subsequent adsorption of albumin (Mw ≈ 66 kDa) on the aminated beads' surface can potentially block the DFOB molecules (Mw = 560.684 g/mol) and physically hinder them from effectively chelating the iron. This concern was particularly justified given that the DFOB was closely linked to the latex surface via SPDP, which has a relatively short spacer arm length of 6.8 Å, in addition to the reported strong adsorption of BSA on both hydrophobic and hydrophilic surfaces (Jeyachandran et al., 2009; Jeyachandran et al., 2010; Hecker et al., 2018).

Additionally, given that the large blood protein fibrinogen (Mw ≈ 340 kDa) was found to adsorb efficiently and almost irreversibly on hydrophobic surfaces, causing blood clotting and platelet adhesion upon its conversion to fibrin strands, we were interested in determining its effects on the chelation activity of DFOB and the resulting amount of chelated iron. (Silverthorn, 2006; Cao et al., 2006; Halperin, 1999; Unsworth et al., 2008).

In this chapter, the effects of surface adhesion of albumin and fibrinogen on the activity of DFOB attached to aminated polystyrene beads have been investigated by adding bovine serum albumin and equine plasma to the Fe(III)-citrate solutions and subsequently measuring the iron formation on the beads.

4.3 Materials and Methods

4.3.1 Surface Blocking of DFOB-Functionalized Beads with Bovine Serum Albumin (BSA)

Prior to introducing Fe(III)-citrate-albumin solutions to DFOB-activated beads, we were interested in investigating the effects of covering the beads' surface with bovine serum albumin (BSA) (Mw ≈ 66 kDa) on the ability of the immobilized DFOB to chelate Fe(III)-citrate.

For that purpose, tubes with similar SH coverage of approximately 35% were coupled to a PDS-DFOB solutions prepared using a DFOB: SPDP molar ratio of 5:1 and PDS: Surface SH ratio of 60:1 (DFOB-activation of beads detailed in Chapter 2 - Section 2.3.1 through 2.3.5). Subsequently, two washing solutions were prepared; the first consisted of our usually used washing PBS buffer (20 mM sodium phosphate, 150 mM NaCl, pH=7.5), while the second was prepared by adding BSA (Sigma-Aldrich, lyophilized powder, ≥96%) to PBS. The BSA concentration in PBS was 40 mg/mL, similar to that observed in human serum. The BSA was stirred very gently to avoid foaming and left to dissolve in the buffer. Subsequently, 1 mL of these two buffers were separately added to the tubes. After gently suspending the beads in the buffers for less than 1 minute, the tubes were centrifuged for 5 minutes at 13.2 RCF and the buffers were decanted. This washing procedure was repeated 4 times and the last centrifugation lasted for 12 minutes.

Later on, 1 mL of 75 μM Fe(III)-citrate solutions were added to the suspended beads and left to interact for 180 minutes under end-over-end mixing at room temperature. Finally the remaining iron amounts in the supernatants of the beads washed with PBS and BSA-PBS were measured and compared (details on iron measurement in Chapter 2 - Section 2.3.9).

4.3.2 Fe(III)-Citrate-Albumin Solution Preparation and Testing under Physiological pH

In order to investigate the ability of DFOB-activated beads to remove iron in the presence of albumin at physiological concentrations (40 mg/mL), Fe(III)-citrate-albumin solutions were prepared similarly to the method outlined by Evans et al. (2008); BSA was dissolved in a solution of Fe(III)-citrate-HEPES (2 mM HEPES, 150 mM NaCL, pH = 7.4) having a citrate: iron ratio of 100:1 and 75 μM iron concentration. The pH was adjusted to 7.4 (± 0.05) and the mixture was allowed to stabilize for 2 hours at room temperature before being added to the DFOB-activated tubes.

It is worth noting that the DFOB-activated beads (initial SH coverage ≈ 25%, DFOB: SPDP molar ratio of 5:1, PDS: Surface SH ratio of 60:1) were washed with PBS and not BSA-PBS prior to use. Subsequently, 1 mL of 75 μM Fe(III)-citrate-albumin solutions were added to the beads and the reaction was allowed to proceed for 180 minutes under end-over-end mixing at room temperature. Lastly, the concentrations of iron remaining in the tubes and the amount of ferrioxamine (FO) formed on the surface were measured and compared to the ones observed under Fe(III)-citrate (ferrioxamine measurement detailed in Chapter 2 - Section 2.3.15).

4.3.3 Fe(III)-Citrate-Plasma Solution Preparation and Testing under Physiological pH

In this work, the DFOB was linked to the latex surface via the SPDP heterocrosslinker having a spacer arm length of 6.8 Å, and no di-block or tri-block copolymers were used to repel the proteins and prevent their adsorption to the surface. Additionally, despite the hydrophilic nature of the aminated latex beads, the fact that these particles are polystyrene-based leads them to retain some hydrophobic characteristics (Molecular Probes, 2004). Consequently, we were

interested in determining the effects of fibrinogen in the iron solution on the ability of surface DFOB to chelate iron. For that reason, Fe(III)-citrate-plasma solutions were prepared by diluting sterile equine plasma (HemoStat Laboratories, Dixon, CA, USA, SHP125) to 25% v/v in Fe(III)-citrate in HEPES (2 mM HEPES, 150 mM NaCL, pH = 7.4) immediately before use. The final citrate-bound Fe(III) concentration in the mixture was 75 μM while the citrate: iron ratio was 100:1. Although the total measured iron concentration in the Fe(III)-citrate-plasma samples was 92 μM, this excess amount of iron (92 – 75 = 17 μM) was mostly strongly bound to plasma proteins thus it was not immediately available for chelation by the DFOB (Manning et al., 2009). It is worth noting that the measured iron concentration of 17 μM is reasonably consistent with the reported iron amounts in the serum of healthy horses (Osbaldiston and Griffith, 1972).

Finally, 1 mL of these iron-citrate-plasma solutions were added to DFOB-activated beads (initial SH coverage ≈ 25%, 60:1, DFOB: SPDP molar ratio of 5:1, PDS: Surface SH ratio of 60:1), while the iron and ferrioxamine concentrations were measured after 180 minutes of contact time.

4.4 Results and Discussion

4.4.1 Effect of BSA Surface Coverage on Fe(III) Chelation

The ability of DFOB-activated beads to chelate Fe(III) following surface coverage with BSA during the washing stage has been investigated. **Figure 4.3** shows the concentrations of iron remaining after 180 minutes of contact with microspheres having similar DFOB coverage but subjected to different washing buffer solutions. It can be noticed that 39 μM of iron was chelated after 180 minutes of contact with the beads washed with PBS buffer. Conversely, this concentration decreased to 17 μM for the beads washed with a solution of BSA-PBS (BSA concentration of 40 mg/mL). Although the total duration of the washing procedure was slightly more than 30 minutes (of which 27 minutes of centrifugation), its effects on the ability of the immobilized DFOB to chelate the iron solute was noticeable. These results strongly suggest that albumin adhesion on the beads' surface severely hindered the ability of DFOB to chelate iron from the supernatant. Additionally, given the findings of Evans et al. (2008) which showed that adding albumin to Fe(III)-citrate did facilitate the chelation of iron by DFOB in solution via creating rapidly chelated iron-citrate species, coupled to the fact that albumin was not found to bind strongly to iron-citrate, we can deduce that the observed decrease in iron chelation under the beads washed with BSA-PBS was most likely due to diffusion limitations and not reaction ones. Knowing that BSA modeled as ellipsoids has larger dimensions than DFOB at 41.6 x 41.6 x 140.9 Å and 21.2 x 10 x 106.6 Å, respectively (Wright and Thompson, 1975; Dhungana et al., 2001), coupled with the findings of Sun and Zhu (2016) which showed that at a BSA concentration of 0.5 mg/mL and a reaction time of 10 minutes was enough to block 98% of the surface of epoxy-coated substrates, with both side-on and end-on monolayer of BSA forming on the surface under BSA concentrations of less than 5 mg/mL, we can conclude that the expected

high surface adhesion of BSA, in addition to its larger size relative to DFOB, can potentially lead to the observed reduction of Fe(III) chelation. Although it is important to note that the DFOB dimensions will strongly depend on the conformation of that molecule, we can expect that the presence of the larger BSA can possibly hinder the DFOB's hydroxamates groups from binding to the Fe(III) in the monomeric FeCit, thus preventing the formation of the DFOB-Fe-Cit intermediate complex, which is critical for the transfer of Fe(III) from the citrate to the chelator. Additionally, the presence of BSA on the polystyrene's surface can potentially prevent the initial dimeric iron citrate complex ($FeCit_2$) from reaching the immobilized chelator, thus preventing the initiation of the ligand-exchange mechanism by the iron. **Figure 4.4** shows a graphical comparison of the sizes of BSA and DFOB in both end-on and side-on orientations.

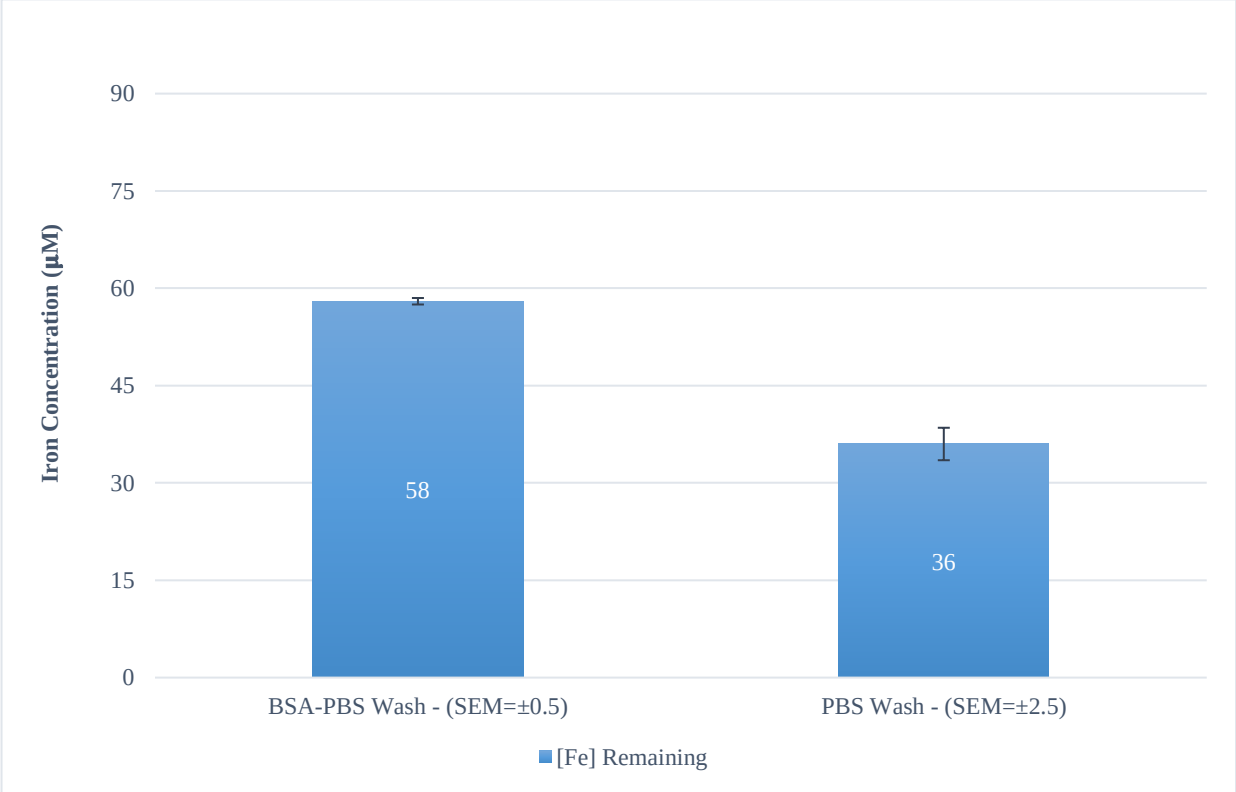

Figure 4.3 Remaining Fe(III) concentrations after 180 min of contact with DFOB-activated beads washed with BSA-PBS and PBS. Initial Fe(III) concentration=75 µM

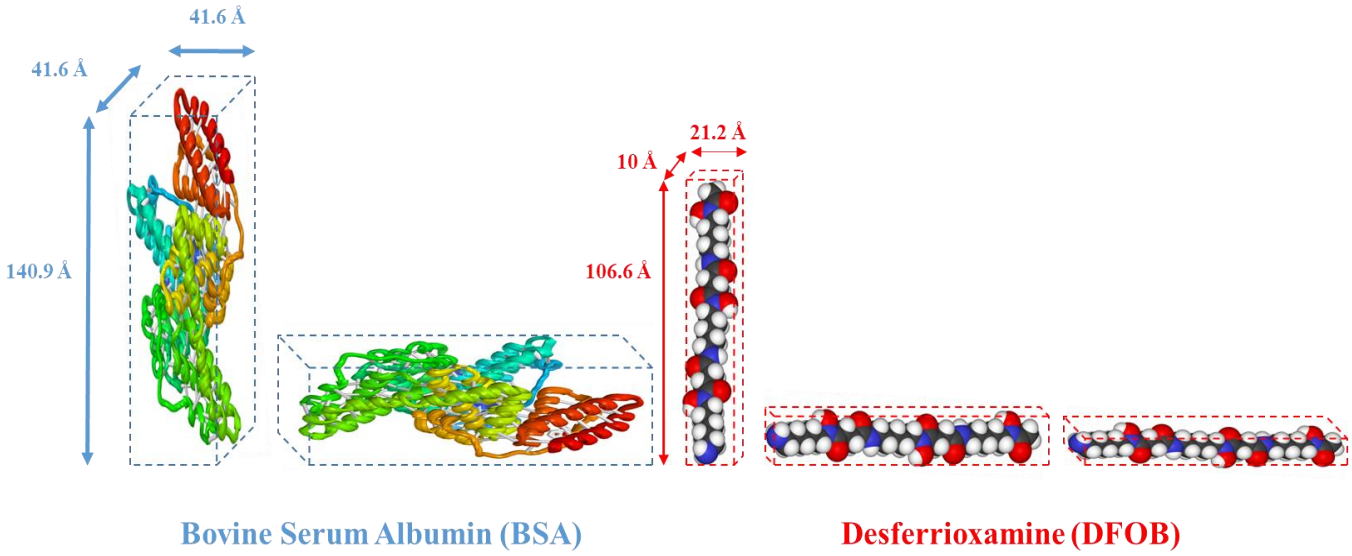

Figure 4.4 BSA and DFOB in both end-on and side-on orientations

4.4.2 Ability of DFOB-Functionalized Beads to Chelate Iron in Fe(III)-Citrate-Albumin and Fe(III)-Citrate-Plasma

The effects of albumin and plasma proteins (especially fibrinogen) on the activity of immobilized DFOB have been investigated. Three different iron solutions: Fe(III)-citrate, Fe(III)-citrate-albumin and Fe(III)-citrate-plasma were introduced to beads having similar DFOB loading. The amounts of iron chelated under the different iron solutions were derived after 180 minutes from the determination of the ferrioxamine formed on the beads' surfaces. The iron measurements yielded highly fluctuating readings for reasons that were not investigated. As shown in **Figure 4.5,** 37, 7 and 11 μM of Fe(III) were chelated from Fe(III)-citrate, Fe(III)-citrate-albumin and Fe(III)-citrate-plasma, respectively. The negative effects of proteins on the activity of immobilized DFOB seen in the previous section seemed to persist and increase when the proteins (albumin and plasma proteins) were added as a component of the iron solution. In

the previous section, we found that washing the DFOB-activated beads with BSA-PBS buffer (BSA concentration of 40 mg/mL) for a total exposure time of 30 minutes, was sufficient to reduce the DFOB's ability to chelate iron by more than 50%. In this section, we can notice that adding albumin to the iron-citrate solution at the same concentration of 40 mg/mL and a total exposure time of 180 minutes (reaction time), decreased the amount of chelated iron by approximately 80% compared to the Fe(III)-citrate solution. These results may be explained by the high effectiveness of BSA to cover the beads' surfaces, especially considering that the exposure time was longer in this experiment. As for the Fe(III)-citrate-plasma solution, containing the large fibrinogen protein in addition to the albumin, we notice that the iron chelation level was approximately 70% lower than that of Fe(III)-citrate, but 30% higher than that of the iron-albumin solution. However, it is very important to note that the equine plasma used was diluted to 25% v/v of its initial concentration.

These results clearly show that the effects of protein surface adhesion on the DFOB's activity cannot be neglected. Consequently, any biomedical system that involves contacting immobilized DFOB with serum proteins must involve coating the surface with protein repelling hydrophilic "brushes" such as PEO-PBD-PEO or PEO-PPO-PEO in order to preserve, at least partially, the chelator's activity (Li et al., 1996; Schilke, 2009; Heintz, 2012).

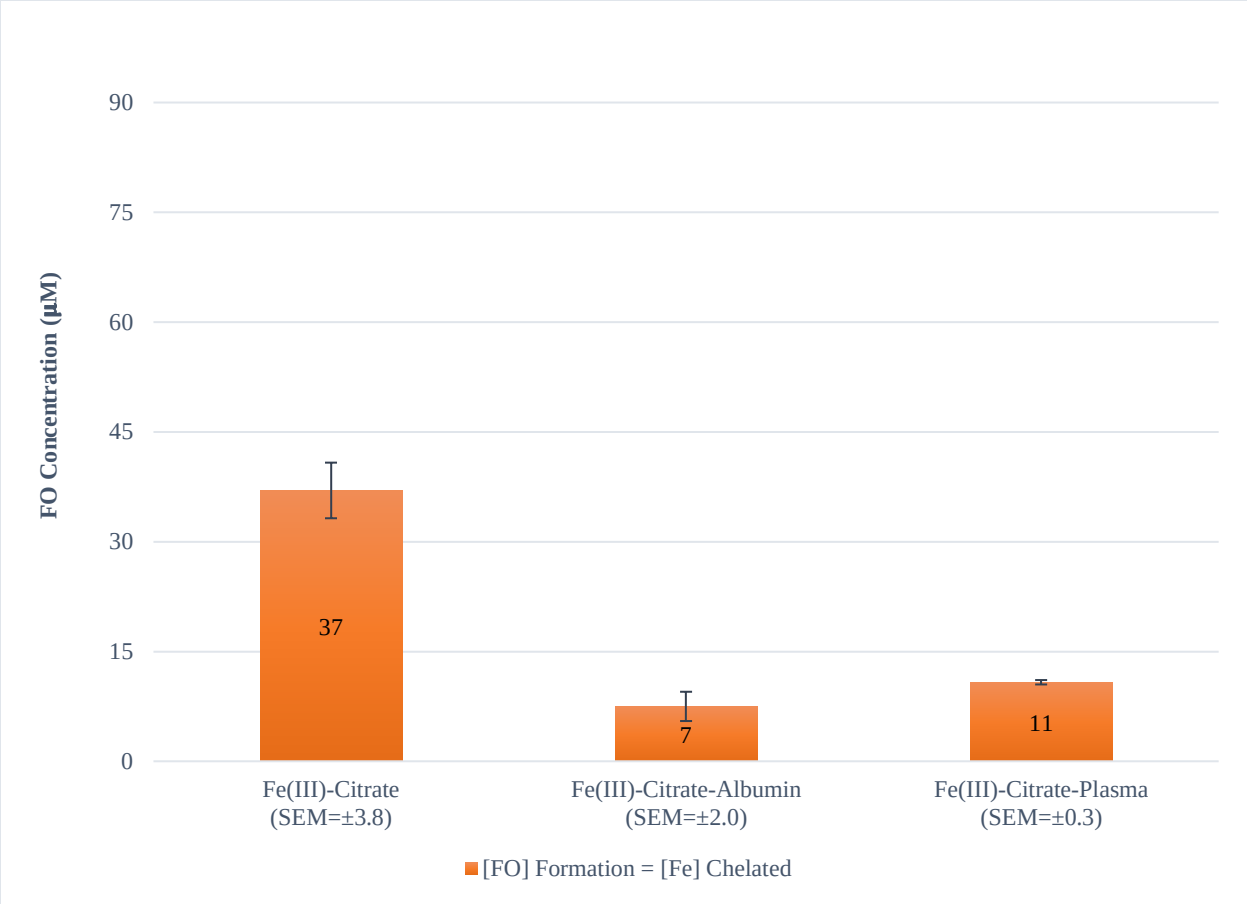

Figure 4.5 Ferrioxamine formation (i.e. Fe(III) chelated) after 180 min of contact with DFOB-beads under Fe(III)-citrate, Fe(III)-citrate-albumin, Fe(III)-citrate plasma. Initial iron concentration=75 uM

4.5 Conclusions

In this chapter, the effects of surface adhesion of bovine serum albumin and plasma proteins (such as fibrinogen) on the ability of immobilized DFOB to chelate citrate-bound Fe(III) have been investigated, with the following findings:

- The surface coverage of DFOB-polystyrene beads with albumin via washing with BSA-PBS buffer (40 mg/mL BSA) for a total exposure time of 30 minutes reduced the DFOB's ability to chelate Fe(III)-citrate by more than 50%. It was hypothesized that the high adhesion of BSA to the surface, coupled with its relative large size compared to that of the chelator, did inhibit the ligand transfer mechanism of Fe(III) from citrate to DFOB.
- Adding albumin (40 mg/mL) to iron-citrate solution decreased the chelated iron amount by approximately 80% after reacting for 180 minutes with DFOB-activated beads. This reduced activity has been observed despite the reported beneficial effects of albumin on the chelation of Fe(III)-citrate by DFOB.
- Adding 25% v/v diluted equine plasma to iron-citrate solution decreased the chelated iron amount by approximately 70% after reacting for 180 minutes with the DFOB-activated beads.
- These results strongly suggest that exposing DFOB-activated supports to protein-rich biological fluids should take into account the detrimental effects of protein surface adhesion on the activity of the chelator. Consequently, a surface treatment to render it more hydrophilic via attaching polymers with hydrophilic tethers such as PEO-PPO-PEO or PEO-PBD-PEO can potentially improve the DFOB's performance.

4.6 Future Directions

In this chapter, the detrimental effects of serum proteins surface adhesion on the activity of DFOB immobilized on polystyrene beads have been confirmed. This reduced performance was observed despite the relatively hydrophilic nature of the aliphatic amine beads. Consequently, the following studies can prove beneficial to mitigate the problem or improve the understanding of the physiological applications and limitations of immobilized DFOB:

- This work was limited in its investigation to the activity of DFOB in a relatively simple iron citrate solution with added BSA or diluted plasma (25% v/v). However, an actual assessment of the DFOB's operation in physiological conditions must be based on experimenting with real complex biological fluids such as serum and urine samples (Alberti et al., 2014).
- Future work can seek to covalently link DFOB via its amine terminal to surface-adsorbed copolymers. This can minimize the surface adhesion of proteins and extend the reach of DFOB into the iron solution. Similar to previous studies on covalently binding functionalized-polymers to biomolecules, EGAP-PDS (Fry et al., 2010) or NHS-activated tri-blocks (Sahin et al., 2009) can be either purchased or prepared and attached to SH-activated DFOB or its amine terminal, respectively. However, given the limitations arising from the hydrolysis of NHS esters under the high pH levels required to bind the DFOB's terminal amine, it is preferable to create imidoesters groups on the polymers, which are more convenient to use under high alkaline conditions (Similar to Scheme 2.10).

5 CONCLUSIONS

This work has sought to reversibly immobilize desferrioxamine B (DFOB) on a polystyrene support and test this system's ability to adsorb the physiologically and environmentally relevant Fe(III)-citrate. The selection of the chelator was based on its ability to form highly stable complexes with different metals, an attribute that expanded the scope of its biomedical, environmental and industrial applications. Additionally, due to the polystyrene's suitability for mass production of biosensors and microfluidics devices, immobilizing the DFOB on that polymer can prove a valuable tool in enhancing access to healthcare in distant communities, along other environmental applications.

After developing the required protocols to reversibly bind DFOB on the polymer support, the activity of the chelator and the effectiveness of its conjugation have been assessed under different operational conditions. Additionally, the polystyrene surface has been successfully regenerated to support fresh batches of DFOB, and achieved iron chelation levels similar to those observed under new beads.

Moreover, a kinetics and equilibrium study for the adsorption of Fe(III)-citrate on DFOB-activated beads have been investigated. The importance of this iron form arises from the critical role of the biosynthesized citrate in the transformation, availability, transportation and uptake of iron in blood plasma, natural waters, plants and pathogenic bacteria. Our findings showed a dependency of the adsorption kinetics and mechanisms on the initial concentration of iron in solution. In turn, these results can constitute a beneficial tool in designing and optimizing DFOB-activated materials for the chelation of iron.

The effects of albumin and serum proteins surface adhesion on the DFOB's activity have also been investigated. The significant decrease of iron chelation levels in the presence of proteins showed the detrimental effects of these compounds on the chelator's activity. Consequently, it was suggested that treating the surface with protein-repulsing copolymers is a necessary step for a successful implementation of DFOB in biomedical devices.

Finally, although our investigation was limited to the chelation of citrate-bound Fe(III) by DFOB-activated polystyrene beads, the versatility of the chelator in terms of complexing different metals, coupled with the industrial relevance of polystyrene, can potentially render this adsorbent a convenient asset in addressing a number of biomedical and environmental topics. Provided an adequate surface treatment with triblock copolymers such as PEO-PPO-PEO or PEO-PBD-PEO to mitigate the negative effects of protein adhesion on the activity of the chelator in biological fluids, a DFOB-activated device can have immediate applications which include its use as an extracorporeal chelation device that can potentially offer a safer metal removal treatment. Additionally, it can be possibly employed to develop simple detection devices of metals and bacteria in physiological and environmental fluids, in addition to the separation of high-valence metals, along other potential applications.

6 BIBLIOGRAPHY

Alberti, G., Emma, G., Colleoni, R., Nurchi, V. M., Pesavento, M., & Biesuz, R. (2014). Simple solid-phase spectrophotometric method for free iron(III) determination. Arabian Journal of Chemistry. doi:10.1016/j.arabjc.2014.08.017

Alberti, G., Emma, G., Colleoni, R., Pesavento, M., Nurchi, V. M., & Biesuz, R. (2014). Novel DFO-functionalized mesoporous silica for iron sensing. Part 2. Experimental detection of free iron concentration (pFe) in urine samples. Analyst, 139(16), 3940-3948. doi:10.1039/c3an01488f

Alberti, G., Quattrini, F., Colleoni, R., Nurchi, V. M., & Biesuz, R. (2015). Deferoxamine-paper for iron(III) and vanadium(V) sensing. Chemical Papers, 69(8), 1024-1032. doi:10.1515/chempap-2015-0112

Alderman, B. W., Ratliff, A. E., & Wirgau, J. I. (2009). A mechanistic study of ferrioxamine B reduction by the biological reducing agent ascorbate in the presence of an iron(II) chelator. Inorganica Chimica Acta, 362(6), 1787-1792. doi:10.1016/j.ica.2008.08.024

Ambrus, C. M., Anthone, S., Deshpande, G., Horvath, C. & Kalghatgi, K. (1987). Extracorporeal removal of iron with immobilized desferrioxamine. Transactions ASAIO 33(3), 744-748

Anthone, S., Ambrus, C. M., Kohli, R., Min, I., Anthone, R., Stadler, A., . . . Vladutiu, A. (1995). Treatment of Aluminum Overload Using a Cartridge with Immobilized Desferrioxamine. Journal of the American Society of Nephrology, 6(4), 1271-1277.

Applichem. (2008). Biological Buffers

Aruoma, O. I., Bomford, A., Polson, R. J., & Halliwell, B. (1988). Nontransferrin-Bound Iron in Plasma from Hemochromatosis Patients - Effect of Phlebotomy Therapy. Blood, 72(4), 1416-1419.

Azizian, S. (2004). Kinetic models of sorption: a theoretical analysis. Journal of Colloid and Interface Science, 276(1), 47-52. doi:10.1016/j.jcis.2004.03.048

Bellanti, F., Del Vecchio, G. C., Putti, M. C., Cosmi, C., Fotzi, I., Bakshi, S. D., . . . Della Pasqua, O. (2016). Model-Based Optimisation of Deferoxamine Chelation Therapy. Pharmaceutical Research, 33(2), 498-509. doi:10.1007/s11095-015-1805-0

Bhadra, P., Shajahan, M. S., Patel, P. N., Bhattacharya, E., Chadha, A., & Sekhar, P. K. (2018). Immobilizing Siderophores on Solid Surfaces for Bacterial Detection. Journal of the Electrochemical Society, 165(8), B3017-B3022. doi:10.1149/2.0041808jes

Biesuz, R., Emma, G., Milanese, C., Dacarro, G., Taglietti, A., Nurchi, V. M., & Alberti, G. (2014). Novel DFO-SAM on mesoporous silica for iron sensing. Part I. Synthesis optimization and characterization of the material. Analyst, 139(16), 3932-3939. doi:10.1039/c4an00179f

Borgias, B., Hugi, A. D., & Raymond, K. N. (1989). Isomerization and Solution Structures of Desferrioxamine-B Complexes of Al-3+ and Ga-3+1. Inorganic Chemistry, 28(18), 3538-3545. doi:DOI 10.1021/ic00317a029

Borgna-Pignatti, C., & Marsella, M. (2015). Iron Chelation in Thalassemia Major. Clinical Therapeutics, 37(12), 2866-2877. doi:10.1016/j.clinthera.2015.10.001

Cabantchik, Z. I., Breuer, W., Zanninelli, G., & Cianciulli, R. (2005). LPI-labile plasma iron in iron overload. Best Practice & Research Clinical Haematology, 18(2), 277-287. doi:10.1016/j.beha.2004.10.003

Cao, L., Sukavaneshvar, S., Ratner, B. D., & Horbett, T. A. (2006). Glow discharge plasma treatment of polyethylene tubing with tetraglyme results in ultralow fibrinogen adsorption and greatly reduced platelet adhesion. Journal of Biomedical Materials Research Part A, 79a(4), 788-803. doi:10.1002/jbm.a.30908

Carlsson, J., Axen, R., & Unge, T. (1975). Reversible, Covalent Immobilization of Enzymes by Thiol-Disulfide Interchange. European Journal of Biochemistry, 59(2), 567-572. doi:DOI 10.1111/j.1432-1033.1975.tb02483.x

Carlsson, J., Drevin, H., & Axen, R. (1978). Protein Thiolation and Reversible Protein-Protein Conjugation - N-Succinimidyl 3-(2-Pyridyldithio)Propionate, a New Heterobifunctional Reagent. Biochemical Journal, 173(3), 723-737. doi:DOI 10.1042/bj1730723

Chan, C. Y., Goral, V. N., Derosa, M. E., Huang, T. J., & Yuen, P. K. (2014). A polystyrene-based microfluidic device with three-dimensional interconnected microporous walls for perfusion cell culture. Biomicrofluidics, 8(4), 046505. doi:10.1063/1.4894409

Chien, S. H., & Clayton, W. R. (1980). Application of Elovich Equation to the Kinetics of Phosphate Release and Sorption in Soils. Soil Science Society of America Journal, 44(2), 265-268. doi:DOI 10.2136/sssaj1980.03615995004400020013x

Chin, C. D., Laksanasopin, T., Cheung, Y. K., Steinmiller, D., Linder, V., Parsa, H., . . . Sia, S. K. (2011). Microfluidics-based diagnostics of infectious diseases in the developing world. Nature Medicine, 17(8), 1015-U1138. doi:10.1038/nm.2408

Corbett, J.F. (1972). Pseudo first-order kinetics. Journal of Chemical Education, 49, 663. doi10.1021/ed049p663.

Dhungana, S., White, P. S., & Crumbliss, A. L. (2001). Crystal structure of ferrioxamine B: a comparative analysis and implications for molecular recognition. Journal of Biological Inorganic Chemistry, 6(8), 810-818. doi:DOI 10.1007/s007750100259

Doi 10.1016/S1040-8428(01)00218-9

Dzombak, D. A., & Morel, F. M. M. (1986). Sorption of Cadmium on Hydrous Ferric-Oxide at High Sorbate/Sorbent Ratios - Equilibrium, Kinetics, and Modeling. Journal of Colloid and Interface Science, 112(2), 588-598. doi:Doi 10.1016/0021-9797(86)90130-X

Elovich, S. Y. & Larinovov, O. G. (1962). Theory of Adsorption from Solutions of Non Electrolytes on Solid (I) Equation Adsorption from Solutions and the Analysis of Its Simplest Form, (II) Verification of the Equation of Adsorption Isotherm from Solutions. Izvestiya Akademii Nauk. SSSR, Otdelenie Khimicheskikh Nauk, 2, 209-216

Enyedy, E. A., Pocsi, I., & Farkas, E. (2004). Complexation and divalent of desferricoprogen with trivalent Fe, Al, Ga, InFe, Ni, Cu, Zn metal ions: effects of the linking chain structure on the metal binding ability of hydroxamate based siderophores. Journal of Inorganic Biochemistry, 98(11), 1957-1966. doi:10.1016/j.jinorgbio.2004.08.017

Evans, R. W., Rafique, R., Zarea, A., Rapisarda, C., Cammack, R., Evans, P. J., . . . Hider, R. C. (2008). Nature of non-transferrin-bound iron: studies on iron citrate complexes and thalassemic sera. Journal of Biological Inorganic Chemistry, 13(1), 57-74. doi:10.1007/s00775-007-0297-8

Evers, A., Hancock, R. D., Martell, A. E., & Motekaitis, R. J. (1989). Metal-Ion Recognition in Ligands with Negatively Charged Oxygen Donor Groups - Complexation of Fe(Iii), Ga(Iii), in(Iii), Al(Iii), and Other Highly Charged Metal-Ions. Inorganic Chemistry, 28(11), 2189-2195. doi:DOI 10.1021/ic00310a035

Faller, B., & Nick, H. (1994). Kinetics and Mechanism of Iron(Iii) Removal from Citrate by Desferrioxamine-B and 3-Hydroxy-1,2-Dimethyl-4-Pyridone. Journal of the American Chemical Society, 116(9), 3860-3865. doi:DOI 10.1021/ja00088a022

Farkas, E., Enyedy, E. A., & Csoka, H. (1999). A comparison between the chelating properties of some dihydroxamic acids, desferrioxamine B and acetohydroxamic acid. Polyhedron, 18(18), 2391-2398. doi:Doi 10.1016/S0277-5387(99)00144-8

Ferreira, C. M. H., Pinto, I. S. S., Soares, E. V., & Soares, H. M. V. M. (2015). (Un)suitability of the use of pH buffers in biological, biochemical and environmental studies and their interaction with metal ions - a review. Rsc Advances, 5(39), 30989-31003. doi:10.1039/c4ra15453c

Fierro, V., Torne-Fernandez, V., Montane, D., & Celzard, A. (2008). Adsorption of phenol onto activated carbons having different textural and surface properties. Microporous and Mesoporous Materials, 111(1-3), 276-284. doi:10.1016/j.micromeso.2007.08.002

Fontecave, M., Gerez, C., Mansuy, D., & Reichard, P. (1990). Reduction of the Fe(Iii)-Tyrosyl Radical Center of Escherichia-Coli Ribonucleotide Reductase by Dithiothreitol. Journal of Biological Chemistry, 265(19), 10919-10924.

Fraas, R., & Franzreb, M. (2017). Reversible covalent enzyme immobilization methods for reuse of carriers. Biocatalysis and Biotransformation, 35(5), 337-348. doi:10.1080/10242422.2017.1344229

Freundlich, H.M.F. (1907). Over the Adsorption in Solution. The Journal of Physical Chemistry, 57, 385-470

Fry, A. K., Schilke, K. F., McGuire, J., & Bird, K. E. (2010). Synthesis and anticoagulant activity of heparin immobilized "end-on" to polystyrene microspheres coated with end-group activated polyethylene oxide. Journal of Biomedical Materials Research Part B-Applied Biomaterials, 94b(1), 187-195. doi:10.1002/jbm.b.31640

G-Biosciences Application Note. (N.D.). Determine the Reactivity of NHS Esters on Biotinylation and Crosslinkering Reagents.

Genc, G. E., Ozturk, Z., Gumuslu, S., & Kupesiz, A. (2016). Mineral Levels in Thalassaemia Major Patients Using Different Iron Chelators. Biological Trace Element Research, 170(1), 9-16. doi:10.1007/s12011-015-0441-1

Gimbert, F., Morin-Crini, N., Renault, F., Badot, P. M., & Crini, G. (2008). Adsorption isotherm models for dye removal by cationized starch-based material in a single component systera: Error analysis. Journal of Hazardous Materials, 157(1), 34-46. doi:10.1016/j.jhazmat.2007.12.072

Halperin, A. (1999). Polymer brushes that resist adsorption of model proteins: Design parameters. Langmuir, 15(7), 2525-2533. doi:DOI 10.1021/la981356f

Heintz, K. (2012). Synthesis and Evaluation of PEO-Coated Materials for Microchannel-Based Hemodialysis. MSc. Thesis, Oregon State University, Corvallis, Oregon, USA

Hermanson, G. T. (2008). Bioconjugate Techniques, 2nd Edition. Burlington: Elsevier Science

Hernlem, B. J., Vane, L. M., & Sayles, G. D. (1996). Stability constants for complexes of the siderophore desferrioxamine B with selected heavy metal cations. Inorganica Chimica Acta, 244(2), 179-184. doi:Doi 10.1016/0020-1693(95)04780-8

Ho, Y. S. (2006). Review of second-order models for adsorption systems. Journal of Hazardous Materials, 136(3), 681-689. doi:10.1016/j.jhazmat.2005.12.043

Ho, Y. S., & McKay, G. (1999). Pseudo-second order model for sorption processes. Process Biochemistry, 34(5), 451-465. doi:Doi 10.1016/S0032-9592(98)00112-5

Ho, Y. S., & McKay, G. (2002). Application of kinetic models to the sorption of copper(II) on to peat. Adsorption Science & Technology, 20(8), 797-815. doi:Doi 10.1260/026361702321104282

Ho, Y. S., Wase, D. A. J., & Forster, C. F. (1996). Removal of lead ions from aqueous solution using sphagnum moss peat as adsorbent. Water Sa, 22(3), 219-224.

Ho, Y., & Mckay, G. (1998). Kinetic Model for Lead(II) Sorption on to Peat. Adsorption Science & Technology, 16(4), 243-255. doi:10.1177/026361749801600401

Ito, H., Fujii, M., Masago, Y., Waite, T. D., & Omura, T. (2015). Effect of ionic strength on ligand exchange kinetics between a mononuclear ferric citrate complex and siderophore desferrioxamine B. Geochimica Et Cosmochimica Acta, 154, 81-97. doi:10.1016/j.gca.2015.01.020

Ito, H., Fujii, M., Masago, Y., Yoshimura, C., Waite, T. D., & Omura, T. (2011). Mechanism and Kinetics of Ligand Exchange between Ferric Citrate and Desferrioxamine B. Journal of Physical Chemistry A, 115(21), 5371-5379. doi:10.1021/jp202440e

Iyer, K.S., Klee, W.A. (1973). Direct Spectrophotometric Measurement of the Rate of Reduction of Disulfide Bonds The reactivity of the disulfide bonds of bovine α-lactalbumin. The Journal of Biological Chemistry, 248(2):707-10

Jeyachandran, Y. L., Mielczarski, J. A., Mielczarski, E., & Rai, B. (2010). Efficiency of blocking of non-specific interaction of different proteins by BSA adsorbed on hydrophobic and hydrophilic surfaces. Journal of Colloid and Interface Science, 341(1), 136-142. doi:10.1016/j.jcis.2009.09.007

Jeyachandran, Y. L., Mielezarski, E., Rai, B., & Mielczarski, J. A. (2009). Quantitative and Qualitative Evaluation of Adsorption/Desorption of Bovine Serum Albumin on Hydrophilic and Hydrophobic Surfaces. Langmuir, 25(19), 11614-11620. doi:10.1021/la901453a

Kiss, T., Farkas, E. (1998). Metal-binding Ability of Desferrioxamine B. Journal of Inclusion Phenomena and Molecular Recognition in Chemistry 32, 2-3, 385–403

Klykov, O., & Weller, M. G. (2015). Quantification of N-hydroxysuccinimide and N-hydroxysulfosuccinimide by hydrophilic interaction chromatography (HILIC). Analytical Methods, 7(15), 6443-6448. doi:10.1039/c5ay00042d

Koizumi, M., Endo, K., Kunimatsu, M., Sakahara, H., Nakashima, T., Kawamura, Y., Watanabe, Y., Saga, T., Konishi, J., Yamamuro, T., Hosoi, S., Toyama, S., Arano, Y. & Yokoyama A.

(1988). ^{67}Ga-labeled Antibodies for Immunoscintigraphy and Evaluation of Tumor Targeting of Drug-Antibody Conjugates in Mice. Cancer Research, 48(5), 1189-1194

Kumar, K. V., & Sivanesan, S. (2006). Pseudo second order kinetics and pseudo isotherms for malachite green onto activated carbon: Comparison of linear and non-linear regression methods. Journal of Hazardous Materials, 136(3), 721-726. doi:10.1016/j.jhazmat.2006.01.003

Lagergren, S. (1898) About the Theory of So-Called Adsorption of Soluble Substances. Kungliga Svenska Vetenskapsakademiens Handlingar, 24, 1-39

Langmuir, I. (1918). The Adsorption Of Gases On Plane Surfaces Of Glass, Mica And Platinum. Journal of the American Chemical Society, 40(9), 1361-1403. doi:10.1021/ja02242a004

Largitte, L., & Pasquier, R. (2016). A review of the kinetics adsorption models and their application to the adsorption of lead by an activated carbon. Chemical Engineering Research & Design, 109, 495-504. doi:10.1016/j.cherd.2016.02.006

Li, J. T., Carlsson, J., Lin, J. N., & Caldwell, K. D. (1996). Chemical modification of surface active poly(ethylene oxide)-poly(propylene oxide) triblock copolymers. Bioconjugate Chemistry, 7(5), 592-599. doi:DOI 10.1021/bc960048v

Lin, J. X., & Wang, L. (2009). Comparison between linear and non-linear forms of pseudo-first-order and pseudo-second-order adsorption kinetic models for the removal of methylene blue by activated carbon. Frontiers of Environmental Science & Engineering in China, 3(3), 320-324. doi:10.1007/s11783-009-0030-7

Liu, Y., & Shen, L. (2008). From Langmuir Kinetics to First- and Second-Order Rate Equations for Adsorption. Langmuir, 24(20), 11625-11630. doi:10.1021/la801839b

Liu, Y., & Wang, Z. W. (2008). Uncertainty of preset-order kinetic equations in description of biosorption data. Bioresource Technology, 99(8), 3309-3312. doi:10.1016/j.biortech.2007.06.026

Manning, T., Kean, G., Thomas, J., Thomas, K., Corbitt, M., Gosnell, D., . . . Phillips, D. (2009). Iron Chelators in Medicinal Applications - Chemical Equilibrium Considerations in Pharmaceutical Activity. Current Medicinal Chemistry, 16(19), 2416-2429. doi:10.2174/092986709788682128

May, P. M., Linder, P. W., & Williams, D. R. (1977). Computer simulation of metal-ion equilibria in biofluids: Models for the low-molecular-weight complex distribution of calcium(II), magnesium(II), manganese(II), iron(III), copper(II), zinc(II), and lead(II) ions in human blood plasma. Journal of the Chemical Society, Dalton Transactions, (6), 588. doi:10.1039/dt9770000588

Miyazaki, M., Kaneno, J., Kohama, R., Uehara, M., Kanno, K., Fujii, M., . . . Maeda, H. (2004). Preparation of functionalized nanostructures on microchannel surface and their use for enzyme microreactors. Chemical Engineering Journal, 101(1-3), 277-284. doi:10.1016/j.cej.2003.11.010

Mohamad, N. R., Marzuki, N. H. C., Buang, N. A., Huyop, F., & Wahab, R. A. (2015). An overview of technologies for immobilization of enzymes and surface analysis techniques for immobilized enzymes. Biotechnology & Biotechnological Equipment, 29(2), 205-220. doi:10.1080/13102818.2015.1008192

Monzyk, B., & Crumbliss, A. L. (1982). Kinetics and Mechanism of the Stepwise Dissociation of Iron(Iii) from Ferrioxamine-B in Aqueous Acid. Journal of the American Chemical Society, 104(18), 4921-4929. doi:DOI 10.1021/ja00382a031

Moussout, H., Ahlafi, H., Aazza, M., & Maghat, H. (2018). Critical of linear and nonlinear equations of pseudo-first order and pseudo-second order kinetic models. Karbala International Journal of Modern Science, 4(2), 244-254. doi:10.1016/j.kijoms.2018.04.001

Neff, J. A., Caldwell, K. D., & Tresco, P. A. (1998). A novel method for surface modification to promote cell attachment to hydrophobic substrates. Journal of Biomedical Materials Research, 40(4), 511-519. doi:Doi 10.1002/(Sici)1097-4636(19980615)40:4<511::Aid-Jbm1>3.3.Co;2-M

Netto, L. E. S., & Stadtman, E. R. (1996). The iron-catalyzed oxidation of dithiothreitol is a biphasic process: Hydrogen peroxide is involved in the initiation of a free radical chain of reactions. Archives of Biochemistry and Biophysics, 333(1), 233-242. doi:DOI 10.1006/abbi.1996.0386

Neubauer, U., Nowack, B., Furrer, G., & Schulin, R. (2000). Heavy metal sorption on clay minerals affected by the siderophore desferrioxamine B. Environmental Science & Technology, 34(13), 2749-2755. doi:DOI 10.1021/es990495w

Osbaldiston, G. W., & Griffith, P. R. (1972). Serum Iron Levels in Normal and Anemic Horses. Canadian Veterinary Journal, 13(5), 105-+.

Panday, K. K., Prasad, G., & Singh, V. N. (1984). Removal of Cr(Vi) from Aqueous-Solutions by Adsorption on Fly-Ash Wollastonite. Journal of Chemical Technology and Biotechnology a-Chemical Technology, 34(7), 367-374.

Pandey, E., Srivastava, K., Gupta, S., Srivastava, S., & Mishra, N. (2016). Some Biocompatible Materials Used in Medical Practices- a Review. International Journal of Pharmaceutical Sciences and Research, 7(7), 2748-2755. doi:10.13040/Ijpsr.0975-8232.7(7).2748-55

Parkes, H. G., Allen, R. E., Furst, A., Blake, D. R., & Grootveld, M. C. (1991). Speciation of Non-Transferrin-Bound Iron Ions in Synovial-Fluid from Patients with Rheumatoid-Arthritis by Proton Nuclear-Magnetic-Resonance Spectroscopy. Journal of Pharmaceutical and Biomedical Analysis, 9(1), 29-32. doi:Doi 10.1016/0731-7085(91)80233-Y

Petrik, M., Zhai, C., Haas, H., & Decristoforo, C. (2016). Siderophores for molecular imaging applications. Clinical and Translational Imaging, 5(1), 15-27. doi:10.1007/s40336-016-0211-x

Pootrakul, P., Breuer, W., Sametband, M., Sirankapracha, P., Hershko, C., & Cabantchik, Z. L. (2004). Labile plasma iron (LPI) as an indicator of chelatable plasma redox activity in iron-overloaded beta-thalassemia/HbE patients treated with an oral chelator. Blood, 104(5), 1504-1510. doi:DOI 10.1182/blood-2004-02-0630

Richardson, D. R. (2002). Iron chelators as therapeutic agents for the treatment of cancer. Critical Reviews in Oncology Hematology, 42(3), 267-281. doi:Pii S1040-8428(01)00218-9

Rose, A. L., & Waite, T. D. (2003). Kinetics of hydrolysis and precipitation of ferric iron in seawater. Environmental Science & Technology, 37(17), 3897-3903. doi:10.1021/es034102b

Rudzinski, W., & Plazinski, W. (2006). Kinetics of solute adsorption at solid/solution interfaces: A theoretical development of the empirical pseudo-first and pseudo-second order kinetic rate equations, based on applying the statistical rate theory of interfacial transport. Journal of Physical Chemistry B, 110(33), 16514-16525. doi:10.1021/jp061779n

Rudzinski, W., & Plazinski, W. (2007). Theoretical description of the kinetics of solute adsorption at heterogeneous solid/solution interfaces - On the possibility of distinguishing

between the diffusional and the surface reaction kinetics models. Applied Surface Science, 253(13), 5827-5840. doi:10.1016/j.apsusc.2006.12.038

Sahin, E., & Kiick, K. L. (2009). Macromolecule-Induced Assembly of Coiled-Coils in Alternating Multiblock Polymers. Biomacromolecules, 10(10), 2740-2749. doi:10.1021/bm900474k

Schilke, K. (2009). Functional Polymers and Proteins at Interfaces. Ph.D. Dissertation, Oregon State University, Corvallis, Oregon, USA

Schilke, K. F., & McGuire, J. (2011). Detection of nisin and fibrinogen adsorption on poly(ethylene oxide) coated polyurethane surfaces by time-of-flight secondary ion mass spectrometry (TOF-SIMS). Journal of Colloid and Interface Science, 358(1), 14-24. doi:10.1016/j.jcis.2011.03.014

Selo, I., Negroni, L., Creminon, C., Grassi, J., & Wal, J. M. (1996). Preferential labeling of alpha-amino N-terminal groups in peptides by biotin, application to the detection of specific anti-peptide antibodies by enzyme immunoassays. Journal of Immunological Methods, 199(2), 127-138. doi:Doi 10.1016/S0022-1759(96)00173-1

Sharma, D. C., & Forster, C. F. (1993). Removal of Hexavalent Chromium Using Sphagnum Moss Peat. Water Research, 27(7), 1201-1208. doi:Doi 10.1016/0043-1354(93)90012-7

Sharma, Y. C., Gupta, G. S., Prasad, G., & Rupainwar, D. C. (1990). Use of Wollastonite in the Removal of Ni(Ii) from Aqueous-Solutions. Water Air and Soil Pollution, 49(1-2), 69-79. doi:Doi 10.1007/Bf00279511

Silva, A. M. N., Kong, X., Parkin, M. C., Cammack, R., & Hider, R. C. (2009). Iron(III) citrate speciation in aqueous solution. Dalton Transactions(40), 8616-8625. doi:10.1039/b910970f

Silverthorn, D. U. (2006). Human Physiology: An Integrated Approach. 4th Edition. United States of America: Pearson

Singh, A. K., Singh, D. P., Panday, K. K., & Singh, V. N. (1988). Wollastonite as Adsorbent for Removal of Fe(Ii) from Water. Journal of Chemical Technology and Biotechnology, 42(1), 39-49.

Su, B. L., Moniotte, N., Nivarlet, N., Chen, L. H., Fu, Z. Y., Desmet, J., & Li, J. (2011). Fl-DFO molecules@mesoporous silica materials: Highly sensitive and selective nanosensor for dosing with iron ions. Journal of Colloid and Interface Science, 358(1), 136-145. doi:10.1016/j.jcis.2011.02.050

Sun, Y. S., & Zhu, X. D. (2016). Characterization of Bovine Serum Albumin Blocking Efficiency on Epoxy-Functionalized Substrates for Microarray Applications. Jala, 21(5), 625-631. doi:10.1177/2211068215586977

Takagai, Y., Takahashi, A., Yamaguchi, H., Kubota, T., & Igarashi, S. (2007). Adsorption behaviors of high-valence metal ions on desferrioxamine B immobilization nylon 6,6 chelate fiber under highly acidic conditions. Journal of Colloid and Interface Science, 313(1), 359-362. doi:10.1016/j.jcis.2007.02.079

Tiffin, L. O. (1966). Iron Translocation II. Citrate/Iron Ratios in Plant Stem Exudates. Plant Physiology, 41(3), 515-518. doi:10.1104/pp.41.3.515

Tinoco, I., Sauer, K., & Wang, J. C. (1995). Physical chemistry: Principles and applications in biological sciences. Englewood Cliffs, NJ: Prentice-Hall

Tran, R., Ahn, B., Myers, D. R., Qiu, Y., Sakurai, Y., Moot, R., . . . Lam, W. A. (2014). Simplified prototyping of perfusable polystyrene microfluidics. Biomicrofluidics, 8(4), 04650. doi:10.1063/1.4892035

Unsworth, L. D., Sheardown, H., & Brash, J. L. (2008). Protein-resistant poly(ethylene oxide)-grafted surfaces: Chain density-dependent multiple mechanisms of action. Langmuir, 24(5), 1924-1929. doi:10.1021/la702310t

Wang, Y. L., Balowski, J., Phillips, C., Phillips, R., Sims, C. E., & Allbritton, N. L. (2011). Benchtop micromolding of polystyrene by soft lithography. Lab on a Chip, 11(18), 3089-3097. doi:10.1039/c1lc20281b

Wenk, J., Foitzik, A., Achterberg, V., Sabiwalsky, A., Dissemond, J., Meewes, C., . . . Scharffetter-Kochanek, K. (2001). Selective pick-up of increased iron by deferoxamine-coupled cellulose abrogates the iron-driven induction of matrix-degrading metalloproteinase 1 and lipid

peroxidation in human dermal fibroblasts in vitro: A new dressing concept. Journal of Investigative Dermatology, 116(6), 833-839. doi:DOI 10.1046/j.1523-1747.2001.01345.x

Wright, A. K., & Thompson, M. R. (1975). Hydrodynamic Structure of Bovine Serum-Albumin Determined by Transient Electric Birefringence. Biophysical Journal, 15(2), 137-141. doi:Doi 10.1016/S0006-3495(75)85797-3

Yehuda, Z., Hadar, Y., & Chen, Y. (2003). Immobilized EDDHA and DFOB as iron carriers to cucumber plants. Journal of Plant Nutrition, 26(10-11), 2043-2056. doi:10.1081/Pln-120024263

Yehuda, Z., Hadar, Y., & Chen, Y. N. (2012). FeDFOB and FeEDDHA immobilized on Sepharose gels as an Fe sources to plants. Plant and Soil, 350(1-2), 379-391. doi:10.1007/s11104-011-0923-7

Yuen, P. K., & DeRosa, M. E. (2011). Flexible microfluidic devices with three-dimensional interconnected microporous walls for gas and liquid applications. Lab on a Chip, 11(19), 3249-3255. doi:10.1039/c1lc20157c

Zeldowitsch, J. (1934). über Den Mechanismus der Katalytischen Oxidation Von CO a MnO_2. URSS, Acta Physiochim, 1, 2, 364-449